Theses and Dissertations

Theses, Dissertations, and Senior Projects

January 2015

Experimental Investigation Of Thermophysical Properties, Pressure Drop And Heat Transfer Of Non-Newtonian Silica Colloid Flow In Tubes

Md Tanveer Sharif

Follow this and additional works at: https://commons.und.edu/theses

EXPERIMENTAL INVESTIGATION OF THERMOPHYSICAL PROPERTIES,
PRESSURE DROP AND HEAT TRANSFER OF NON-NEWTONIAN SILICA
COLLOID FLOW IN TUBES

by

Muhammad Tanveer Sharif
Bachelor of Science, Islamic University of Technology, 2010

A Thesis

Submitted to the Graduate Faculty

of the

University of North Dakota

In partial fulfillment of the requirements

for the degree of

Master of Science

Grand Forks, North Dakota

May

2015

The Thesis, submitted by Md Tanveer Sharif in partial fulfillment of the requirements of the Degree of Master of Science from the University of North Dakota, has been read by the faculty advisory committee under whom the work has been done and is hereby approved.

6-May-2015

Dr. Clement Tang, Chairperson

6 May 2015

Dr. Forrest Ames, Committee Member

6 May, 2015

Dr. Nanak Grewal, Committee Member

This thesis meets the standard for appearance, conforms to the style and format requirements of the graduate school of the University of North Dakota and is hereby approved.

Dr. Wayne Swisher, Dean of School of Graduate Studies

May 7, 2015

Date

iii

PERMISSION

Title   Experimental Investigation of Thermophysical Properties, Pressure Drop and Heat Transfer of Non-Newtonian Silica Colloid Flow in Tubes

Department   Mechanical Engineering

Degree   Master of Science

In presenting this thesis in partial fulfillment of the requirements for a graduate degree from the University of North Dakota, I agree that the library of this University shall make it freely available for inspection. I further agree that permission for extensive copying for scholarly purposes may be granted by the professor who supervised my thesis work or, in his absence, by the chairperson of the department or the dean of the Graduate School. It is understood that any copying or publication or other use of this thesis or part thereof for financial gain shall not be allowed without my written permission. It is also understood that due recognition shall be given to me and to the University of North Dakota in any scholarly use which may be made of any material in my thesis.

_____
Md Tanveer Sharif

5/7/2015
Date

TABLE OF CONTENTS

LIST OF FIGURES

LIST OF TABLES

ACKNOWLEDGEMENTS

I would like to thank the University of North Dakota for giving me the opportunity of pursuing Master of Science degree in Mechanical Engineering program. I am also thankful to the Department of Mechanical Engineering for its continuous support throughout the duration of my study.

My heartiest thanks to Dr. Clement Tang, my advisor, whose teaching, advising and mentoring has helped me to complete my research work. I am also thankful to Dr. Forrest Ames and Dr. Nanak Grewal for their encouragement and support. I would like to include Sanjib Tiwari, Matthew Cox and Sarbottam Pant on my thanks list due to their immense support with the experimental setup and procedure.

Words are not enough to describe the contribution of my parents to my study. It is due to their support that I reached this stage today. My brother's and sister's supports are also worth mentioning. Finally, all praise to the Almighty for providing me with such an excellent opportunity and helping me to complete my graduate study.

ABSTRACT

Thermophysical properties and rheological behavior of silica (SiO_2) nanoparticle colloidal suspension with 9.58% volume concentration in water were analyzed. The laminar flow of the fluid through tubes of different diameter was studied to compare its pressure drop and heat transfer performance with those of water.

Thermal conductivity of the silica suspension was found to be 0.99% to 3.6% higher than the same property of water when measured from 7°C to 50°C. Within the temperature range, thermal conductivity of the silica suspension and water increased by 9.88% and 11.1% respectively, with increase in temperature.

It was observed that the colloidal dispersion of silica behaved as non-Newtonian shear thickening fluid whose viscosity increased with increasing shear rate when temperature was kept constant. Power law model for non-Newtonian fluid could fairly predict the viscosity of the fluid at certain shear rate. While measuring viscosity data with a rotary viscometer at fixed shear rate and temperature, the fluid viscosity showed a change in value with time for first 12-15 second of shear application and then obtained a constant value.

Pressure drop analysis showed that the friction factor of the silica suspension and the friction factor of water have no significant difference after a Reynolds number of 750. Before that, silica suspension has higher friction factor than that of water and the highest increase observed was 63%. Conventional correlation to predict the friction factor of single phase fluid can also be used in case of silica colloidal dispersion. As the diameter of the test section got smaller, the increase in the friction factor of silica dispersion enhanced compared to the friction factor of water.

There was no eminent difference between the heat transfer performance of silica suspension and water. Correlation that is used for water was found to be suitable for nanoparticle dispersion too. The highest value of Nusselt number for silica suspension and water was 17.54 and 13.42 respectively, when the fluids were circulated through the tube with the biggest diameter.

NOMENCLATURE

A_i Inside cross-sectional area [m²]

C_{pbf} Specific heat of base fluid [J.kg^{-1}.K^{-1}]

C_{pp} Specific heat of nanoparticle [J.kg^{-1}.K^{-1}]

D Diameter [m]

D_o Outside diameter[m]

D_i Inside diameter [m]

d diameter of particle[nm]

du/dy Velocity gradient, shear rate [s^{-1}]

d_p Diameter of nanoparticles [nm]

f Friction Factor

Gz Graetz number

h Convective heat transfer coefficient[W.m^{-2}.K^{-1}]

h_p	Plank constant [J.s]
I	Current supplied [Amp]
K	Consistency index
k	Thermal conductivity [W.m^{-1}.K^{-1}]
k_b	Thermal conductivity of test section material [W.m^{-1}.K^{-1}]
k_{bf}	Base fluid thermal conductivity [W.m^{-1}.K^{-1}]
κ	Boltzmann constant (= 1.3807×10^{-23} J.K^{-1})
k_s	Effective thermal conductivity of nanoparticle colloidal suspension [W.m^{-1}.K^{-1}]
k_e	Thermal conductivity of the suspension [W.m^{-1}.K^{-1}]
k_O	Thermal conductivity of base fluid [Wm^{-1}K^{-1}]
k_p	Thermal conductivity of the particles [Wm^{-1}K^{-1}]
L	Length [m]
$\dot{m}$	Mass flow rate [kg.s^{-1}]
n	Flow behavior index
n_{sf}	Empirical shape factor
Nu	Nusselt number

ΔP	Pressure drop [Pa]
Pe	Peclet number
Pr	Prandtl number
Q	Heat/power supplied [W]
Q_a	Heat absorbed [W]
Q_l	Heat loss [W]
q	Heat flux [W.m^{-2}]
Re	Reynolds number
T	Temperature [°C]
T_{boil}	Boiling point temperature of water [K]
t	Time [s]
T_b	Bulk fluid temperature [°C]
$T_{b,out}$	Outlet fluid bulk temperature [°C]
$T_{b,in}$	Inlet fluid bulk temperature [°C]
$T_{b,x}$	Bulk fluid temperature at axial location x [°C]
T_o	Reference temperature [K]
$T_{w,i}$	Inside wall temperature [°C]

$T_{w,o}$	Outside wall temperature [°C]
V	Velocity [m.s^{-1}]
V	Voltage supplied [Volts]
x	Axial distance [m]

Greek Symbols

η	Heat transfer rate per pump power and per temperature difference
μ	Dynamic Viscosity [Pa.s, cP]
μ_a	Apparent viscosity of non-Newtonian fluid [Pa.s, cP]
μ_{bf}	Viscosity of base fluid [Pa.s]
μ_s	Viscosity of nanoparticle colloidal suspension [Pa.s]
$\emptyset$	Particle volume fraction
ρ	Density [kg/m^3]
ρ_{bf}	Density of base fluid [kg/m^3]
ρ_p	Density of the nanoparticle [kg.m^{-3}]
τ	Shear stress [N.m^{-2}. dyne.cm^{-2}]
γ	Shear rate [s^{-1}]
$\dot{\gamma}$	Shear rate [s^{-1}]

Abbreviations

CNT	Carbon Nanotube
DI	Distilled
DVI	Degree of Viscosity Increase
GA	Gum Arabic
HVAC	Heating, Ventilation and Air Conditioning
ID	Inner Diameter
MWCNT	Multi-Wall Carbon Nanotube
OD	Outer Diameter

CHAPTER I

INTRODUCTION

Researches have been going on for decades in search of more effective heat transfer fluids, other than water or air, to increase the efficiency of thermal systems and develop more compact designs. One technique has been to introduce additives in convectional fluids, such as water, ethylene glycol, oil, Therminol, etc., to enhance their heat transfer capabilities. From such ideas, the notion of using nanometer-sized particles as colloidal suspensions in conventional heat transfer fluids advanced. Utilization of nanoparticle colloidal dispersion is relatively a new field, not older than two decades. The application of such fluid can be seen in automotive radiator, nuclear reactor, power plant, HVAC system, graphics processor unit cooling of a desktop computer. The science of nanoparticle colloidal dispersion is being studied by researchers all over the world. It has promising features to be used in micro-electro mechanical system, fuel cells, boiler flue gas temperature reduction, solar energy to enhance the efficiency of solar thermal system and many other things.

The suspended nanoparticles bring about change in the transport properties and heat transfer characteristics of the base fluids. One of the main reasons for the enhancement in heat transfer of nanoparticle colloidal suspension is the increase of thermal

conductivity of the suspension compared to the base fluid. But there are concerns of high pressure drop in pumping these colloids. The prepared suspension is usually more viscous than the base fluid. So, the enhancement in heat transfer must outweigh the penalty in pressure drop to make the use of nanoparticle colloids feasible. Prasher et al. (2006) deduced that the increase in the viscosity needs to be four times greater than the increase in the thermal conductivity for the nanoparticle colloidal suspension to be not beneficial at all.

Nanoparticles of metallic or non-metallic oxides are used to prepare colloidal dispersion. Carbon nanotube and graphene (a crystalline form of carbon) are also regarded as a highly promising material to be used in this kind of solution. Most commonly used materials to prepare nanoparticle suspension are alumina, copper dioxide, zinc oxide etc. Beside these, the use of titanium oxide, silicon dioxide, gold and silver is also common. Every particle material has its own merit to make its way in the study of nanoparticle suspension.

Preparation of nanoparticle suspension varies from researcher to researcher. Several researchers use surfactant to increase the stability of the suspension. Due to the difference in preparation method, two different suspensions of same material and same concentration can exhibit different properties. Some suspensions may act as Newtonian fluid, which has a constant viscosity whereas some other suspensions may behave as shear thinning or shear thickening non-Newtonian fluid. Increase of thermal conductivity may be significant for one suspension, but trivial for another one. Pressure drop and heat transfer performance may vary from sample to sample. Hence, a thorough experiment is

required to study the properties of nanoparticle colloidal dispersion so that the relation between the properties can be understood better and improvement can be made.

The main objective of this research is to get a thorough understanding of the nanoparticle colloidal suspension in terms of thermophysical properties, pressure drop and heat transfer. An accurate experimental setup and methodology for the measurement of various thermophysical properties, pressure drop and heat transfer for nanoparticle colloidal dispersion will be developed. The thermophysical properties such as thermal conductivity and viscosity play important role on the flow and heat transfer characteristics. Understanding and accurately quantifying these terms are essential in understanding the flow and heat transfer characteristics of the colloidal suspension. Comparison of the properties and characteristics should be made with a standard fluid, preferably water, in order to know where the nanoparticle colloidal suspension lies with respect to the standard fluid.

This manuscript provides an insight about the experimental study of the thermophysical properties, rheological behavior and pressure drop and heat transfer characteristics of nanoparticle suspension flow. Chapter II discusses the work of researchers regarding the thermal conductivity, viscosity, friction factor and convective heat transfer phenomena of nanoparticle suspension. Chapter III provides the description of experimental setup, instrument calibration process and the uncertainty associated with the measurements. Validation of the experimental setup and a thorough discussion of the experimental result are provided in Chapter IV. Chapter V summarizes the outcome of the experiment and discusses the scope of future development of the current research.

CHAPTER II

LITERATURE REVIEW

To use nanoparticle colloidal suspension as a cooling fluid in various operations, proper characterization of its parameters such as viscosity, thermal conductivity, heat transfer coefficient and pressure drop must be done. These properties are very important in designing the fluid flow system. Numerous studies have been done on these parameters. Factors such as particle material, particle concentration, size and shape of nanoparticle, Brownian motion etc., have been reported to affect the properties and performance of nanoparticle colloidal suspension. This chapter discusses the findings of researchers regarding the thermal conductivity, rheology, heat transfer and pressure drop performance of such colloidal dispersion.

2.1 Thermal Conductivity of Nanoparticle Colloidal Suspension

Maxwell (1954) was one of the first to develop a correlation for the thermal conductivity of a dilute suspension of randomly suspended spherical particles. His developed correlation takes into account the thermal conductivity of the particles substance and the same property of the medium in which the particles are suspended. Another factor that is considered in this model is the volume fraction of the particle. The correlation is given by

$$k_s = \frac{k_p + 2k_{bf} - 2(k_{bf} - k_p)\emptyset}{k_p + 2k_{bf} + (k_{bf} - k_p)\emptyset} k_{bf} \tag{2.1}$$

Hamilton and Crosser (1962) studied the influence of included particle shape, composition and pure component conductivity on the thermal conductivity of heterogeneous two-component mixtures consisting of a continuous and a discontinuous phase. They measured thermal conductivities for mixtures of balsa wood and aluminum particles as several shapes in rubber at certain compositions. They proposed an equation based on Maxwell model to predict the thermal conductivity of the mixture which is given by

$$k_s = \frac{k_p + (n_{sf} - 1)k_{bf} - (n_{sf} - 1)(k_{bf} - k_p)\emptyset}{k_p + (n_{sf} - 1)k_{bf} + (k_{bf} - k_p)\emptyset} k_{bf} \tag{2.2}$$

where n is the empirical shape factor. The value of n is dependent on the shape of the particles and the ratio of the conductivities of the two phases. They suggested that the value of n can be taken as 3 for mixtures in which the conductivity of the discontinuous phase is larger by less than a factor of 100 and in such case, the shape of the particle does not influence the value of n.

Models developed by Maxwell and Hamilton-Crosser do not take into account factors like interaction between particles, the size of the particles, temperature, Brownian motion etc. While studying thermal conductivity of nanoparticle suspensions, researchers reported effects of many other factors besides thermal conductivity of the particles, thermal conductivity of the suspension medium and volume fraction of particles. Philip and Shima (2012) reviewed different researchers' work on this area and reported the influence of volume fraction, nanoparticle size and diameter, additives, pH value, temperature, base fluid nature, type of nanoparticle material etc. on the thermal

conductivity of the suspensions. Within their report, there is no unvarying effect of one certain factor on the thermal conductivity.

Sahoo et al. (2013) carried out the investigation of thermal conductivity of silicon dioxide (SiO_2) nanoparticles dispersed in a base fluid of 60% ethylene glycol and 40% water by mass. They conducted experiments in a temperature range of 298 K to 365 K and used several particle volumetric concentrations up to 10%. They observed that the ratio of thermal conductivity of nanofluid to that of the base fluid increased with an increase in temperature and volumetric concentration. They modified Hamilton and Crosser correlation based on their experimental results, to take into account the temperature and particle size dependency of thermal conductivity. Their proposed correlation is given by

$$k_s = \frac{k_p + 2k_{bf} - 2(k_{bf} - k_p)\emptyset}{k_p + 2k_{bf} + (k_{bf} - k_p)\emptyset} k_{bf} + 5 \times 10^4 \beta \emptyset \rho_{bf} C_{pbf} \sqrt{\frac{\kappa T}{\rho_p d_p}} f(T, \emptyset) \qquad (2.3)$$

where κ = Boltzmann constant = 1.381×10^{-23} (J/K), $\beta = 1.9526 (100\emptyset)^{-1.4594}$ and

$f(T, \emptyset) = (2.8217 \times 10^{-2} \emptyset + 3.917 \times 10^{-3})\left(\frac{T}{T_o}\right) + (-3.0669 \times 10^{-2} \emptyset - 3.91123 \times 10^{-3})$ for $1\% \leq \emptyset \leq 10\%$, $298\,K < T < 365K$ and $T_o = 273\,K$. This correlation predicted their experimental values with a maximum deviation of 3.35%.

Kihm et al. (2011) developed another thermal conductivity model of nanoparticle suspension. In their opinion, Brownian particle velocities in published literature are often found not too fast to account for the relatively higher thermal conductivity of nanoparticle suspension. They attributed this increase in thermal conductivity to heat propagation velocity, which is of the same order as the sonic velocity, rooted in a modified kinetic principle. Their proposed model is

$$\frac{k_s}{k_{bf}} = 1 + C \frac{\emptyset^a \rho_p C_{pp} \kappa T^{1.5}}{k_{bf} h_p \cdot \mu_{bf}^{0.5} d_p^{0.5}} \exp\left(-\frac{3.8 T_{boil}}{T}\right) \left(\frac{C_{pbf}}{C_{pp}}\right)^b \tag{2.4}$$

where h_p is the Planck constant, T_{boil} is the boiling point temperature of the base fluid, C is a modified constant, a and b are empirical constants, the values of which represent the effect of coagulation and heat dissipation of nanoparticles. They got the values $a =$ 0.70, $b =$1.5 and $C =$3.58×10^{-14} by regression analysis of published experimental data of Chan Hee et al. (2005) for the case of alumina nanoparticles. Then they compared their model with five published models by analyzing experimental data of 47nm Al_2O_3 at 1 and 4% and 30 nm CuO at 1%. For both suspensions and for all the tested conditions of temperatures and volume concentrations, the model was in consistent agreement with the experimental data.

Beck et al. (2009) provided the following correlation based on their experimental data for seven different alumina colloidal suspensions

$$\frac{k_s - k_{bf}}{k_{bf}} = 4.4134 \emptyset (1 - e^{-0.025 d_p}) \tag{2.5}$$

Hwang et al. (2006) measured the thermal conductivity of CuO, SiO_2 and multiwalled carbon nanotubes (MWCNTs) suspensions in distilled water and CuO suspension in ethylene glycol. They used the transient hot-wire method for thermal conductivity measurement. They observed that MWCNT suspension had the highest thermal conductivity and SiO_2 nanoparticle suspension had the lowest thermal conductivity. For CuO nanoparticle suspension, the thermal conductivity enhancement of ethylene glycol-based suspension was higher than that of water based suspension. They saw 11.3%

increases in thermal conductivity for MWCNT suspension at a volume fraction of 0.01

whereas the increase of the same property for SiO_2 suspension was about 3.1%.

Huifei et al. (2014) analyzed the thermal conductivity of silica nanoparticle suspension in

mineral oil at temperatures between 10 to 80 ^{o}C. They experimented with volume

fractions of 0.01% and 0.1% and compared the results with the thermal conductivity of

mineral oil. Both 0.01% and 0.1% silica suspensions resulted in about 1.6% decrease of

the thermal conductivity when the temperature was above 40°C. The accuracy of their

used system was ±1 to 2%. So, they concluded that the effect of adding up to 0.1% silica

nanoparticles in mineral oil is negligible on the thermal conductivity of mineral oil.

Following model was developed by Abbaspoursani et al. (2011) considering that the

effective thermal conductivity of nanoparticle suspension (k_s) is a function of the thermal

conductivity of the base fluid (k_{bf}), the solid particle (k_p), the interfacial shell (k_i), the

particle diameter (d_p), the volume fraction of the particle ($\emptyset$), the interfacial shell

thickness (t), the temperature of nanofluid (T), and the half of the base fluid boiling

temperature (T_c)

$$\frac{k_s}{k_{bf}} = 1 + m\frac{\emptyset^\alpha}{(d_p)^\beta}T^\delta + n\emptyset\left(1 - \frac{d_c}{d_p}\right)T \quad \text{for} \quad d_p \geq d_c \qquad (2.6)$$

where m is a factor that depends on the properties of the solid particle, base fluid and

interfacial shell; α and β are empirical constant determined from experimental data; n is

a factor dependent on the properties of the base fluid, d_c and δ are model parameters

whose values for alumina-water system are 21 and 1 respectively.

Mariano et al. (2013) investigated the thermal conductivity of non-Newtonian ethylene

glycol-based SnO_2 nanoparticle suspension. The temperature points for the experiment

were 283.15, 303.15 and 323.15 K. Concentrations of SnO_2 nanoparticles up to 25% in

weight fraction were used. They observed that thermal conductivity of the suspension was larger than that of the base fluid and it kept increasing with enhancement in particle concentration. Average increase was between 1% for the lowest particle fraction and 14% for the highest fraction. Their experimental results were over predicted by Maxwell model.

The effect of aggregation on the thermal conductivity of water based alumina suspension was explored by Hong and Kim (2012). They used solutions of 1%, 3% and 5% by volume alumina and aggregated the solutions by inducing NaCl solution. The concentrations of NaCl in each sample were 0.05M and 0.5M. While the 3% and 5% alumina solutions aggregated, the 1% solution did not form any gel. They applied 3ω method for the measurement of thermal conductivity of both well-dispersed fluidic suspensions with NaCl and aggregated suspensions. The thermal conductivity results were found to be increasing with the degree of aggregation and the aggregated nanofluids showed greater thermal conductivities than the fluidic samples with maximum increase being 22%.

Sun et al. (2013) measured effective thermal conductivity (ETC) of water-based silicon dioxide nanoparticle suspension in shear flow fields using a rotating Couette apparatus. The diameters of silica particle used for the experiment were 10, 20, 40 and 60 nm and for each diameter, they prepared suspensions of four different concentrations with silica volume fraction being 1.96%, 3.92%, 8.57% and 12.85%. Their results indicated that the ETC of the suspension in shear flow fields was significantly higher than that in static states within a shear rate range of 89-820 1/s. The highest increase they achieved was 17% for 12.85% volume fraction suspension of 60 nm particle diameter. They also

observed that thermal conductivity increased asymptotically with increasing shear rate for the lower shear rates and reached a plateau as the applied shear rate was higher than a certain value. This critical shear rate value varied for each solution and was higher for a higher concentrated suspension (Figure 2.1).
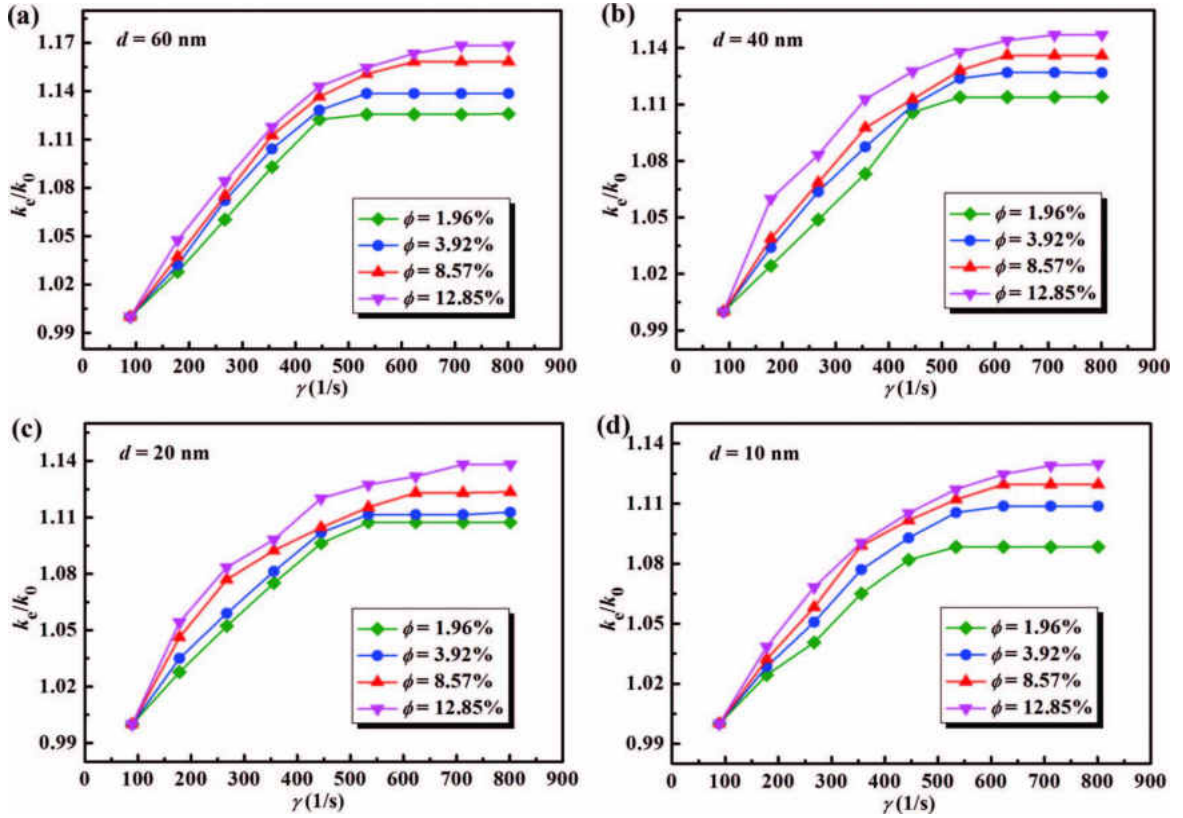
Figure 2.1: Ratios of the ETC k_e to the zero-shear thermal conductivity k_0 vs. the shear rate γ for the nanofluids suspending the nanoparticles with diameter d = 60 nm (a), d = 40 nm (b), d = 20 nm (c), and d = 10 nm (d), respectively. For each diameter, four different nanoparticle volume fractions (∅ = 1.96%, 3.92%, 8.57%, and 12.85%) are involved, Sun et al. (2013)

H. Wang et al. (2011) investigated the influence of size and fraction of SiO_2-organic composite nanorods on the thermal conductivity of nanoparticle suspension. The nanorods were synthesized in cetyltrimethylammonium bromide-tetraethylortho-silicate-ammonia solution-water media. Then the nanorods were dispersed in water to prepare

aqueous nanoparticle suspension. The length and aspect ratio of the nanorods were decreased by increasing addition of water. The thermal conductivity increased with an increase in the fraction of nanorods for all the fluids. But at the same fraction, enlarging the size of the nanorods did not enhance thermal conductivity. They suggested that at the same fraction of nanorods, number of nanoparticles was the maximum for the shortest size of nanorods and hence, thermal conductivity was the maximum. They achieved the maximum thermal conductivity with the sample that was synthesized with the maximum water addition whereas the minimum value was obtained for the sample synthesized with the moderate water addition.

2.2 Viscosity of Nanoparticle Colloidal Suspension

Jo and Banerjee (2014) experimented with the effect of shear rate and nanoparticle aggregation on the viscosity of multi-walled carbon nanotube (MWCNT) suspension in molten salts for a shear rate range of 1 to 1000 s^{-1} at 550 °C . They used an alkali carbonate eutectic composed of lithium carbonate and potassium carbonate by molar ratio of 62:38 as a base fluid. MWCNT, 10–30 nm in diameter and 1.5 μm in length, were dispersed into the eutectic to make suspensions of 1%, 2%, and 5% by mass. Equipment used for the viscosity measurement was a rotational rheometer and a cone-and-plate test section. Two types of suspensions were prepared, one with application of Gum Arabic (GA) to disperse nanoparticles homogenously and the other without GA, to observe the effect of aggregation of the nanotubes on the rheological behavior of the suspensions. The suspensions exhibited non-Newtonian behavior in low shear rate region and the same behavior was extended to higher shear rates with increase in the mass concentration of the nanoparticles. At a shear rate of 1000 s^{-1} where asymptotic value for the viscosity was

observed, the viscosity increased by 11%, 93%, and 1130% for the MWCNT mass concentrations of 1%, 2%, and 5% respectively than that of the base fluid (Figure 2.2). As for the effect of aggregation, they found that the viscosity of the suspension synthesized without using GA was about 18% higher than that of the synthesized using GA for MWCNT suspension of 1% by mass.
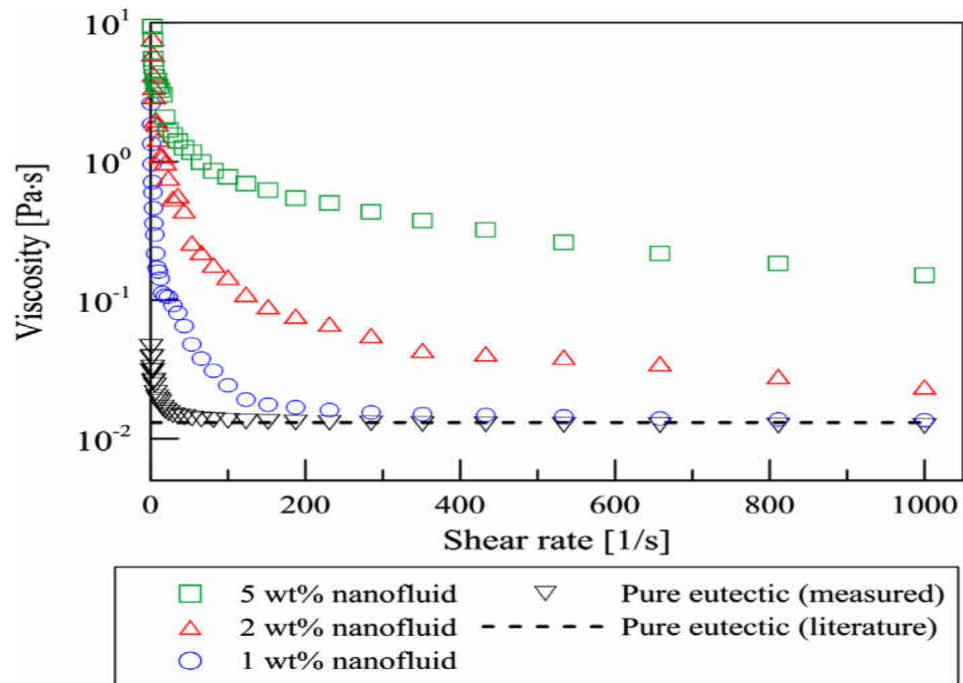
Figure 2.2: Viscosity of MWCNT colloidal suspension as a function of shear rate for various nanotube concentrations at 550 °C, Jo and Banerjee (2014)

Pastoriza-Gallego et al. (2011) studied the rheological behavior of ethylene glycol-based hexagonal scalenohedral-shaped α-Fe_2O_3 nanoparticles suspension, sizing 29 ± 18 nm in diameter and particle weight concentrations up to 25%, at 303.15 K. A cone-plate Physica MCR rheometer was used by them. The allowed value of torques to be applied and controlled by the equipment were between 0.5 μN·m and 125 mN·m and normal force from 0.1 to 30N. The applied shear rate ranged from 0 to 1000 s^{-1}. They found shear thinning (pseudoplastic) non-Newtonian behavior for the nanoparticle suspension. The

value of viscosity increased as the concentration got higher. The suspension also showed time dependency of its viscosity at a given shear rate.

The shear rate and temperature dependencies of viscosity of alumina nanospheres and nanorods suspension in polyalphaolefins lubricant were studied experimentally by Zhou et al. (2010). They prepared four samples of 1% alumina nanospheres, 3% alumina nanospheres, 1% alumina nanorods, and 3% alumina nanorods by volume particle suspension and termed them as NF1, NF2, NF3 and NF4 respectively. The rheological properties were measured at 25°C by a stress-controlled rheometer in a cone-plate configuration. They applied a shear rate of 500 s^{-1} and decreased the value stepwise until it reached 0.01 s^{-1}. By analyzing the trend of viscosity with shear rate, they considered sample NF1, NF2 and NF3 as Newtonian fluid within the experimental range, though they stated that these sample showed certain non-Newtonian feature and might behave as non-Newtonian under higher shear rate. Sample NF4 showed an apparent non-Newtonian shear thinning behavior but had a Newtonian plateau for shear rate lower than 1 s^{-1}. They observed that the viscosity in suspension of nanorods was larger than that of nanospheres suspension for the same volume fraction. They mentioned the aspect ratio of rods being larger than that of spheres as the key to this larger value. For suspension of the same nanoparticle shape, the viscosity of nanofluid increased with the increasing volume fractions in their experiment. The relative viscosity of the first three samples was found to be temperature independent whereas for the fourth sample, the relative viscosity decreased with an increase in temperature. Based on their study of several experimental results from literature, they suggested the relative viscosity of most nanoparticle suspension is independent of temperature because the rheological behavior of

nanoparticle suspension is mainly dominated by the base fluid even after the addition of nanoparticles. Thus the temperature dependence of viscosity of nanofluids follows that of base fluid resulting in the constant relative viscosity at different temperatures.

Yang et al. (2012) worked with colloidal dispersion of copper (Cu) nanoparticles in viscoelastic aqueous solution of cetyltrimethylammonium chloride/sodium salicylat. The average size of the particles was 50 nm. The volume fractions of Cu (spherical) nanoparticles used in their experiment were 0.05 vol%, 0.1 vol%, 0.15 vol%, 0.2 vol%, 0.6 vol%, 1.0 vol%, 1.6 vol% and 2.5 vol%. A stress-controlled rotational rheometer with concentric rotating cylinder carried out the viscosity test at a series of temperature. The torque range of the rheometer was 0.05 µN.m to 200 mN.m. In their experiment, the viscosity of each suspension decreased dramatically at small and moderate shear rate when the shear rate increased, indicating shear thinning behavior. But at large shear rate (order of hundreds), all the samples demonstrated shear-thickening behavior. They attributed this kind of behavior of the fluids to the flow transition happening in the Taylor–Couette flow of viscoelastic fluid; since the viscoelasticity induced flow transition at large shear rate will result in an abrupt increase in shear stress measured by the rheometer and consequently a sudden shear viscosity increase estimated from the measured shear stress. They also investigated the effect of temperature on viscosity. They found that at a relatively large volume fraction of nanoparticles, the temperature has a strong effect on the viscosity of the samples. The viscosity decreased radically as temperature was raised. But for lower volume fraction of Cu nanoparticles, the effect of temperature is insignificant on viscosity (Figure 2.3).
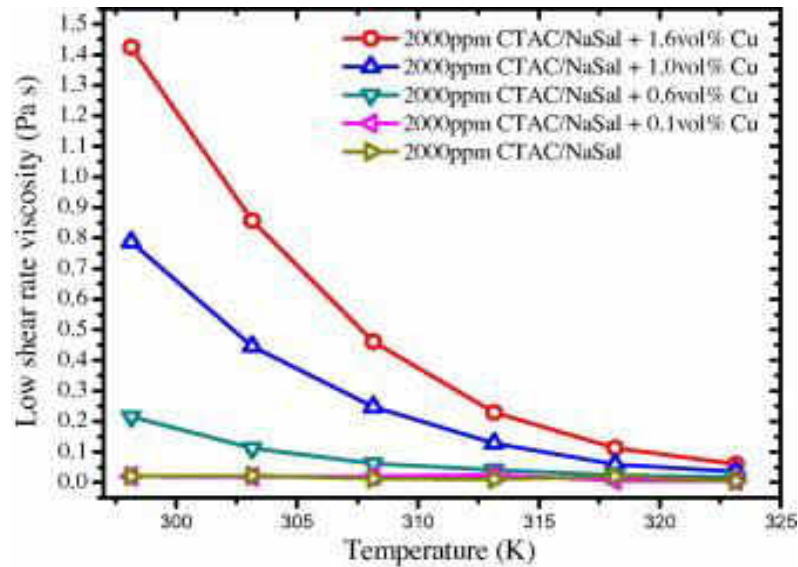
Figure 2.3: Low-shear-rate viscosity variation with temperature for different Cu nanoparticle colloidal suspension, Yang et al. (2012)

P. K. Namburu et al. (2007) investigated the rheological properties of ethylene glycol/water based silicon dioxide nanoparticle suspension. They measured the properties at suspensions of 2, 4, 6, 8 and 10% volume fraction of silica particle within a temperature range of -35 to 50 ^{o}C. They prepared the suspensions with particle diameter size of 20, 50 and 100 nm. Their samples showed non-Newtonian behavior at temperature lower than -10 ^{o}C but Newtonian behavior at temperature higher than -10 ^{o}C. The viscosity of the nanoparticle suspension was higher than that of the base fluid and the highest increase was 180% for 10% volume fraction suspension. They observed that as the volumetric nanoparticle concentration was higher, the viscosity value was also higher compared to that for the lower concentrated suspension. In their experiment, the viscosity decreased exponentially as temperature went higher. The ratio of difference between the nanoparticles suspension viscosity and the base fluid viscosity to the base fluid viscosity, termed as degree of viscosity increase or DVI, was also analyzed. DVI value decreased with increase in temperature but increased with an increase in volume concentration. The

15

highest and lowest values of DVI were 90% for suspension of 10% volume fraction and 5% for suspension of 2% volume fraction. At a certain concentration, the viscosity increased as the diameter size decreased and this was the case for all concentrations. Based on their experimental results, they developed a new empirical correlation between the viscosity, nanoparticle volume concentration and temperature of silica nanoparticle suspension in ethylene glycol and water solution. The maximum deviation between the equation value and the experimental data was ±8.4%. The correlation is given by

$$\log(\mu_s) = Ae^{-BT} \tag{2.7}$$

where A and B are the functions of particle volume concentration and can be calculated from

$$A = 0.1193\emptyset^3 - 1.9289\emptyset^2 - 2.245\emptyset + 167.17$$

$$B = -7 \times 10^{-6}\emptyset^2 - 0.00045\emptyset + 0.0192$$

Duan et al. (2012) studied the viscosity of 1, 2, 3 and 4% volume fraction of graphite nanoparticle (4 nm diameter) suspension in water. All their experiments were carried out at 298.15 K. They found the effective dynamic viscosity to decrease with increasing shear rate at a certain particle volume fraction. The suspensions acted as shear thinning non-Newtonian at lower shear rates and achieved constant dynamic viscosity at higher shear rate. They also studied aggregation effect by testing newly made and three days old sample. The relative effective dynamic viscosity at infinite rate of shear was found to be 2.92 for the fresh sample at 4 vol% in comparison of the base fluid and 24.86 for the sample of same volume fraction held for 3 days. The microstructure of the diluted nanofluids showed that the agglomeration of nanoparticles is much higher in the 3-days old fluids than that in the fresh fluids. They suggested that aggregation would happen in

nanoparticle suspensions which have not been treated specially by adding the surfactant, controlling the pH value, etc.

Hojjat et al. (2011b) studied rheological characteristics of γ-Al_2O_3, TiO_2 and CuO nanoparticle dispersion in 0.5 wt.% aqueous solution of carboxymethyl cellulose (CMC). Solutions of 0.1, 0.2, 0.5, 1, 1.5, 3 and 4% volume fraction nanoparticles were tested between 5 to 45 $^{\circ}$C and found to be non-Newtonian shear thinning fluids. All solutions obeyed the power law model of non-Newtonian fluid which is given by $\mu = K\dot{\gamma}^{n-1}$ where K is consistency index and n is power law index. The power law index for Al_2O_3 and TiO_2 suspension decreased with an increase in particle concentration but for CuO suspension, the opposite trend was observed. For all suspensions, the power law index increased with temperature. As for consistency index, it increased with higher concentration for Al_2O_3 and TiO_2 suspensions and decreased for CuO suspension. Temperature had a decreasing effect on consistency index in their study. They also observed that relative apparent viscosity of Al_2O_3 and TiO_2 suspensions was larger for higher volume concentration and almost independent of volume concentration in case of CuO.

Baghbanzadeh et al. (2014) experimented with silica nanospheres, multiwall carbon nanotubes (MWCNT), two types of hybrid nanostructures (80 wt.% silica nanosphere/20 wt.% MWCNT and 50 wt.% silica nanosphere/50 wt.% MWCNT) suspensions in distilled water and compared the rheological properties. 0.1%, 0.5% and 1% mass concentration of nanoparticle suspensions were prepared. They observed that viscosity increased with particle concentration and highest increase was for MWCNT. But temperature had decreasing effect on the viscosity. Degree of viscosity increase (DVI)

was lowest at 20 ^{o}C for all suspensions and the highest value of DVI was for MWCNT. For silica suspension, the highest DVI was around 14% at 40 ^{o}C for 1 wt% solution. They commented that the optimum operating conditions for using the nanomaterials inside the fluids to obtain the least increase in the viscosity of distilled water are 20 ^{o}C and 1 atm.

Aladag et al. (2012) analyzed the effect of temperature and shearing time on viscosity of alumina nanoparticles and carbon nanotubes (CNT) suspended in water. Both suspensions were 1% by weight fraction of nanoparticles and contained 1% by volume of surfactant. A stressed control rheometer in a parallel plate configuration was used to measure the rheological properties. Temperature points were chosen to be 2, 5, 7 and 10 ^{o}C and the time of shear stress ramp were 120, 180, 240 and 300 s. They saw hysteresis loops for both suspensions under increasing and decreasing ramp in shear stress. The flow curve for increasing ramp in shear stress was greater than that of decreasing shear stress ramp in their study. The shape of the hysteresis loop varied depending on nanoparticle type and shear time. The CNT suspension behaved as non-Newtonian shear thinning under their experimental condition but it tended to Newtonian plateau for shear rate over 100 s^{-1}. So they considered it as Newtonian fluid at high shear rate. Its apparent viscosity decreased with an increase in temperature. The alumina nanoparticle suspension behaved as non-Newtonian shear thickening fluid within a shear rate range of 0-4000 s^{-1}. They described the shear thickening behavior by saying that it might be related to a transition of suspension structure from an ordered state to a rather disordered state and increasing the shear stress caused the particles or clusters to displace from their equilibrium position to become a disorder structure which dissipates more energy during flow leading to the increase of viscosity. They determined the power law model indices

18

and saw that the consistency index decreased by 57% from 2 to 10 $^{\circ}$C whereas flow index increased by 5.57% over the same temperature range.

Kole and Dey (2010) prepared alumina nanoparticle suspension in car engine coolant using oleic acid as surfactant and reported its rheological behavior. Both the base fluid and the solution of base fluid and surfactant were Newtonian under experimental condition. For alumina volume fraction of 0.004% or lower, the suspension was Newtonian at higher temperatures. All other alumina suspensions were found to be shear thinning non-Newtonian over the whole temperature range. Their experimental data agreed well with the correlation given by Masoumi et al. (2009) and Praveen K Namburu et al. (2007).

2.3 Heat Transfer and Pressure Drop of Nanoparticle Colloidal Suspension

Sajadi and Kazemi (2011) studied the effect of the concentration of dilute particles on heat transfer and pressure drop. They used TiO_2/water based colloidal suspension in fully developed turbulent regime in a circular tube. Nanoparticle volume concentrations used for the experiment were 0.05, 0.1, 0.15, 0.20 and 0.25%. Sajadi and Kazemi found that heat transfer coefficient of nanoparticle suspension increased with the suspension of a small amount of TiO_2 nanoparticles compared to that of pure water. They also found that with increasing Reynolds number, the rate of the heat transfer coefficient enhancement of nanoparticle suspension to that of pure water decreased. They found no effect of increasing the concentration of nanoparticles on the enhancement of heat transfer. In their experiment, the pressure drop of the suspension increased with increasing volume fraction of nanoparticles. They derived a new correlation of Nusselt number with respect to their experimental data to predict the heat transfer coefficient of nanoparticle

dispersion with a volume concentration ≤0.25% and a Reynolds number range between 5000 and 30000. The correlation is given by

$$Nu = 0.067Re^{0.71}Pr^{0.35} + 0.0005Re \qquad (2.8)$$

The majority of their data fell within ±8% of the above equation. As for pressure drop, they found that nanoparticle concentration enhancement increased the pressure drop of suspension but increasing Reynolds number decreased it. Pressure drop increment was 5-25% greater compared to that of water.

J. Wang et al. (2013) investigated the convective heat transfer and pressure drop of the laminar flow of dilute suspension containing multi walled carbon nanotubes (MWCNTs) in a horizontal circular tube and compared the results with those of distilled water (DI). They observed that Nu increased with the increase of Re. They observed a considerable increase in the convective heat transfer of nanoparticle suspension at Re > 100 in comparison with that of DI water and the enhancement became more obvious for high concentration of nanoparticles. E.g., when Re was about 120, the heat transfer coefficient increased up to about 70% with concentration of 0.05 vol% and 190% with concentration of 0.24 vol%. This enhancement of heat transfer coefficient was attributed to the increase of thermal conductivity and mostly to the reduction in thermal boundary layer. The pressure drop for different fluids in the horizontal tube was found to vary linearly with Re confirming the flow pattern to be laminar. It was found that the heat transfer rate per pump power and per temperature difference, η of DI water was nearly Re independent, while η for nanofluid flow increases monotonously with increasing Re, and the effect of CNT concentration on η was not obvious. They also found that at relatively high flow rate, i.e., Re > 100, η of nanofluids is much larger than that of DI water due to the

considerable enhancement in the heat transfer rate. All in all, Wang et al. concluded that CNT nanoparticle suspension is a promising heat transfer media as their result indicated that at low concentration, these suspensions will increase the heat transfer, but at the expense of pumping power.

Fotukian and Nasr Esfahany (2010) investigated heat transfer performance and pressure drop of very dilute suspension of CuO nanoparticle in water inside a circular tube in turbulent regime. In their experiment, they found that heat transfer coefficient of the suspension increased about 25% compared to pure water and the increase in concentration of the nanoparticles did not have much effect on heat transfer enhancement in turbulent regime in the range of concentrations they studied. Comparing their experimental results with Dittus-Boelter equation, they said that this equation underestimated the Nusselt number of the suspension. They also observed a reduction in the ratio of convective heat transfer coefficient of nanoparticle suspension to that of pure water with increasing Reynolds number. It was observed that the wall temperature of the test tube decreased considerably when the suspension flowed in the tube and with increasing Reynolds number. They thought of the augmented thermal energy transfer from the wall to the fluid flowing in the tube in the presence of nanoparticles as the cause of this temperature decrease. In the observation of pressure drop, they found a maximum pressure drop of about 20% for nanoparticle suspension with a volume concentration of 0.03%.

Kayhani et al. (2012) studied the effect of nanoparticle concentration on forced convective heat transfer of TiO_2-water colloidal suspension in turbulent flow regime under constant heat flux at the wall. They also studied the effect on pressure drop. The

concentrations used in the experiments were 0.1, 0.5, 1, 1.5 and 2 vol%. The Reynolds numbers were between 6,000 and 16,000. They found that the heat transfer coefficient and Nusselt number of all the suspensions were significantly higher than those of base fluid and these properties increased with increasing Reynolds number. The maximum enhancement of heat transfer (h_{nf}/h_w) was 1.17 for 2% volume fraction at a Reynolds number of 11,780. The maximum Nu_{nf}/Nu_w also occurred at the same volume concentration and Reynolds number which was 1.08. Their experimental values fell well within the prediction by Dittus-Boelter (-3% to +15%) and Gnielinski (-1% to +10%) correlations. They did not find any significant increase in pressure drop.

Hashemi and Akhavan-Behabadi (2012) studied the heat transfer and pressure drop characteristics of CuO nanoparticles suspended in base oil. The suspension was flown inside horizontal helical tube under constant heat flux. They prepared suspensions with different particle weight concentrations of 0.5%, 1% and 2%. For a given helical tube and at a same flow conditions, they found a noticeable increase in heat transfer coefficient as well as pressure drop of nanoparticle suspension compared to that of base liquid. They also found that at the same flow condition and for a given fluid with constant particle concentration, helical tube enhanced the heat transfer rates most compared to that of the straight tube. Compared to base oil flow, maximum heat transfer enhancement of 18.7% and 30.4% was obtained for flow with 2 wt.% concentration inside the straight tube and helical tube, respectively. They introduced a new parameter called performance index, $\eta=(h^*/h_{ST.BF})/(\Delta P^*/\Delta P_{ST.BF})$ in which, h^* and ΔP^* represent mean heat transfer coefficient and pressure drop of the flow resulted by applying enhanced heat transfer techniques, respectively. $h_{ST,BF}$ and $\Delta P_{ST,BF}$ are the mean heat transfer coefficient and pressure drop

22

of the base oil flow inside the straight tube, respectively. For the straight tube, the highest performance index was 1.052 for the nanofluid flow with 2 wt.% at Reynolds number of 90.2. For the helical tube, the maximum value of this parameter for base oil flow was 1.16 at Reynolds number of 21.9 whereas it was 1.26 for nanoparticles suspension at Reynolds number of 41.3. They developed a correlation to predict the nanofluid flow heat transfer coefficient inside the helical tube which predicted their experimental data within an error band of −15% and +18%. The correlation is:

$$\text{Nu} = 41.730\text{Re}^{0.364}Pr^{-0.286}(1 + \emptyset)^{0.180} \tag{2.9}$$

Duangthongsuk and Wongwises (2010) studied the heat transfer coefficient and friction factor of the TiO_2-water colloidal suspension flowing in a horizontal double tube counter-flow heat exchanger under turbulent flow conditions, experimentally. TiO_2 nanoparticles with diameters of 21 nm dispersed in water with volume concentrations of 0.2–2 vol.% were used as the test fluid. They found that the heat transfer coefficient of the suspension was higher than that of the base liquid and increased with increasing Reynolds number and particle concentrations. The heat transfer coefficient of the suspension was approximately 26% greater than that of pure water. But they found that heat transfer coefficient of the suspension at a volume concentration of 2.0 vol.% was approximately 14% lower than that of base fluids for given conditions. Pak and Cho correlation predicted the heat transfer coefficient of nanofluids and gave results that corresponded well with the experimental results for the volume concentration of 0.2% but not for volume concentration of 0.6% and 1.0%. The pressure drop and friction factor of the suspensions increased while increasing Reynolds number. Enhancement in particle concentrations increased pressure drop and friction factor slightly.

Kannadasan et al. (2012) compared the heat transfer and pressure drop characteristics of water based CuO nanoparticle suspension in a helically coiled heat exchanger held in horizontal and vertical positions. They conducted experiments in the turbulent flow regimes using water and CuO nanoparticle suspension of 0.1% and 0.2% volume concentrations. They found that Nusselt number at 0.1% and 0.2% volume concentration suspension increased by 36% and 45% respectively when compared with water turbulent flow in horizontal position. For vertical position, the Nusselt number at same nanoparticle concentration was found to be increased by 37% and 49% respectively when compared with water turbulent flow. They attributed the greater increase of heat transfer in vertical position than in horizontal position to rapid developments of secondary flow due to increase in thermal conductivity of nanofluids. They found that pressure drop increased with volume concentration of nanoparticles. The average increase in friction factor of 0.2% volume concentration CuO suspension compared to water was 24% for the horizontal helically coiled heat exchanger whereas the increase for same property was 23% for vertical helically coiled heat exchanger.

Heyhat et al. (2013) presented an experimental study of the heat transfer coefficient and friction factor of nanoparticle dispersion flowing in a horizontal tube under laminar flow conditions. They conducted the experiment on fully developed region under the constant wall temperature condition. The test fluid they experimented with was Al_2O_3 nanoparticles with diameters of 40 nm dispersed in distilled water with volume concentrations of 0.1–2 vol.%. They found that the heat transfer coefficient of the alumina dispersion increased with increasing Reynolds number. The same trend was observed for increasing particle volume concentration. The heat transfer coefficient

increased by 32% at 2 vol.% compared to that of pure water. The enhancement in heat

transfer coefficient was larger than that of the effective thermal conductivity at the same

volume concentration. From this observation, they commented that the augmentation of

thermal conductivity of nanofluids cannot be the sole reason for heat transfer

enhancement and other factors are also involved in affecting the convective heat transfer

of nanofluids. In their study, the traditional correlation failed to predict the average

Nusselt number of the nanoparticle dispersion in laminar flow. In their study, pressure

drop was significantly high for higher volume concentration (5.7 times for 2% volume at

Re≈360) but very small increase was seen for lower volume concentration fluid.

Wu et al. (2009) performed experimental investigations on the single-phase flow and heat

transfer characteristics through the silicon-based trapezoidal microchannels with a

hydraulic diameter of 194.5 µm using Al_2O_3-H_2O nanoparticle colloidal dispersion with

particle volume fractions of 0, 0.15% and 0.26%. Their investigation examined the

effects of Reynolds number, Prandtl number and nanoparticle concentration on the

pressure drop and convective heat transfer. With the combined use of a microscope and

CCD camera, they also examined the deposition and adhesion behavior of the Al_2O_3

nanoparticles in silicon microchannels. In their study, using the dispersion of low particle

volume fractions ($\phi \leq 0.26\%$) instead of pure water gave rise to an obvious increase in the

convective heat transfer coefficient and the Nusselt number. The Nusselt number of the

suspensions increased with increasing Reynolds number, Prandtl number and

nanoparticle concentration. They observed that Al_2O_3 nanoparticles deposited and

adhered to the inner wall of silicon microchannels more easily with increasing wall

temperature and decreasing flow rate, and once boiling commenced, there was a severe

deposition and adhesion of nanoparticles to the inner wall, which makes the boiling heat transfer of nanoparticle dispersion in silicon microchannels questionable. The pressure drop increased with the increase in the volumetric flow rate for both base fluid and colloidal dispersion. At a certain volumetric flow rate, the pressure drop increased very slightly for nanoparticle dispersion as compared to that of the pure water. The pressure drops of 0.15% and 0.26% volume concentration suspension increased by 3–4.2% and 3.4–5.5%, respectively, as compared to that of the pure water.

Darzi et al. (2012) worked with SiO_2 nanoparticle suspension in water to study the heat transfer and pressure drop performance of its flow through plain and helically corrugated tube. For plain tube, the heat transfer coefficient was higher for nanoparticle suspension than that of water. But increase of volume concentration of nanoparticles (0.5% vol. to 1% vol.) had negligible effect on heat transfer coefficient increase. For corrugated tubes, tube with small corrugation pitch and higher height showed significant heat transfer enhancement for nanoparticles increase. For high pitch of corrugation, this effect was trivial. They explained that higher height and lower pitch of corrugation intensified the mixing flow and reduced the thickness of boundary layer where the ejection of nano-particles from laminar sub layer to main flow enhanced and thus caused the increase in heat transfer increase. The friction factor was higher for nanoparticle suspension and increased with particle volume concentration but decreased with increasing Reynolds number in both type of tubes.

Hojjat et al. (2011a) studied forced convective heat transfer characteristics of γ-Al_2O_3, TiO_2 and CuO nanoparticle dispersion in 0.5 wt.% aqueous solution of carboxymethyl cellulose (CMC). The dispersions were flown inside a uniformly heated circular tube.

The base fluid and all nanoparticle suspensions used in their tested demonstrated non-Newtonian shear thinning behavior. They observed that the heat transfer coefficient for the nanoparticle suspensions was always higher than that of base fluid. At a certain Peclet number, higher volume concentrated suspension obtained higher heat transfer coefficient. As Peclet number kept increasing, the heat transfer coefficient also kept increasing. They observed similar trend while studying Nusselt number of the flow. At a specified Peclet number and axial distance from the tube inlet, the local heat transfer coefficient of nanoparticle suspension boosted with an increase in the nanoparticle concentration. For a certain Peclet number and nanoparticle concentration, the local heat transfer coefficient fell with increasing axial distance. In their opinion, this was due to the increasing boundary layer thickness occurring along the axial distance. They also saw that the entrance region for nanoparticle suspension was longer than that of the base fluid, and the length increased with an increase in nanoparticle concentration. They developed a new correlation based on their experimental result which is

$$Nu = 7.135 \times 10^{-4} Re^{0.9545} Pr^{0.913} (1 + \emptyset^{0.1358}) \tag{2.10}$$

for 2800 < Re < 8400 and 40 < Pr < 73

CHAPTER III

EXPERIMENTAL SETUP AND METHODOLOGY

There have been different reports by different researchers regarding the thermophysical, rheological properties and heat transfer parameters of nanoparticles colloidal suspension. Difference in the method of measurement and data reading may have caused these irregularities. Hence, a proper and organized technique of measuring different parameters of the fluid is essential. The experimental setup and procedure for the present work is divided into the following sections:

1. Preparation of sample fluid

2. Temperature control system

3. Viscosity measurements

4. Thermal conductivity measurement

5. Experimental loop

6. Instrument calibration

7. Experimental procedure

8. Experimental uncertainties

The experimental setup is versatile and can be used to measure different types of fluids other than nanoparticle colloidal suspension.

3.1 Preparation of Nanoparticle Colloidal Suspension

The working fluid used in current experiment is silicon dioxide nanoparticle suspension in distilled water. Silica is a widely used ceramic material which has good abrasion resistance, electrical insulation and high thermal stability. The average diameter for silica particles in the suspension is 20 nanometer (nm). The fraction of silica in the suspension is 20% by mass or 9.58% by volume. A solution of 40% by mass (or 22% by volume) of silica and distilled water is purchased from Alfa Aesar. The densities of the solution and the silica are provided by the manufacturer. This solution is further diluted in the lab to prepare the test fluid of desired concentration with the help of graduated beaker. The prepared sample is observed for 30 days to see if there is any sedimentation or agglomeration of nanoparticles. No sedimentation was observed with normal vision (Figure 3.1).

Figure 3.1: Sample of prepared 20% by mass silica nanoparticle suspension after 30 days of preparation

3.2 Temperature Control System

To measure the rheological and thermal properties of fluid at different operating temperatures, a proper system to maintain a specific temperature is required. This desired temperature is reached with the help of a constant temperature bath from Brookfield Engineering (model TC-550MX). Figure 3.2 shows the equipment. The operating range for this temperature bath is −20°C to 135°C with a temperature stability of 0.07°C. The temperature bath has a reservoir with a volume capacity of 7.0 liters. An opening at the top allows the sample to be submerged into the bath or the fluid can be circulated by a constant speed pump through a tube to other instruments which require a temperature controlled environment.

Figure 3.2: TC 550MX constant temperature bath

3.3 Rheological Property Measurement

A Brookfield viscometer (model DV II+Pro Extra) is used to measure the rheological properties of experimental fluid. The equipment has an accuracy of ±1.0% of the full scale reading. It measures the viscosity and shear stress of the fluid sample at a given shear rate and temperature. The shear rate is applied by submerging a spindle in the fluid and rotating it. The shear rate can be varied by changing the rotational speed of the spindle. The spindle can be set to rotate from 0.01 to 200 RPM, with 0.01 RPM increment from 0.01 to 0.99 RPM, and 0.1 RPM increment from 1 to 200 RPM. The viscous drag force against the spindle is measured by a spring deflection. The spring deflection is measured in terms of torque by a rotary transducer. The full scale torque is 0.0673 mili N.m for the DV II+Pro Extra model. While taking measurements, the measured torque should be between 10–90% of the full scale torque of the calibrated spring to get a good reading. The equipment can be operated either with the help of a panel within itself, or with a computer. The measurement range of the instrument is dependent on the rotational speed, size and shape of the spindle (various spindle come along for measuring various range of viscosity), and the container in which the spindle is rotating. The operating temperature is obtained with the help of a temperature bath (Figure 3.3). The fluid in the temperature bath is circulated through a water jacketing system built around the sample chamber with the help of an Enhanced UL adapter with EZ-lock spindle coupling system. Thus, certain temperature of working fluid is obtained. The viscometer is attached to a PC with a serial USB cable and Rheocalc V3.3 Build 49-1 software is used to operate it and take readings. Readings can be taken manually or by

setting up programs with the help of the software. All the readings from this software can be exported to MS Excel spreadsheet.

Rheological properties measurement method and accuracy of the viscometer are validated by measuring the viscosity of a calibration fluid. This calibration fluid comes along with the viscometer and has a viscosity of 493 cP at 25°C, specified by the manufacturer.

Figure 3.3: DV II+Pro Extra Brookfield viscometer connected to the TC-550MX temperature bath

Following procedures are taken to take accurate readings:

1. It is confirmed that the viscometer is leveled by using a leveling meter at the top of the viscometer and leveling screw at the bottom of it.

2. The viscometer is turned on and external mode is selected to operate it with the help of the Rheocalc software.

3. The torque in the spring is auto zeroed before attaching the spindle to the viscometer. The percentage torque reading between ±0.1 to ±0.2% indicates that auto zeroing is done properly.

4. The desired spindle is attached to the viscometer depending upon the readings to be taken. It is made sure that the spindle is fully immersed in the sample.

5. The temperature bath is set to achieve the desired temperature. Reading is taken 3 minutes after the temperature bath reaches the specified temperature. This ensures the thermal equilibrium between the sample and the bath fluid.

6. Reading is taken at six specified RPM at a certain temperature. RPMs are set in increasing order and then in decreasing order.

7. After taking the readings, the temperature of the bath is increased to next point and the same procedure for taking the readings is followed till the maximum desired temperature is reached.

8. Then the same procedure is followed by decreasing the bath temperature from the highest to the lowest.

3.4 Thermal Conductivity Measurements

The thermal conductivity is measured with the help of a thermal properties analyzer from Decagon Devices (model KD2 Pro) which is presented in Figure 3.4. The equipment has an accuracy of $\pm5\%$ over the range of 0.2 to 2 W/(m.K). Other thermal properties like thermal resistivity, volumetric specific heat capacity and thermal diffusivity can also be measured by the same equipment. Recorded data of the instrument can be downloaded to a PC in spreadsheet form with the help of a serial cable and the KD2 Pro utility software. There are three needle sensors to be inserted in the sample. Selection of sensor depends on the type of sample (liquid or solid). This instrument works on transient heat conduction principle. A small amount of current is supplied through the sensor needle dipped in the sample and the temperature of the sensor needle is monitored over time to

calculate the thermal conductivity. Mathematically, this process of obtaining the thermal conductivity reading can be described by the following equation

$$k = \frac{q}{4\pi} \frac{d\ln(t)}{dT}$$ 3.1

where k is the thermal conductivity in [W.m^{-1}.K^{-1}], q is the applied heat per unit length in [W.m^{-1}], t is the heating time in [s], and dT is the rise in temperature over the heating time in [K].

A small amount of current is supplied so that the heat input is small and thus ensuring minimal sample movement from the sensor and free convection. The KD2 Pro is capable of resolving 0.001°C temperature so the small amount of heat added does not significantly affect the result.
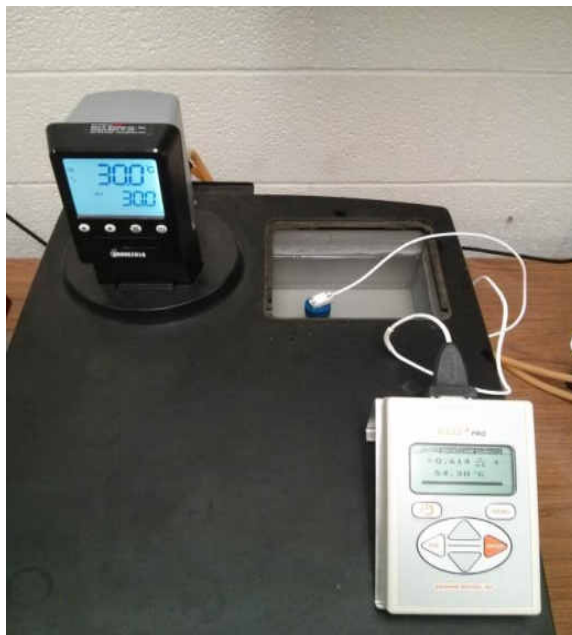
Figure 3.4: Measuring thermal conductivity using KD2 Pro Thermal Property Analyzer. Temperature bath is used to maintain specific temperature

Extra care should be taken to minimize errors in result. Convection or bulk movement of the measuring samples can cause error. The sample should be in thermal equilibrium to avoid thermal gradient in the sample. Otherwise, free convection will occur. The sensor and the sample must stand still to minimize error from forced convection. Readings must be taken during the night time or the weekends so that any vibration from the HVAC system of the room or building does not hamper the results. Other equipment in the lab should be shut down before taking the thermal conductivity reading as they can also be a source of vibration. For accurate readings, the sensor needle should be inserted into the sample as vertically as possible.

Before taking any readings, the accuracy of KD2 Pro and the experimental method should be validated. This is done by calibration against a manufacturer provided standard liquid whose thermal conductivity is 0.285 W/(m.K) at 20°C.

The followings are the procedures to take thermal conductivity reading:

1. 40 ml of the liquid sample is taken in a septum vial. It is ensured that the vial is completely filled and there is no air bubble. The sensor needle is then inserted into the vial through a cap. The sensor needle should not touch the walls of the vial and should line up as close as possible with the axis of the vial. A fixture is used to hold the needle vertically.

2. The vial along with the needle is placed into the temperature bath.

3. The temperature bath is set to a specified temperature at which the reading is to be taken. Once the bath temperature reaches the specified temperature, it is kept running for another 15 minutes to ensure no thermal gradients in the sample.

4. After that, the temperature bath is turned off and 1 minute is allowed for everything to come to a tranquil state before taking a reading to avoid vibration.

5. Then reading is taken. Fifteen minutes should be allowed between two consecutive readings for accuracy.

6. The temperature is increased by 5°C until it reaches highest value and same procedure is followed to take readings at each temperature point.

3.5 Experimental Loop

The experimental loop is a closed loop system which consists of 1) reservoir, 2) gear pump, 3) mass flow meter, 4) pressure transducers, 5) data acquisition unit, 6) thermocouples, 7) DC power supply unit and 8) heat exchangers which are all connected by a pipe network (Figure 3.5). The piping network comprises a ¼ inch stainless steel tubing and flexible PVC tubing. The flexible tubing is integrated in this experimental loop for housing different lengths of the test section. This flow loop can enable experiments for fluids flowing through tubes ranging from 6 mm to 500 μm ID.

A reservoir is used to contain the working fluid. The fluid is then pumped to the flow loop by a gear pump. A counter flow heat exchanger is used just after the gear pump to remove heat added to the fluid by the pump. The mass flow rate in the loop is adjusted by a metering valve. A Coriolis mass flow meter is used to measure the mass flow rate. Pressure transducers, connected at the inlet and the outlet of the test section, measure the pressure drop. The heating of the test section is done by a DC power supply. Thermocouples are attached along the test section for heat transfer analysis. A second heat exchanger right after the test section is used to remove any heat gained by the fluid while passing through the heated test section. The pressure transducer, DC power supply

and the mass flow meter are all connected to the data acquisition system. This system is used to gather, record and analyze data. The fluid goes back to the reservoir after passing through the test section.
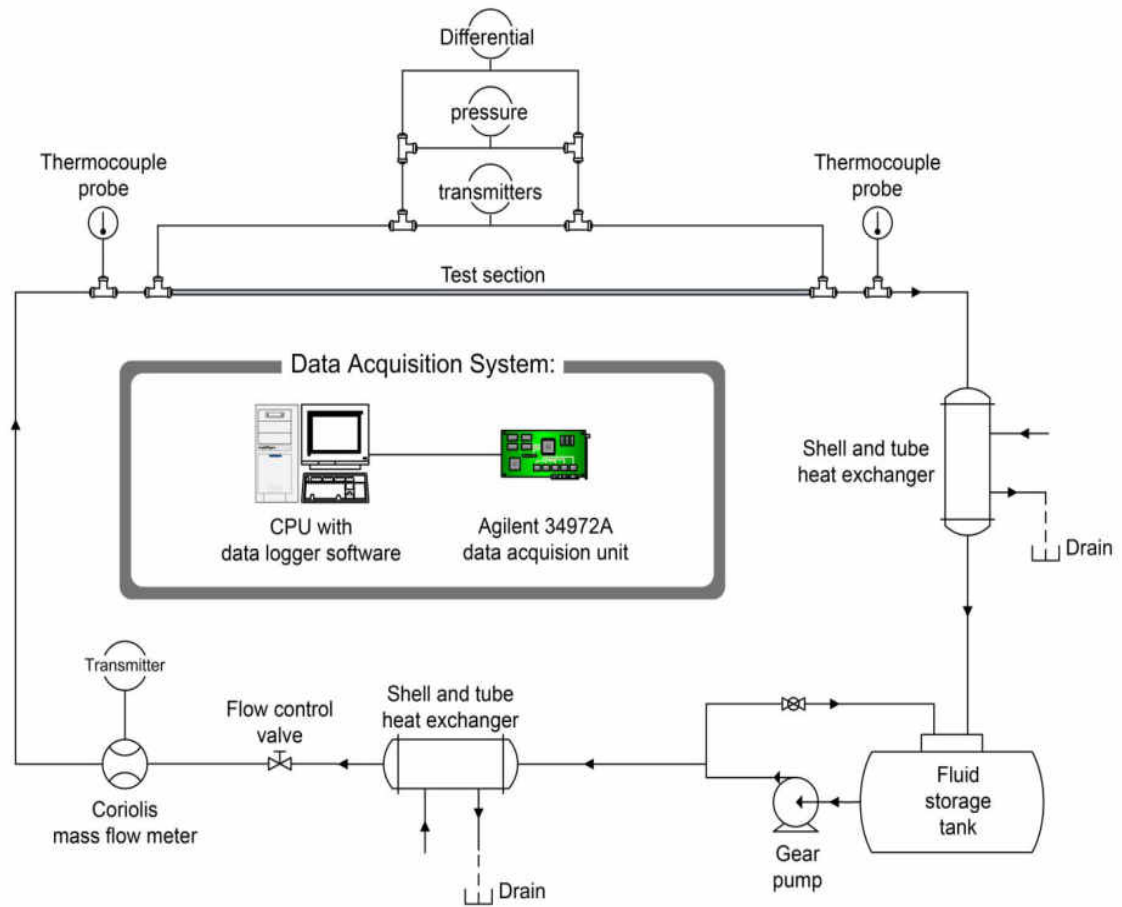
Figure 3.5: Schematic of experimental loop for conducting pressure drop and heat transfer measurements, Tiwari (2012)

3.5.1 Reservoir

The reservoir is shown in Figure 3.6. It is a cylindrical tank made of PVC with diameter of 0.25 m, length of 0.3048 m and a capacity of 15 liters. The reservoir is placed above the gear pump maintaining 1m vertical distance so that the gear pump can have adequate pressure to avoid running dry. The reservoir is connected to the gear pump through a pipe at its bottom. At the top, it is connected to a bypass line and the loop line.

Figure 3.6: Flow loop reservoir

3.5.2 Gear Pump

A Liquiflow sealed gear pump (model 35 F) is used for the experiment (Figure 3.7). It can sustain a maximum flow of 12.8 LPM and maximum pressure difference of 6.9 bar. This pump can be operated at variable speeds with maximum rated speed of 1750 RPM. The suction side of the pump is linked to the reservoir and the discharge side to a T-connector which divides the flow through the closed loop and a bypass.

Figure 3.7: Liquiflow sealed gear pump

3.5.3 Mass Flow Meter

The mass flow meter used in the experiment is a Micro Motion mass flow sensor (model CMFS010M). It is connected to a 1700R model transmitter (Figure 3.8). It has an accuracy of ±0.05% of the flow rate. It can measure a maximum flow rate of 108 kg/hr. The operation of the mass flow meter is based on the principle of the Coriolis effect. The fluid passes through a U-shaped tube in the mass flow sensor which initially vibrates at a given frequency. When the fluid flows through the U- shaped tube, its angular velocity and inertia causes the tube to twist. The twisting of the two legs of the U-shaped tube is detected by an electromagnetic sensor in terms of a phase change. This phase change is calibrated to be measured in terms of mass flow. A metering or needle valve controls the flow going through the mass flow meter. A DC current signal, calibrated linearly in terms of flow rate, is given by the transmitter.

Figure 3.8: Micro Motion mass flow sensor connected to a 1700R transmitter.

3.5.4 Pressure Transducers

Three Rosemount pressure transmitters (model 3051) with accuracy of +0.65% of span

are connected to the inlet and outlet of the test section (see Figure 3.9). The three pressure

transducers have different pressure ranges. One of the transducers can measure a pressure

drop from 0 to 9 psi, the other one from 0 to 36 psi and the last one from 0 to 300 psi. All

of them are attached in parallel connection to read the same pressure drop for a given

flow rate and obtain more accurate reading. The pressure transmitter gives output in DC

current which is calibrated linearly in terms of pressure drop. If a pressure drop reading

exceeds the maximum range for a given transducer, the data acquisition unit is

programmed to generate an alarm. If an alarm goes up, a valve on the pressure transmitter

itself isolates that particular transmitter.
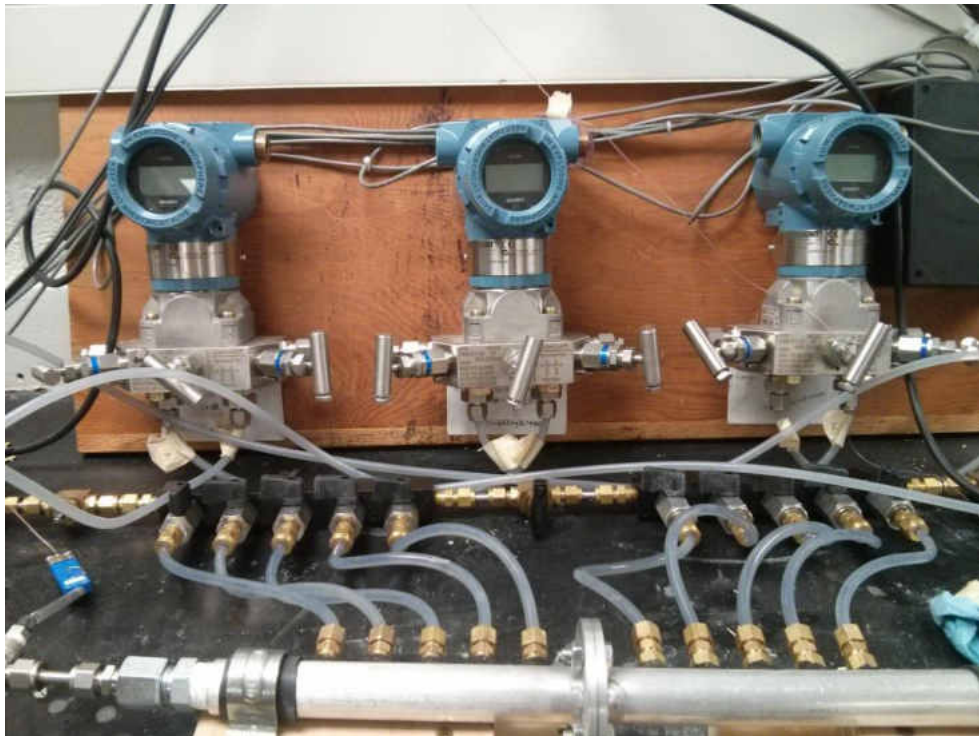
Figure 3.9: Three Rosemount pressure transmitters (model 3051) connected in parallel.

3.5.5 Data Acquisition Unit

An Agilent data acquisition unit (model 34972A) with 20 channel multiplexer (Figure 3.10) is used for the experiment. All the thermocouples, mass flow meter, pressure transducers are connected to the channels of multiplexer. Based on the type of thermocouple, temperature can be sensed by the data acquisition unit. The pressure transducers and the mass flow meter produce their output in DC current. This DC output can be sensed and programmed linearly to give the readings in psi and gm/sec, respectively.

The data acquisition unit is connected to the PC through a USB cable to obtain readings. For programming the channels, setting the reading time and capturing data, Agilent Benchlink Data Logger 3 is used. During the experiment, a read time of 0.1sec is used.

Figure 3.10: Agilent data acquisition unit (model 34972A).

3.5.6 Thermocouples

Two different types of thermocouple are used in the experiment. T-type thermocouple from Omega (model no. TMQSS-020U-6) is used to measure the bulk fluid temperature at the inlet and outlet of the test section. This thermocouple has 0.020 inches sheath diameter and 6 inches length. With the help of a Tee and a reducing compression fitting from Omega (part no. SSLK-116-18, 1/16*1/8), the thermocouple tip is inserted into the middle of the flow path of the fluid. The thermocouple is then connected to the data acquisition unit to record the temperature.

The other type of thermocouple is made from a 36 AWG thermocouple wire from Omega (model TT-T-36-SLE-1000). With the help of a thermocouple welder, the two wire tips are welded to form a thermocouple tip. The tip is made as small as possible. The tips are then connected along the test section (Figure 3.11). A high temperature and thermally conductive epoxy from Omega (part no. 08-101-16) is used to make these connections. Though the epoxy is highly thermally conductive, but it acts as an insulator for DC current. This ensures thermocouple protection and enables accurate temperature readings.
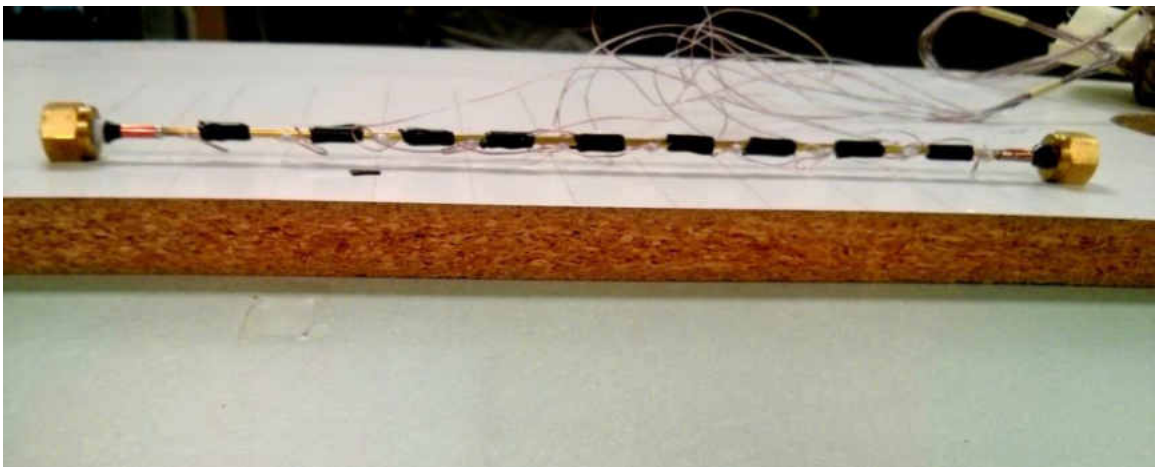
Figure 3.11: Thermocouple wire tip cemented to the test section outer wall with the help of Omega bond cement.

3.5.7 DC Power Supply

To provide the power required for the experiment, an N5761A DC power supply from Agilent Technologies (Figure 3.12) is used. It can provide an output up to 6 V / 180 A, 1080W. The power supply unit can measure data with an accuracy of ±300mA for current and ±6mV for voltage. The output from the DC power supply and the test section is connected through a copper strip soldered to the test section. The DC power supply is accommodated with a remote load sense circuit which is connected to the same copper strip. It enables the DC power supply to compensate for the voltage drop in the wires between the test section and the DC power supply itself.

Figure 3.12: N5761A Agilent DC power supply unit.

3.5.7 Test Section

Three tubes with different dimension are used as the test section. These tubes are made of brass 260. The first one has an outer diameter of 0.125 inch and inner diameter of 0.097 inch. For the second one, the outer diameter and inner diameter are 0.09375 inch and 0.06575 inch respectively. The third tube is 0.0625 inch in outer diameter and 0.0345 inch in inner diameter. All three tubes are 12 inch long and have a wall thickness of 0.014 inch. Teflon (PTFE) bushings keep the test sections connected to the test loop. The advantage of using the PTFE bushings is they act as a reducing fitting and as a sealing

between the experimental loop and the test section. Ten thermocouple wires are connected to each test sections. They are placed along a single axial line on the outside of the tube wall. The spacing for the thermocouples is same for all three test sections (Figure 3.13). With the help of copper strips, the DC power supply is connected to the test section.
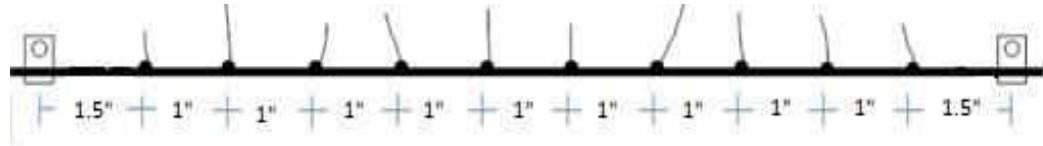
Figure 3.13: Schematic diagram of the test section connected with thermocouples and copper strips

3.5.8 Heat Exchangers

In the experimental loop, a ¼ inch tubing is attached to two counter flow heat exchangers coaxially. One heat exchanger serves the purpose of removing the heat added from the pump to the fluid and maintaining a steady inlet temperature to the test section. This heat exchanger is placed just after the gear pump. Another heat exchanger, placed just after the test section, takes away the heat added to the fluid during heating of the test section for heat transfer experiments.

The heat exchangers are ½ inch in diameter and 38 inches in length. The heat exchangers are fitted through a ½ inch Tee connection and a bore through fitting of ½ inch thread at one end and a ¼ inch compression fitting at the other end. The Tee is connected at the threaded end while a seal is kept between the compression fitting and the ½ inch tubing and the ¼ inch tubing. Cold water is supplied by a ½ inch PVC tubing connected at the other free end.

3.6 Instrument Calibration

It is necessary to calibrate experimental equipment to check their accuracy and reliability before running experiment. The procedures and results of calibration for thermal property analyzer, viscometer and pressure transducer are discussed below.

3.6.1 KD2 Pro Thermal Property Analyzer Calibration

A standard calibration fluid, provided by the manufacturer, is used to calibrate the KD2 Pro to test the accuracy of the experimental setup and procedure. The calibration fluid has a thermal conductivity of 0.285 $W.m^{-1}.K^{-1}$ ±5% at 20°C. This value is given by the manufacturer. The measurements are taken at 20°C. The method of taking reading is the same as described in section 3.4. The comparison between the measured values and the standard value is presented in Figure 3.14.

As mentioned earlier, the temperature bath has a stability of 0.07°C. Repeatable values of thermal conductivity with a standard deviation of 0.003 $W.m^{-1}.K^{-1}$ is observed within the temperature limit. The average value of thermal conductivity deviates by −1.05% from the standard value. This deviation falls well within the uncertainty limit of the equipment.
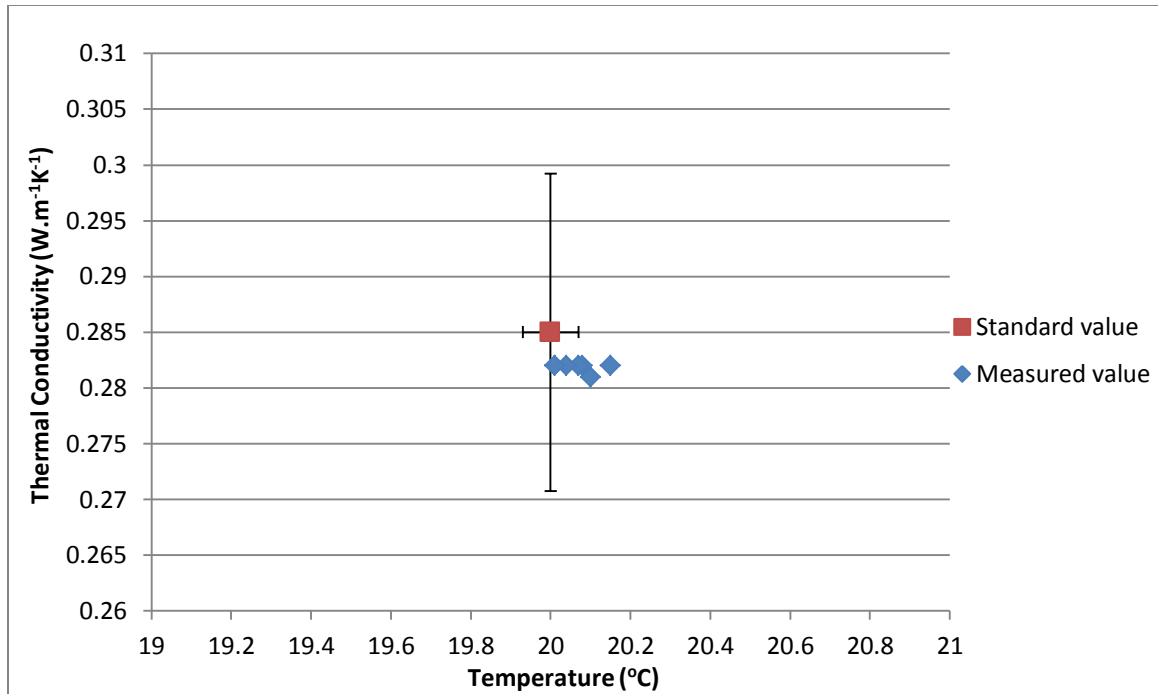
Figure 3.14: Thermal conductivity measurement for a standard calibration fluid at a temperature of 20°C. The error bar represents ±5% in y-axis and ±0.07°C in x-axis.

3.6.2 Pressure Transmitters Calibration

A pneumatic hand pump from Ametek (model T-970, range 0 to 580 psi) and two digital electronic gages from Dwyer (model DPG-107, range 0–300 psi and model DPG-104, range 0–50 psi) are used for the purpose of pressure transducers calibration. A certain amount of pressure is applied by the hand pump and the output voltage from the transducers is recorded. The following procedure is maintained to calibrate the pressure transducers:

1. The digital pressure gauge is connected to the hand pump. Then the hand pump is connected to the high pressure side of the pressure transmitter.

2. Certain amount of pressure is applied by pumping the hand pump. After waiting for 2 minutes, if the pressure reduces, the connections are checked for leak using soapy solution.

3. After checking leak and amending it (if there is any leak), the voltage output corresponding to the pressure is recorded.

4. The applied pressure is then increased and the voltage is recorded.

5. Step 1-4 is repeated until the highest range of the pressure transmitter has been reached.

Calibration results for the three pressure transmitters are presented in Figures 3.16−3.18. A linear curve fitting trend line with respective R^2 value and equation of the graph are also shown in each of the graphs. In the data acquisition unit, this equation is set as a gain ($Mx + B$) to read the output directly with respect to pressure drop.

Figure 3.15: Ametek hand pump attached to Dwyer digital gage
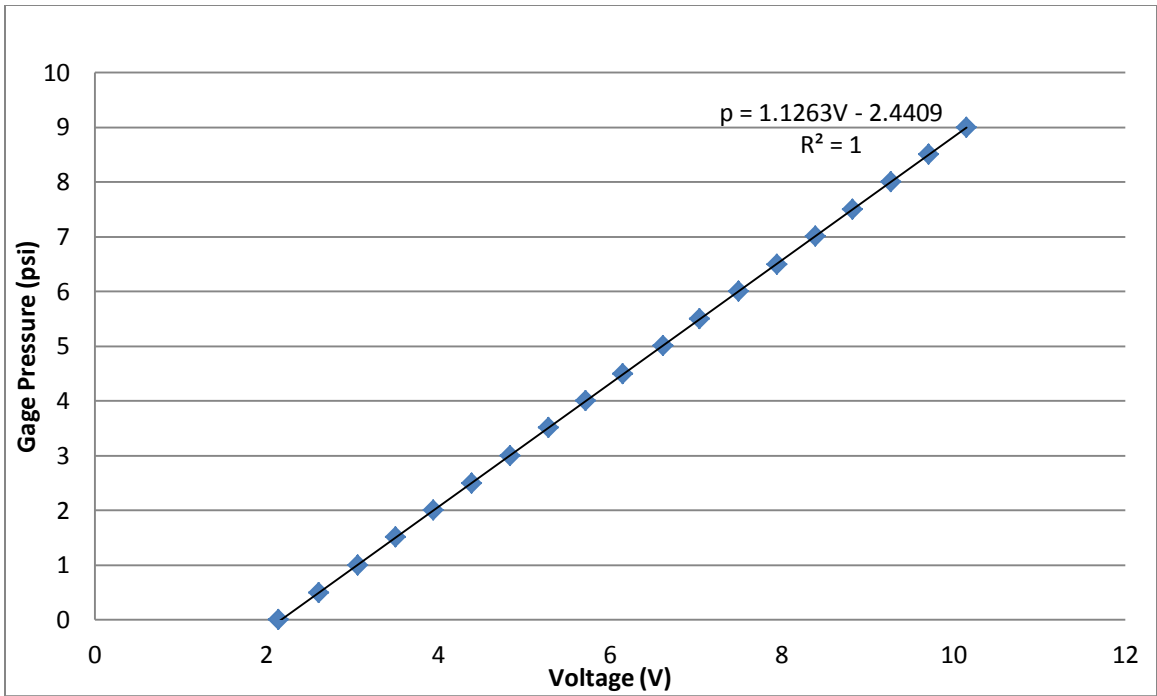
Figure 3.16: Calibration graph for 0–9 psi pressure transmitter
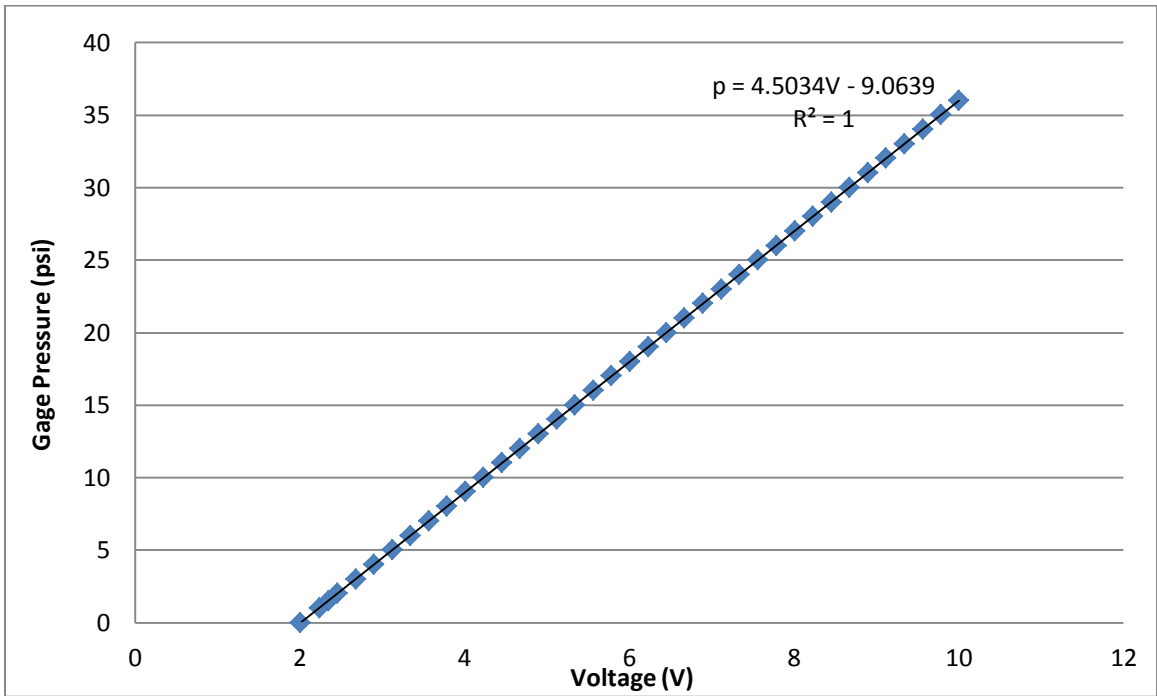
Figure 3.17: Calibration graph for 0–36 psi pressure transmitter
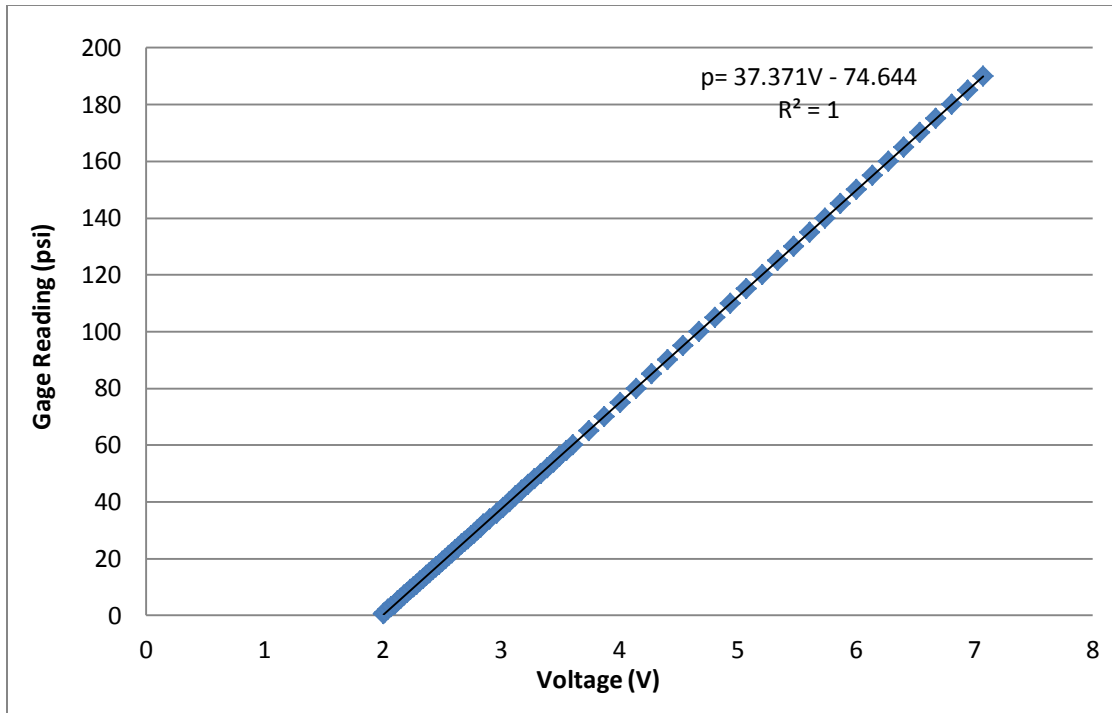
Figure 3.18: Calibration graph for 0–300 psi pressure transmitter

3.6.3 Viscometer Calibration

The Brookfield viscometer is calibrated with respect to the viscosity of a standard calibration fluid that comes with the equipment. The standard fluid has a viscosity of 493 cP at 25°C and the equipment has an accuracy of ±1%. So, viscosity value within 488 cP to 498 cP at 25°C is expected to occur. For calibration measurement, the procedure followed is outlined in Section 3.3. Figure 3.19 shows the results of the calibration. The cooling curve and the heating curve have almost the same path. The viscosity at 25°C is found to be 497.4 cP and 495.9 cP for heating and cooling respectively which fall within the accuracy limit.
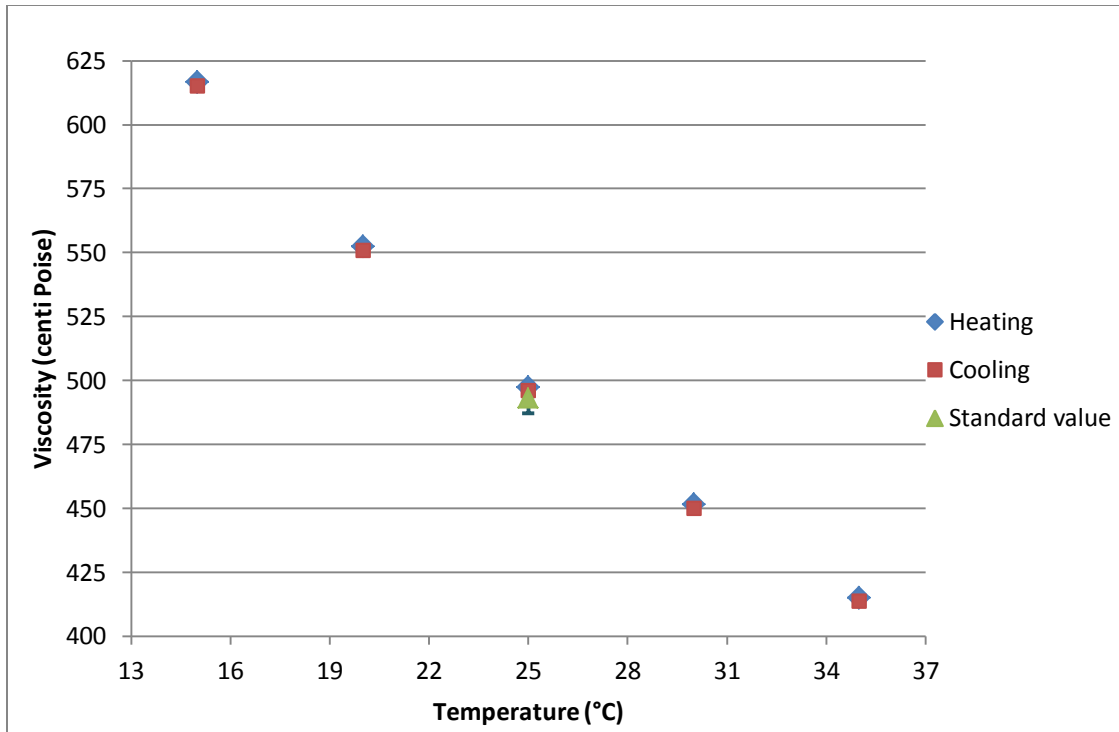
Figure 3.19: Viscosity vs. temperature curve for the given standard viscosity fluid. The fluid has a viscosity of 493 cP at 25°C

3.6.4 Thermocouples Calibration

Thermocouples are calibrated by measuring the temperature of ice bath. All the thermocouples are dipped inside an ice bath. Then the temperature readings are taken using the data acquisition unit. All thermocouples give a reading within ±0.3°C range of 0°C.

3.7 Experimental Procedure

3.7.1 Pressure Drop Measurement

1. The pump, mass flow meter, data acquisition unit and the pressure transducers are started first.

2. The pump speed is set to match the desired flow rate and Reynolds number.

3. It is made sure that the bypass valve is open to limit the strain in the pump.

4. Cold tap water is supplied to the heat exchangers.

5. The metering valve on the mass flow meter is adjusted to fine tune the flow rate.

6. Five minute is allowed for the system to reach steady state. When same continuous readings are obtained from the unit, it is understood that steady state has been reached.

7. The outputs from the mass flow meter, pressure transducers and bulk temperature measuring thermocouples are recorded for 5 minutes.

8. The flow rate is increased to next desired point by fine tuning the metering valve or increasing the speed of the pump and step 1-7 are repeated to take another data point.

3.7.2 Heat Transfer Measurements

1. The test section is well insulated before running any heat transfer experiment.

2. The pump, mass flow meter, data acquisition unit and the pressure transducers are turned on.

3. It is made sure that the bypass valve is open to limit the strain in the pump.

4. Cold tap water is supplied to the heat exchangers.

5. The metering valve on the mass flow meter is adjusted to fine tune the flow rate.

6. The DC power supply is then turned on and desired electricity is supplied to the test section to heat it up.

7. The system is allowed to reach steady state.

8. After reaching steady state, the outputs from the mass flow meter, pressure transducers, DC power supply, thermocouples along the test section and the bulk temperature measuring thermocouples are recorded for 6 minute.

9. The flow rate is increased to next desired point by fine tuning the metering valve or increasing the speed of the pump and step 1-8 are repeated to take another data point.

10. The process is repeated until either maximum flow rate has been achieved or the bulk fluid temperature difference between the inlet and the outlet becomes less than $2.5^{\circ}C$.

11. After finishing experiment, it is made sure that the DC power supply is turned off first and then the pump. Turning off the pump first might cause excessive temperature in the test section resulting in the damage of the thermocouples and the test section. For nanoparticle suspension, excessive heat may cause dry out and clog up the test section.

3.8 Experimental Uncertainties

3.8.1 Friction Factor

The friction factor is calculated from the Darcy-Weisbach equation which is expressed as

$$f = \frac{2\Delta P D_i}{\rho L V^2} \tag{3.2}$$

The velocity, V, can be computed as

$$V = \frac{\dot{m}}{\rho A_i} \tag{3.3}$$

The cross-sectional area for the flow is given by

$$A_i = \frac{\pi D_i^2}{4} \tag{3.4}$$

Putting the value of A in Eq. 3.3, the velocity can be written as,

$$V = \frac{4\dot{m}}{\rho \pi D_i^2} \tag{3.5}$$

From Eq. 3.2 and 3.5,

$$f = \frac{\Delta P D_i^5 \rho \pi^2}{8 L \dot{m}^2} \tag{3.6}$$

From Eq. 3.6, it can be deduced that the friction factor depends upon 1) pressure drop, 2) inside diameter of the tube, 3) density of the fluid flowing through the tube, 4) length of the tube, and 5) mass flow rate of the fluid.

The uncertainty in the measurement of the pressure drop, mass flow rate and the length of the tube can be controlled by monitoring the procedure of taking the data. But uncertainty in the tube diameter depends on the manufacturer's accuracy and methods.

The pressure transmitter measurement accuracy is specified to be ±0.65% of span by the manufacturer. While taking readings, extra care is taken so that the process reaches steady state and all the three transducers read the same pressure drop. However, for water

at low Reynolds number and higher tube diameter, the uncertainty in the measurement of pressure drop seems to be high which is indicated by slight reading variation of the three pressure transmitters. But, while using silica colloidal suspension as test fluid, the situation seems to be better. In such case, the readings from the lower range pressure transmitter are used for data analysis.

The uncertainty with the inside diameter of the test section is a key factor that affects the measurement of friction factor. From Equation 3.6, it is clear that the friction factor is proportional to the fifth power of the inside diameter. The manufacturer provides a tolerance of ± 0.001 inches for the inside diameter of thetube.

The mass flow meter has an accuracy of $\pm 0.05\%$ of the flow rate. Here also, steady state process is attained with extra attention.

The uncertainty in the measurement of tube length is determined by the accuracy of the measurement scale used. Measurements are taken repeatedly to avoid error as much as possible. The uncertainty for the length of the tube is found to be ± 0.25 inches.

The nanofluid density is taken as 1.15 gm/cc. The operating range of the experiment is from 7°C to 60°C. The particle density is assumed to be constant over this range whereas the density of water may change slightly. The maximum uncertainty in density is calculated as $\pm 1.77\%$.

The maximum uncertainty in the measurement of the friction factor is calculated to be $\pm 12.88\%$, as shown in Table 3.1.

Table 3.1: Uncertainty in friction factor

Uncertainty in pressure drop	Uncertainty in inside diameter	Uncertainty in length	Uncertainty in mass flow rate	Uncertainty in density	Maximum Uncertainty in friction factor measurement
0.65%	1.60%	1.66%	0.05%	1.77%	10.87%

3.8.2 Heat Transfer

The heat transfer is presented in terms of the Nusselt number. Equation for the Nusselt number is

$$Nu = \frac{hD_i}{k} \qquad (3.7)$$

where Nu is the Nusselt number, h is the convective heat transfer coefficient in $[W.m^{-2}.K^{1}]$, D_i is the tube inside diameter in $[m]$, and k is the thermal conductivity in $[W.m^{-1}.K^{-1}]$.

The convective heat transfer coefficient is given as

$$h = \frac{q}{T_{w,i} - T_b} \qquad (3.8)$$

where q is the heat flux per unit area and can be expressed as

$$q = \frac{dQ}{\pi D_i dx} \qquad (3.9)$$

where Q is the total heat input to the test section and x is the axial distance along the heated section.

The inside wall temperature, $T_{w,i}$, is calculated from following equation

$$T_{w,i} = T_{w,o} - \frac{qD_ix}{2k_bL} \ln\left(\frac{D_o}{D_i}\right) \tag{3.10}$$

where L is the length of the tube, D_o is the outside diameter, D_i is the inside diameter of the test section, and k_b is the thermal conductivity of the tube wall. For Brass 260, the thermal conductivity value is 120 W.m^{-1}.k^{-1} at 20°C. This value is provided by the manufacturer. The effect of change in thermal conductivity of brass on the inside wall temperature is negligible. So, this value is considered constant for the whole temperature range.

A linear variation of the bulk fluid temperature from the inlet of the test section to the outlet is assumed and for any axial distance along the test section, it is given as

$$T_{b,x} = T_{b,in} + \frac{x}{L}(T_{b,out} - T_{b,in}) \tag{3.11}$$

where $T_{b,in}$ is the inlet fluid bulk temperature in [°C] and $T_{b,out}$ is the outlet fluid bulk temperature in [°C].

Therefore in final form, the Nusselt number can be written as,

$$Nu = \frac{IV}{\pi D_i x \left[T_{wo} - T_{bin} + \frac{x}{L}(T_{bout} - T_{bin}) - \frac{IV}{2\pi k_b L} \ln\left(\frac{D_o}{D_i}\right)\right]} \frac{D_i}{k} \tag{3.12}$$

Eq. 3.12 implies that the Nusselt number is a function of 1) thermal conductivity of the fluid, 2) bulk fluid inlet and outlet temperatures, 3) tube outer wall temperature, 4) length of the heated section, 5) distance of each axial location from inlet, 6) thermal conductivity of the tube, 7) tube inside diameter, 8) tube outside diameter, 9) current supplied by the DC power supply, and 10) Voltage supplied by the DC power supply.

The uncertainty in measurement by the thermocouple is found to be ±0.31°C. The thermal conductivity value of the fluid can have an error of ±5% for the range 0.2−2 W/m.K.

Uncertainty in heat loss is measured by applying energy balance equation to the system. The difference between the heat supplied to the system and the heat absorbed by the fluid is the heat lost to or taken from surroundings. The heat supplied to the system can be written as,

$$Q = IV \tag{3.13}$$

The heat carried away by the fluid is,

$$Q_a = \dot{m}c_p\Delta T \tag{3.14}$$

If Q_l is the amount of heat loss, then from energy balance equation,

$$IV = \dot{m}c_p\Delta T \pm Q_l \tag{3.15}$$

For both water and silica suspension flow through all the test sections, Equation 3.15 is applied to different mass flow rates. The highest amount of heat loss is observed as 3.6%. The average heat loss is 0.93%. Of all the data point that is analyzed, 95% provides a heat loss less than 2%.

Using these uncertainties, the uncertainty in the measurement of Nusselt number is 12% (Table 3.2).

Table 3.2: Uncertainty in measurement of Nu_d.

Uncertainty in measurement of h	Uncertainty in measurement of q	Uncertainty in measurement of T_b	Uncertainty in measurement of T_{wi}	Uncertainty in measurement of k	Uncertainty in measurement of Nu_d
5.50%	3.40%	1.03%	0.54%	5.00%	12.00%

CHAPTER IV

RESULTS AND DISCUSSION

The experimental findings and their comparison with results from different researchers are discussed in this chapter. For most of the experiments, the experimental setup and procedure are validated by checking experimental data of distilled water.

4.1 Results for Experimental Setup Validation Using Water

Before conducting experiments with nanoparticle colloidal suspension, experiments are conducted with distilled water using the same setup to see if the results matched with existing theory. This also helps to predict the accuracy of the flow loop and different instruments connected to it.

4.1.1 Thermal Conductivity Measurements of Water

With the exact procedure outlined in Section 3.4, the thermal conductivity of water is measured. Figure 4.1 represents the plot between the thermal conductivity and temperature for water. Standard value of thermal conductivity of water is taken from the textbook of Kays et al. (2004). The experimental value lies well within the ±5% range of the standard value.
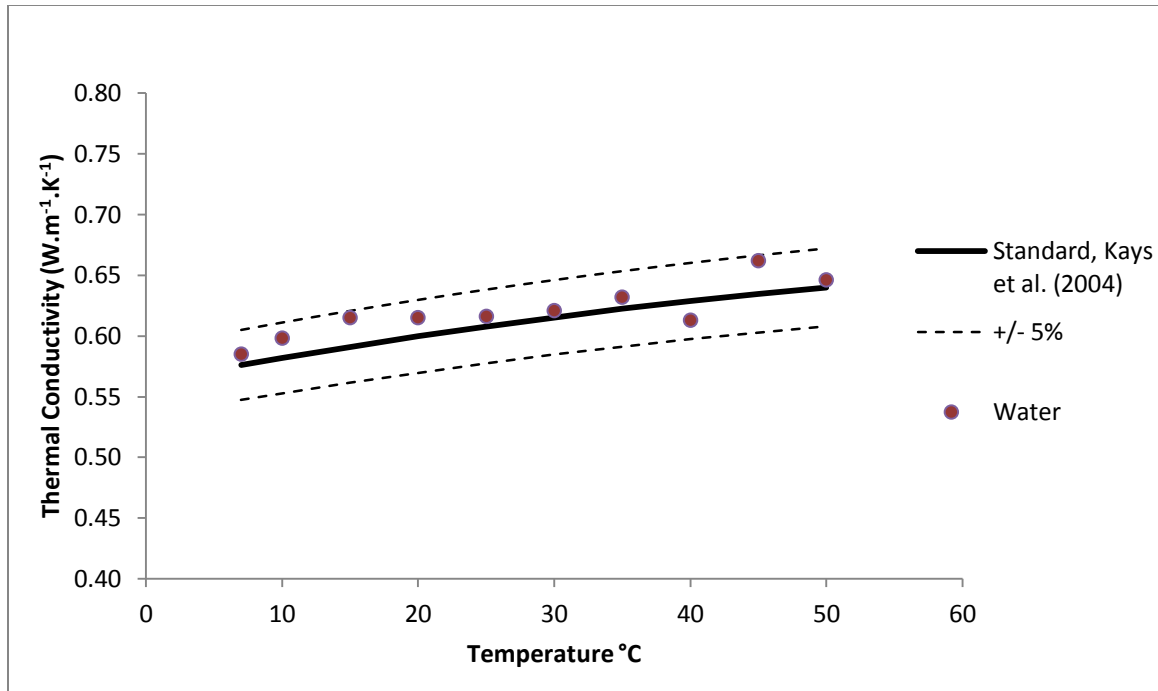
Figure 4.1: Comparison between the experimental value and the standard value, Kays et al. (2004), of thermal conductivity for distilled water

The thermal conductivity of water is measured from 7°C to 50°C. Measurements are not taken above 50°C as the accuracy of the equipment is not reliable above this temperature without special arrangement. At high temperature, free convection is induced in the system. Liquid with a higher viscosity will dampen out the disturbances and the readings will be more accurate. But, due to the lower viscosity of water, readings are not stable and do not represent a true value for the thermal conductivity. Within the measured temperature range, the conformity between the standard value and experimental value of thermal conductivity implies that the procedure of taking the thermal conductivity measurement is accurate and reliable. So, the exact procedure is followed to obtain the thermal conductivity of nanoparticle suspension.

4.1.2 Pressure Drop Measurements of Water

The friction factor can be calculated from the Darcy-Weisbach equation given as

$$f = \frac{\Delta P D_i^5 \rho \pi^2}{8 L \dot{m}^2} \tag{4.1}$$

The values of friction factor are plotted against the Reynolds number and laminar,

transition and turbulence regions are observed. Reynolds number is given by

$$Re = \frac{\rho V D}{\mu} \tag{4.2}$$

Three tubes of outer diameter 1/8 inch, 3/32 inch and 1/16 inch with the same length of

12 inch are taken as the test section.
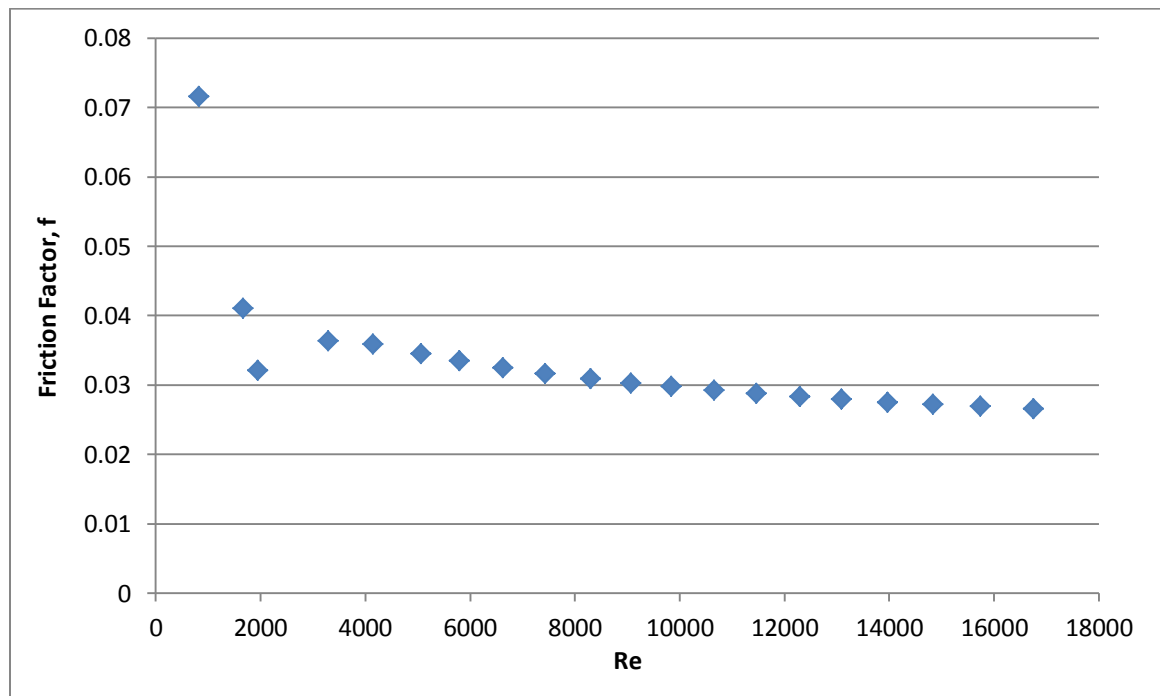
Figure 4.2: Friction factor vs. Reynolds no. for flow of water inside 0.125 inch OD tube
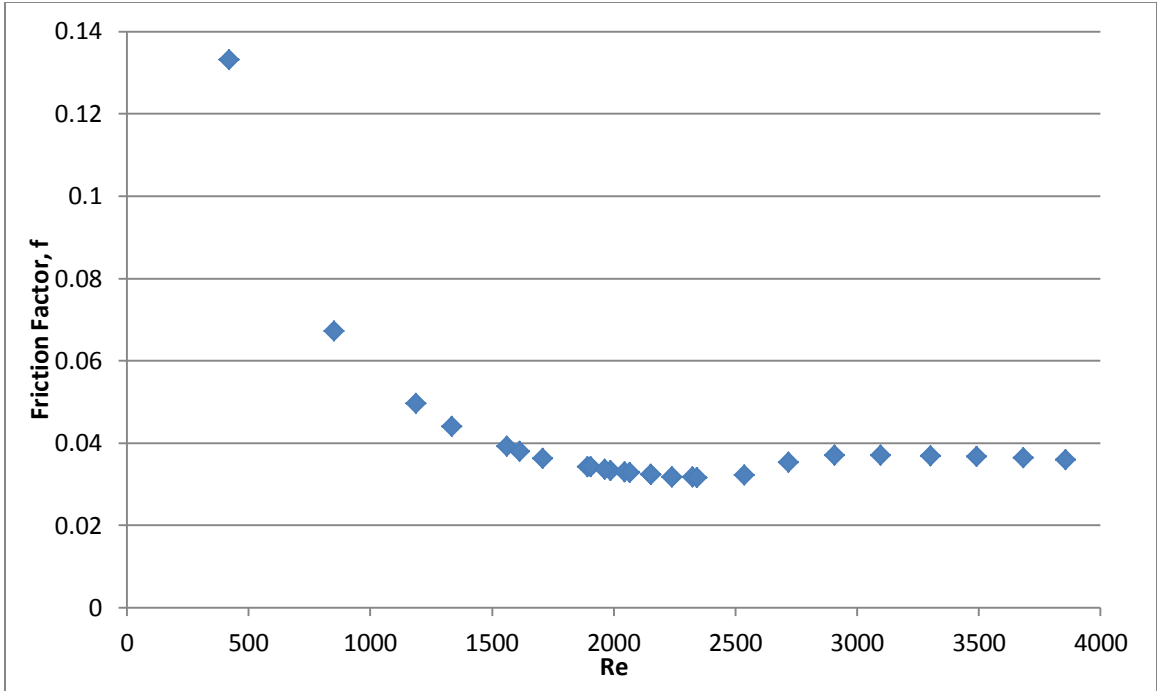
Figure 4.3: Friction factor vs. Reynolds no. for flow of water inside 0.09375 inch OD tube
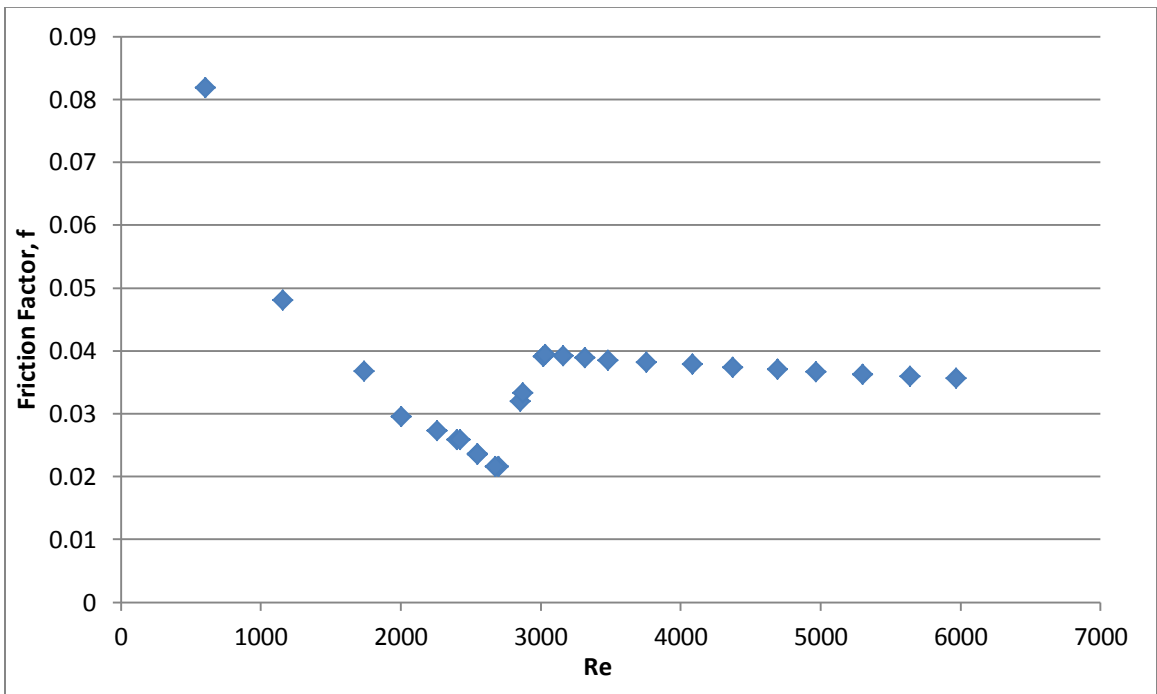
Figure 4.4: Friction factor vs. Reynolds no. for flow of water inside 0.0625 inch OD tube

From Figures 4.2, 4.3 and 4.4, it can be seen that the transition starts around Reynolds number of 1950 for 0.125 inch OD tube, Reynolds number of 2400 for 0.09375 inch OD tube and Reynolds number of 2700 for 0.0625 inch OD tube.

For laminar fully developed flow, friction factor can be determined by the following equation

$$f = \frac{64}{Re} \tag{4.3}$$

Or, in other words, the product of friction factor and Reynolds number is 64. This number 64, is called Poiseuille number.

Hydrodynamic entry length is determined from

$$L_{h,laminar} = 0.05 \text{ Re D} \tag{4.3}$$

For all three test sections, flow is hydrodynamically developed at all Reynolds number.
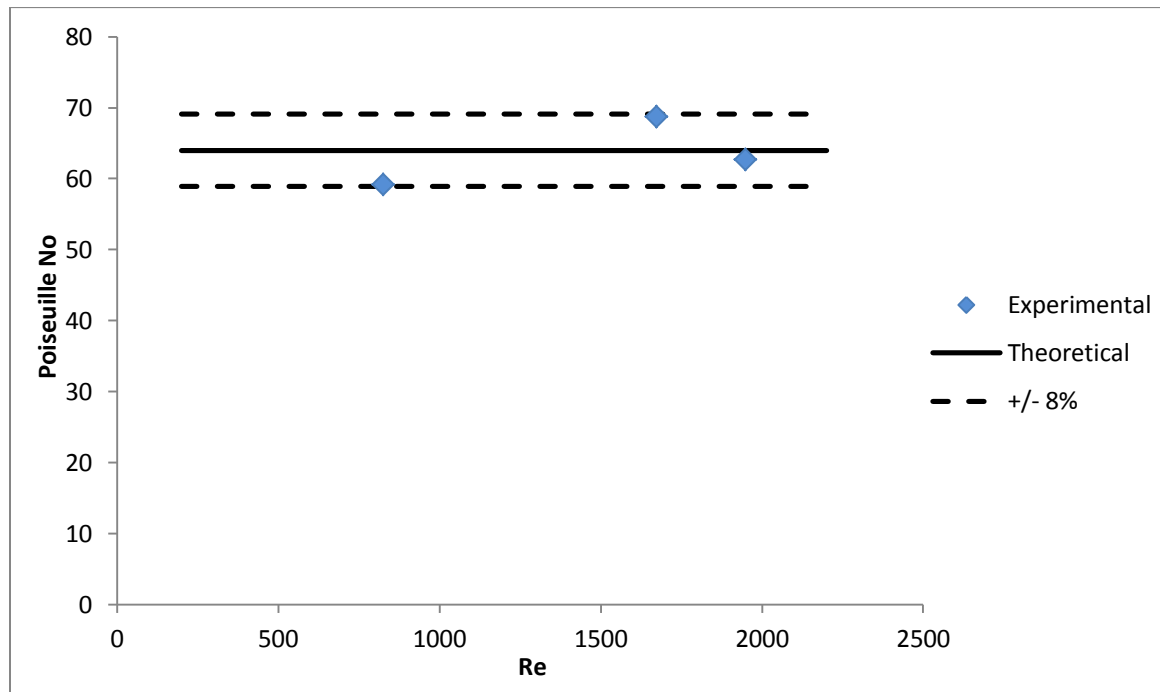
Figure 4.5: Poiseuille no. vs. Reynolds no. for flow of water inside 0.125 inch OD tube
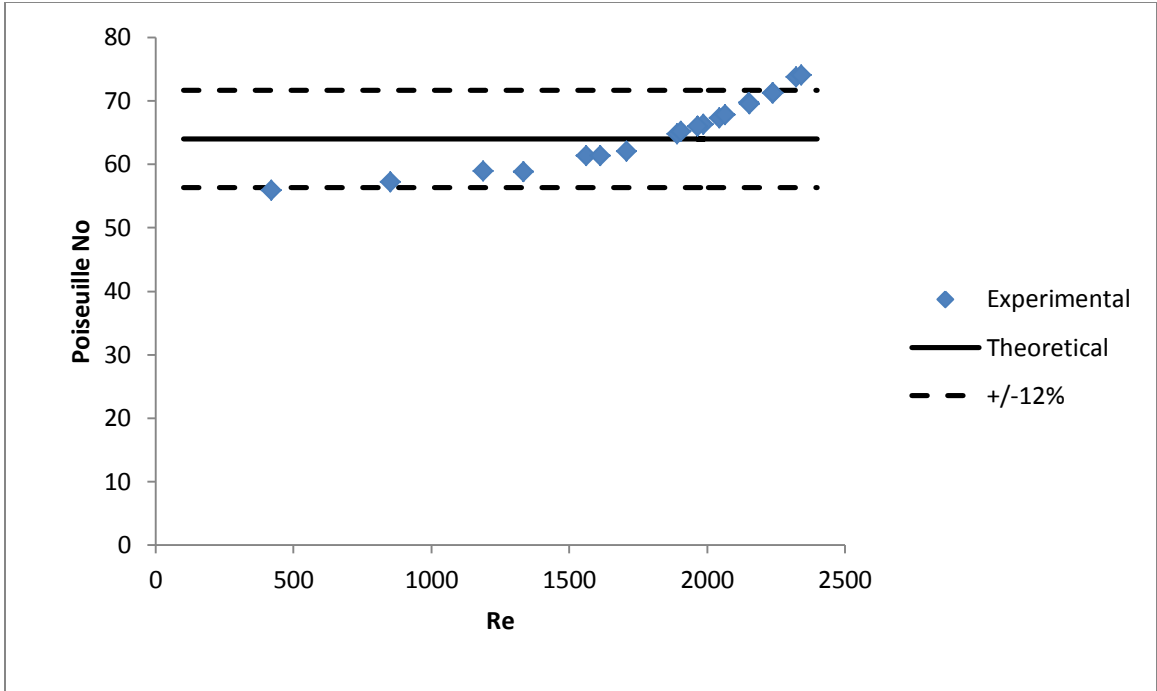
Figure 4.6: Poiseuille no. vs. Reynolds no. for flow of water inside 0.09375 inch OD tube
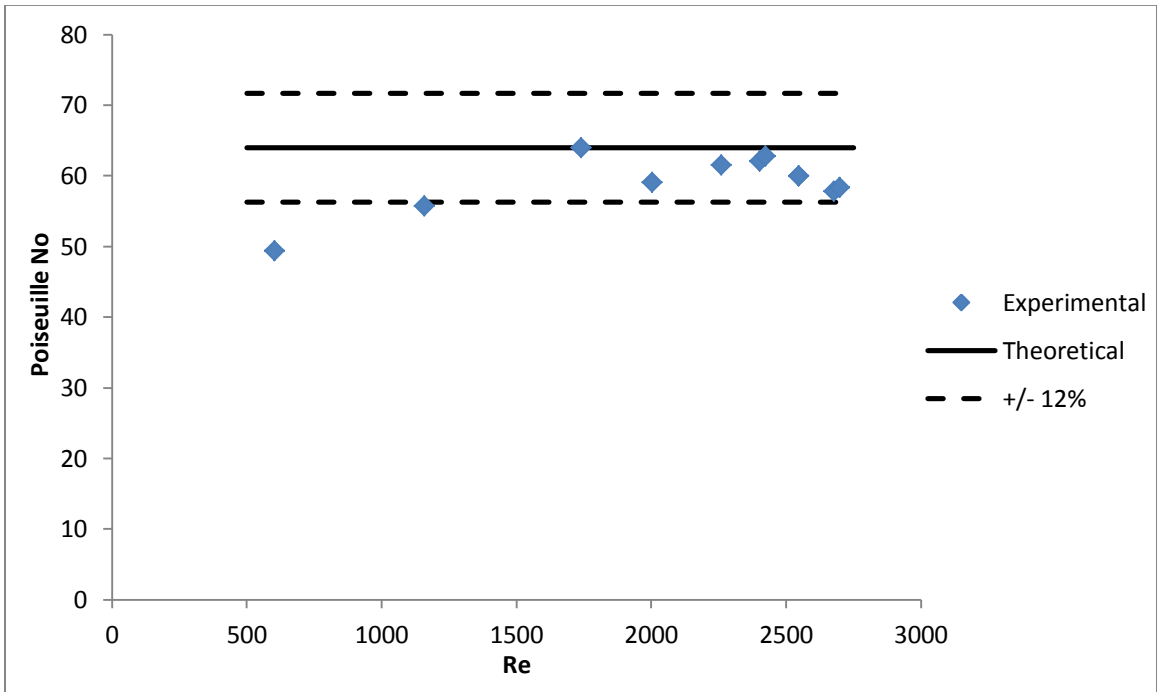
Figure 4.7: Poiseuille no. vs. Reynolds no. for flow of water inside 0.0625 inch OD tube

From Figure 4.5, it can be seen that the Poiseuille number obtained from experimental

data for 0.125 inch OD tube falls within ±8% of predicted values. For other two tubes,

Poiseuille number can be predicted with an accuracy of ±12% (Figures 4.6 and 4.7).

For turbulent flow, experimental friction factor is compared with the friction factor

obtained from the correlation given by Blasius (1913). The correlation is given by

$$f = 0.316 Re^{-0.25}$$

(4.2)
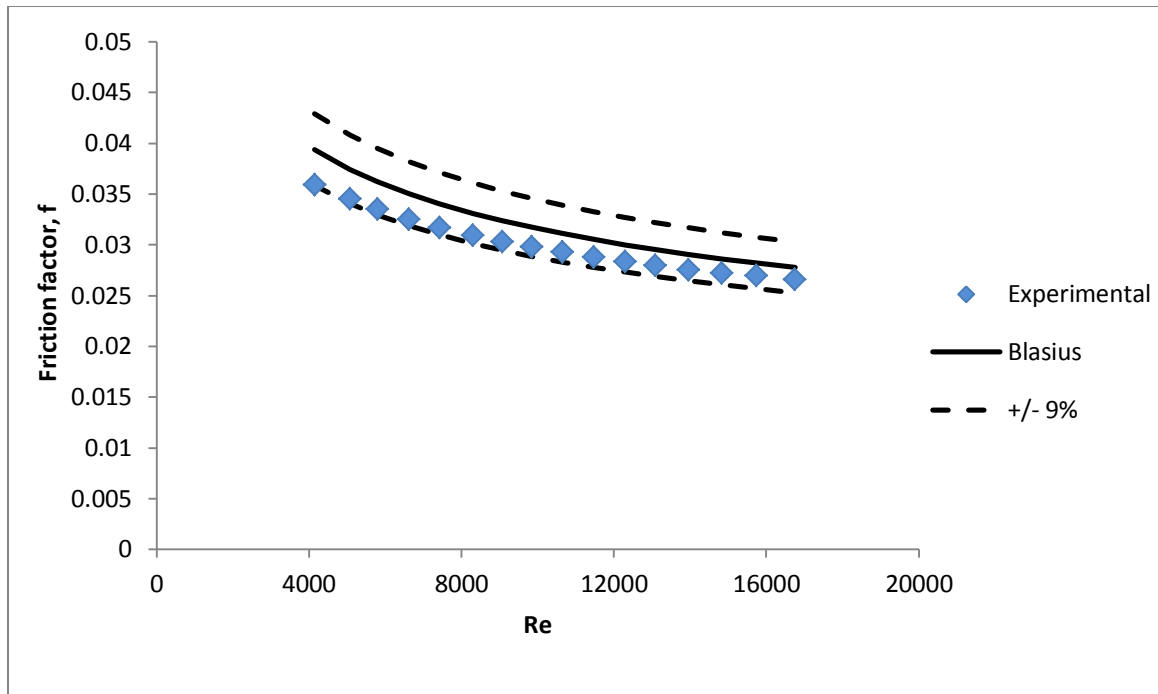
**Figure 4.8: Friction factor vs. Reynolds no. for flow of water inside 0.125 inch OD
tube, comparison with Blasius (1913)**

From Figure 4.8, it is clear that our experimental friction factor of water for 0.125 inch

OD tube relates well with the Blasius correlation. In the experimental flow rate range,

this correlation overpredicts experimental friction factor with a maximum error of 9%.

For the 0.09375 inch and 0.0625 inch OD tubes, Blasius correlation overpredicts the

experimental friction factor for water within an accuracy of 12% and 8%, respectively

(Figures 4.9 and 4.10).
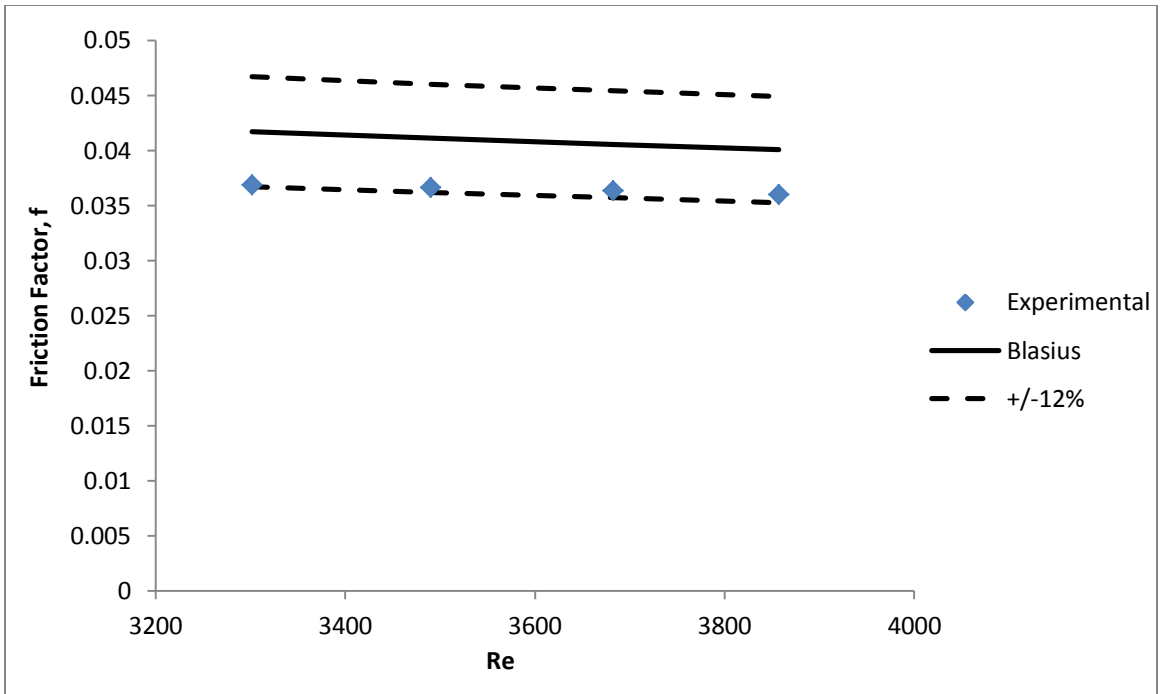
Figure 4.9: Friction factor vs. Reynolds no. for flow of water inside 0.09375 inch OD tube, comparison with Blasius (1913)
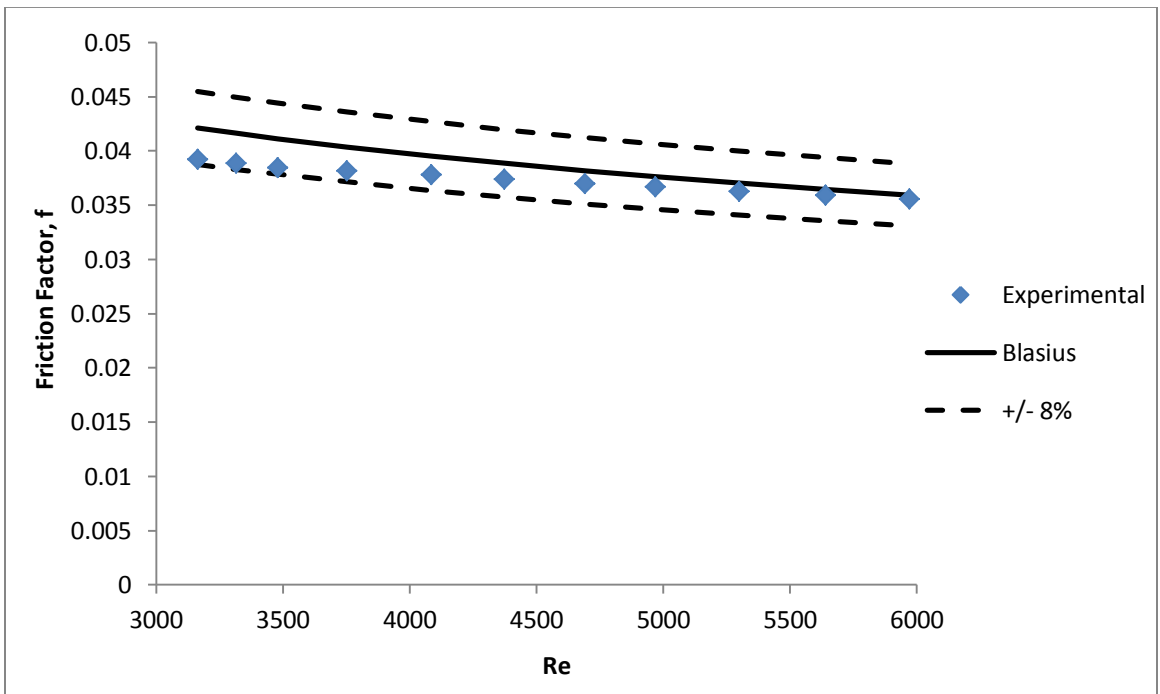
Figure 4.10: Friction factor vs. Reynolds no. for flow of water inside 0.0625 inch OD tube, comparison with Blasius (1913)

4.1.3 Heat Transfer Measurement with Water

Water is circulated through the test section and its heat transfer performance is measured. The test sections used are same in length, but differ in diameter. The outer diameter of the test sections are 0.125 inch, 0.09375 inch and 0.0625 inch. Testing is conveyed in the laminar region. Nusselt number for constant surface heat flux convective heat transfer of a fluid in the laminar flow can be calculated from correlation developed by Lienhard and Lienhard (2012). The correlation is

$$Nu = \begin{cases} 1.302Gz^{1/3} - 1 & for\ 2 \times 10^4 \leq Gz \\ 1.302Gz^{1/3} - 0.5 & for\ 667 \leq Gz \leq 2 \times 10^4 \\ 4.364 + 0.263Gz^{0.506} - e^{-\frac{41}{Gz}} & for\ 0 \leq Gz \leq 667 \end{cases} \qquad (4.3)$$

where $\boldsymbol{Gz}$ is called Graetz number and it is expressed as

$$Gz = \frac{Re_D Pr D}{x} \qquad (4.4)$$

Nusselt number obtained from the experimental data is compared to that calculated from Equation 4.3. The comparison is shown in Figure 4.11 for 0.125 inch OD test section, in Figure 4.12 for 0.09375 inch OD test section and in Figure 4.13 for 0.0625 inch OD test section. Experimental Nusselt numbers lie within ±15% accuracy limit of Lienhard correlation except for few points. Thus, the procedure of heat transfer measurement is validated and can be used to find out the heat transfer performance of silica nanoparticle colloidal suspension.

Figure 4.11: Nusselt number vs. 2/Graetz number for water flow through 0.125 inch OD tube

Figure 4.12: Nusselt number vs. 2/Graetz number for water flow through 0.09375 inch OD tube

68
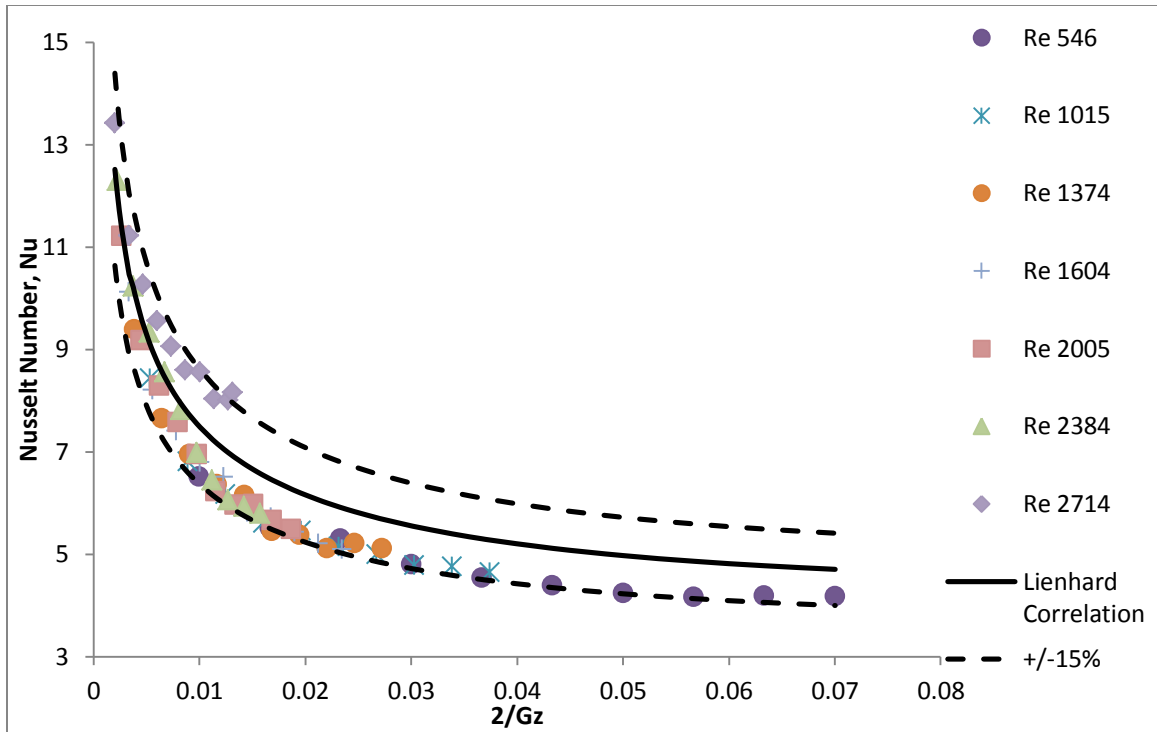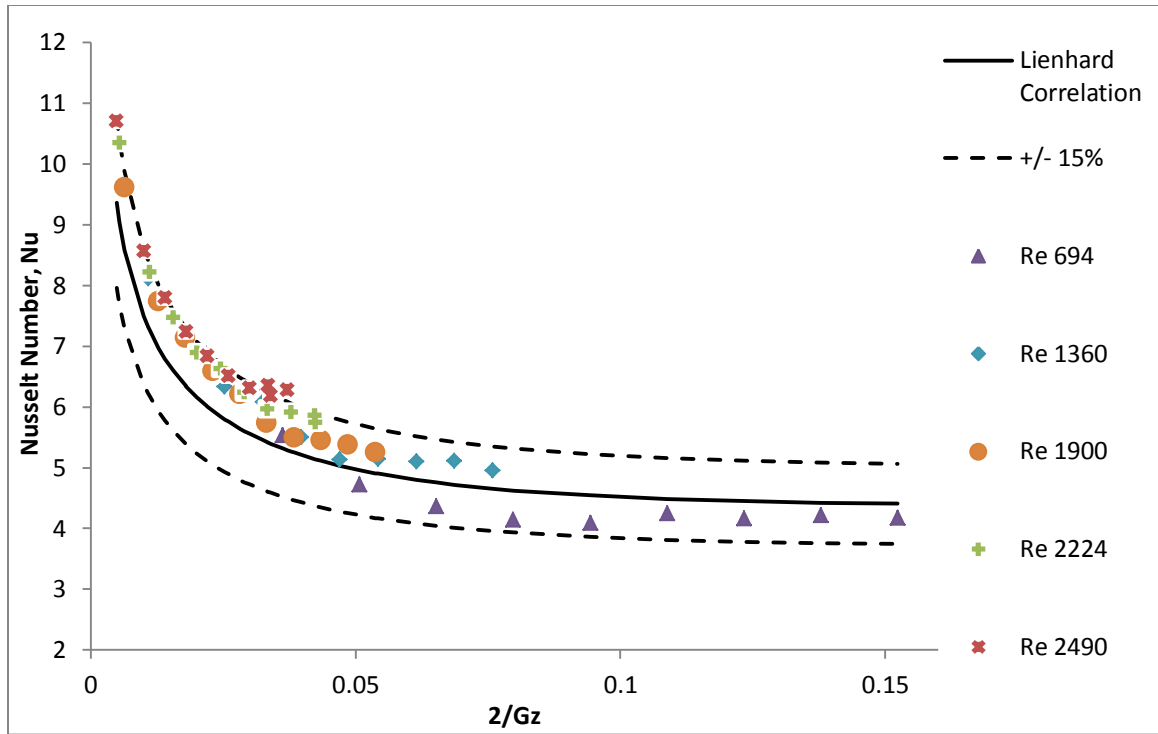
Figure 4.13: Nusselt number vs. 2/Graetz number for water flow through 0.0625 inch OD tube

4.2 Thermal Conductivity of Silica Nanoparticle Colloidal Suspension

The thermal conductivity of silica nanoparticle colloidal dispersion is measured from 7°C to 50°C. Measured values of thermal conductivity of the suspension and theoretical values of thermal conductivity of water are plotted against temperature in Figure 4.14 to make a comparison. Thermal conductivity of silica suspension increases as the temperature goes up. At all temperature, thermal conductivity of the nanoparticle suspension is higher than the thermal conductivity of water. For the suspension, thermal conductivity increases by 9.88% from the lowest to the highest experimental temperature. Within the same temperature range, thermal conductivity of water increases by 11.1%.
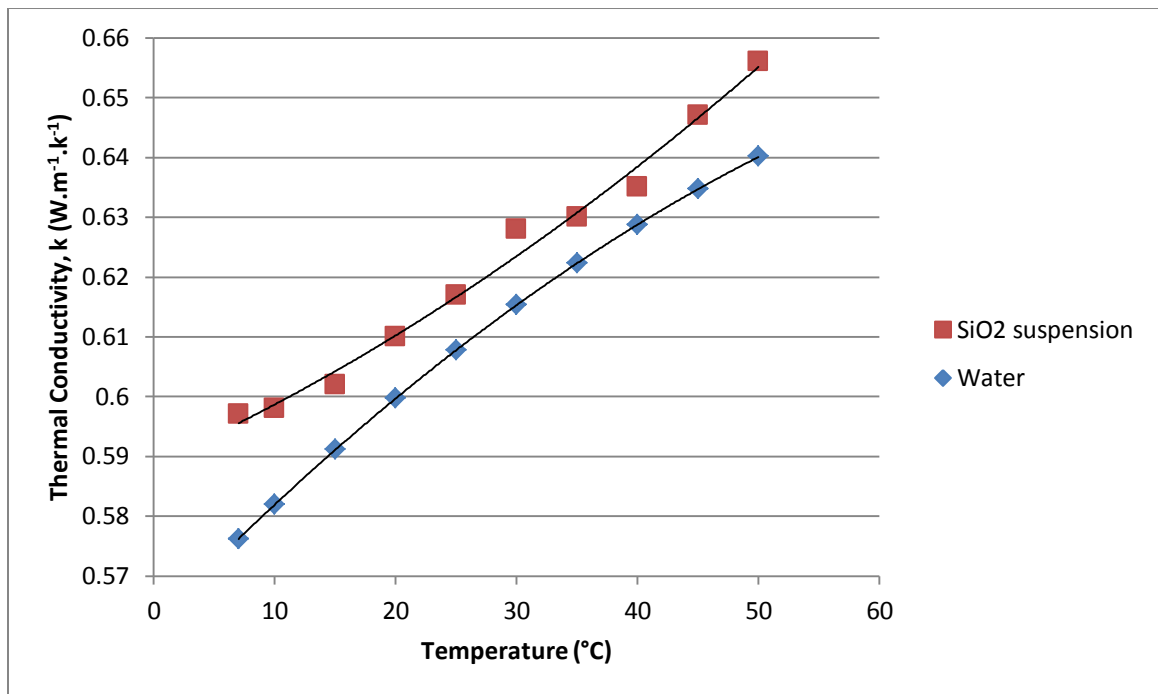
Figure 4.14: Thermal conductivity of water and silica nanoparticle suspension vs. temperature

The relative thermal conductivity, i.e. the ratio of thermal conductivity of silica suspension to the thermal conductivity of base fluid water, is plotted against temperature and shown in Figure 4.15. It can be seen that the relative thermal conductivity follows somewhat a parabolic trend with temperature. From 7°C to 40°C, its value decreases with increasing temperature. After 40°C, the relative thermal conductivity starts to increase with temperature and this trend can be observed up to the highest experimental range of temperature. The highest increase in thermal conductivity of silica suspension compared to that of water is found to be 3.6% at 7°C and the lowest increase is 0.99% at 40°C.
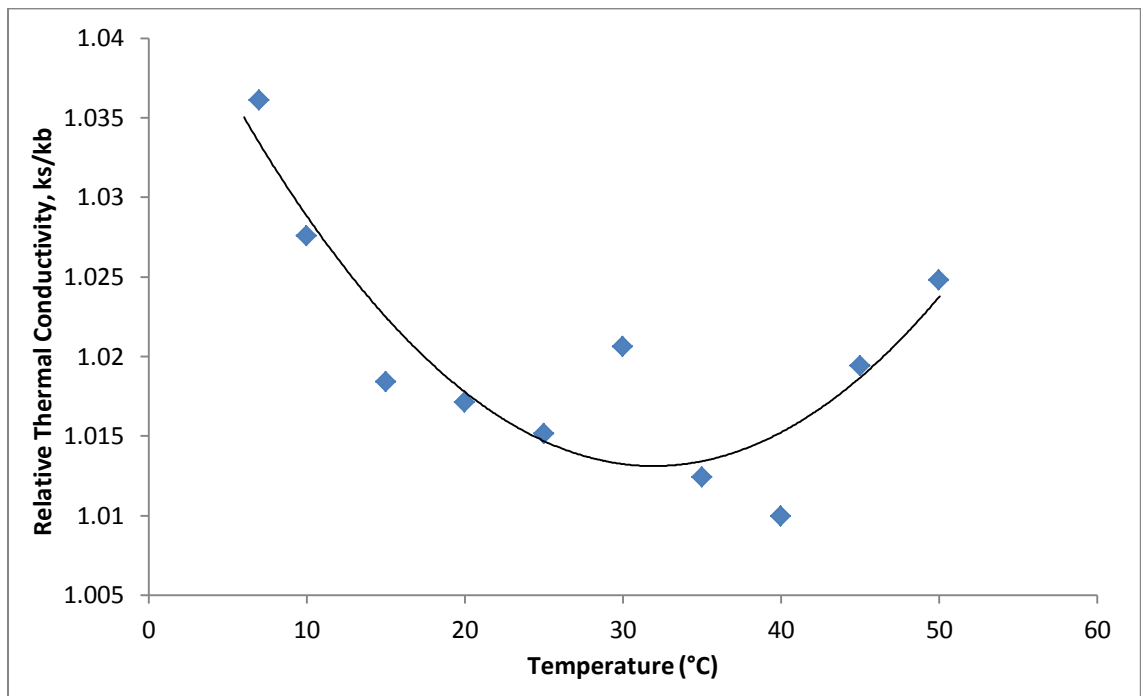
Figure: 4.15: Plot of relative thermal conductivity (k_s/k_b) vs. temperature within a temperature range of 7°-50°C

Several correlations are used to predict the thermal conductivity of the suspension and then compared with the experimental value. Figure 4.16 shows a comparison of thermal conductivity values obtained from the experiment and from Maxwell (1954) correlation. It can be seen that, Maxwell correlation can predict the experimental values with an accuracy of ±2%.
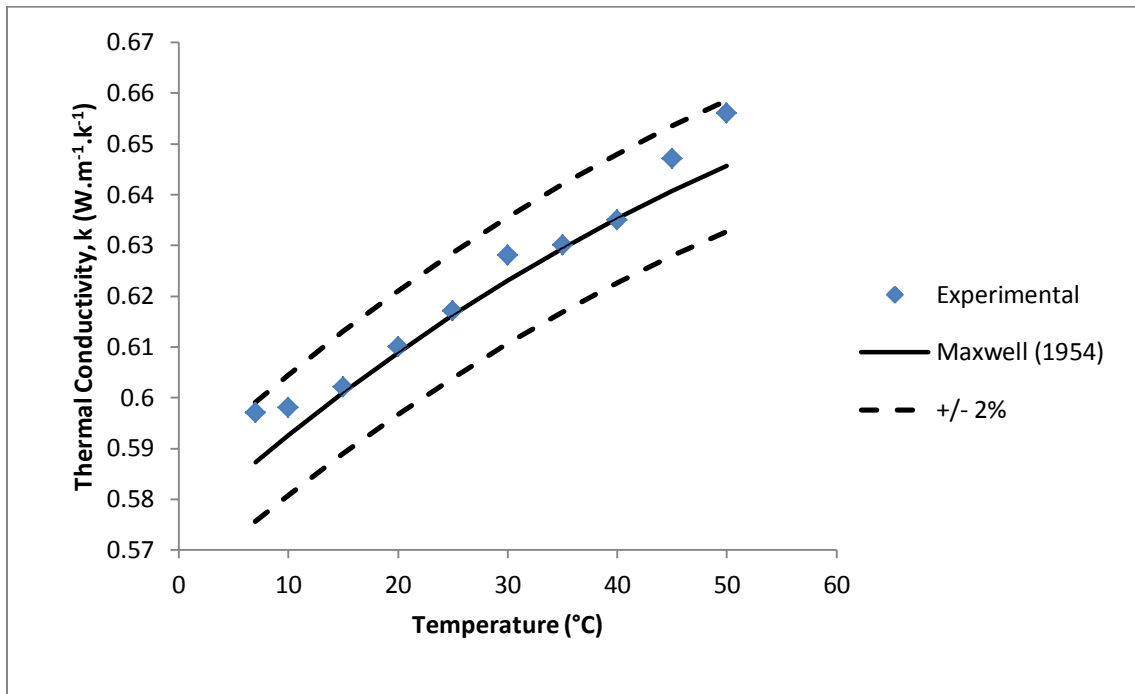
Figure 4.16: Comparison between the thermal conductivity values obtained from current experiment and from Maxwell (1954) correlation

Correlation developed by Kihm et al. (2011) slightly underpredicts our experimental thermal conductivity with a maximum deviation of 4% (Figure 4.17). Their correlation takes into account the effect of coagulation and heat dissipation of nanoparticles.
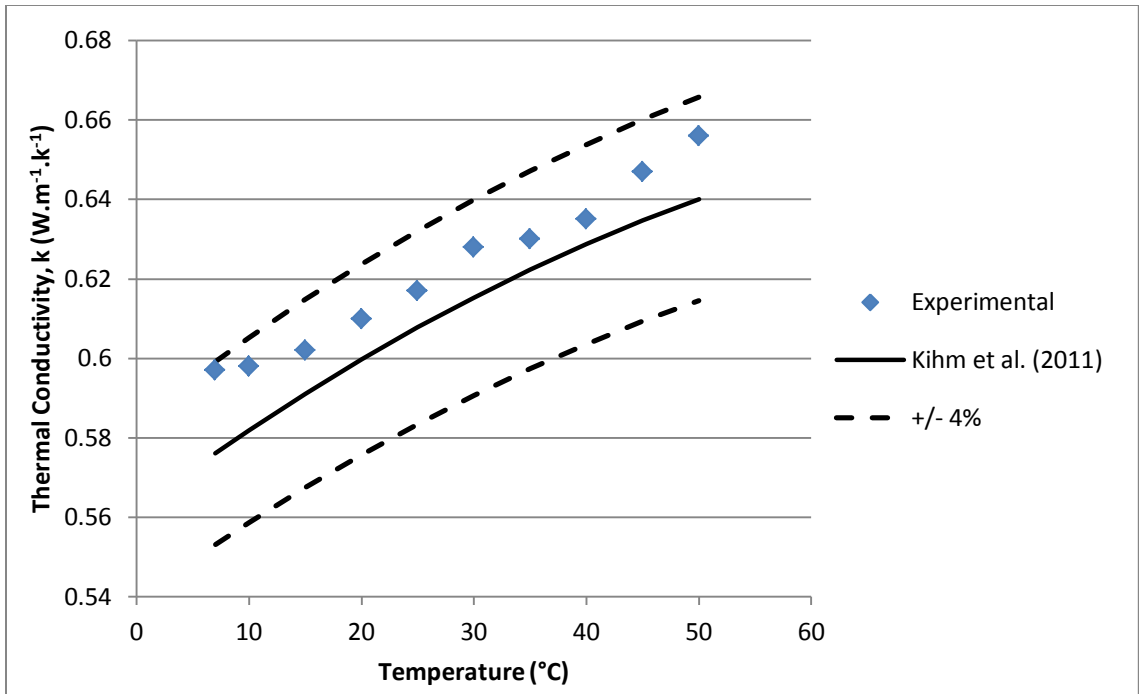
Figure 4.17: Comparison between the thermal conductivity values obtained from current experiment and from Kihm et al. (2011) correlation
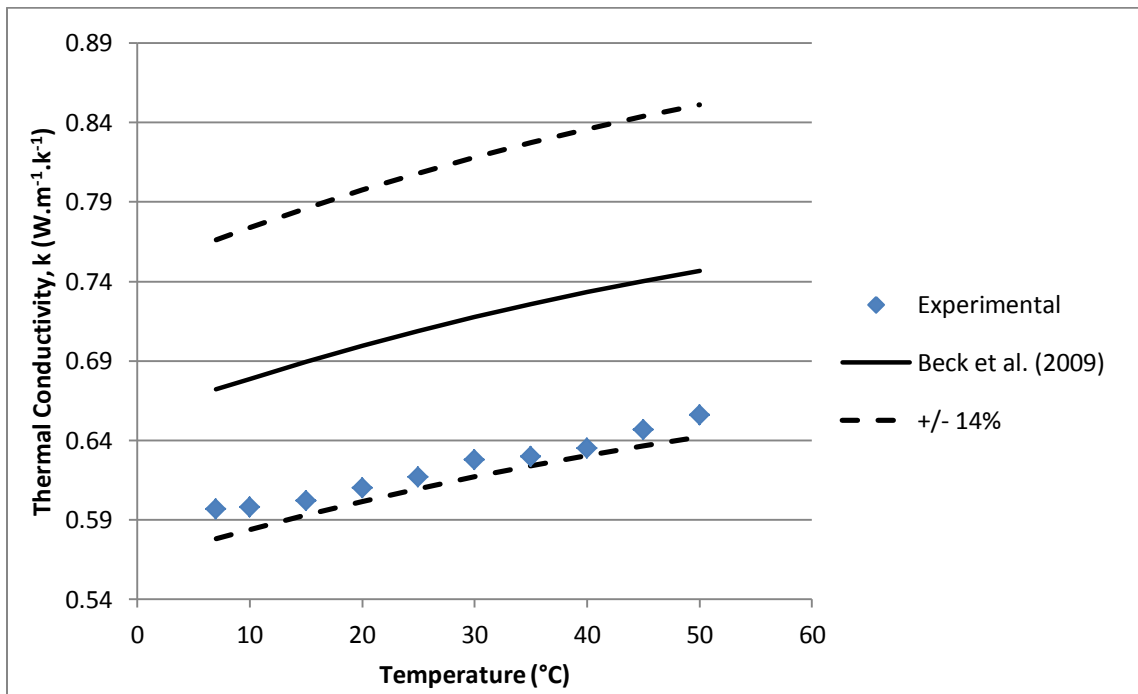
Figure 4.18: Comparison between the thermal conductivity values obtained from current experiment and from Beck et al. (2009) correlation

The correlation developed by Beck et al. (2009) considers the particle volume fraction and particle diameter size to predict the thermal conductivity of the suspension. They developed this correlation based on their experimental data of aluminum nanoparticle suspension. Their correlation overpredicts our experimental results. The prediction deviates from 11% to 14% (Figure 4.18). But the increase in thermal conductivity with temperature shows similar trend in both cases.
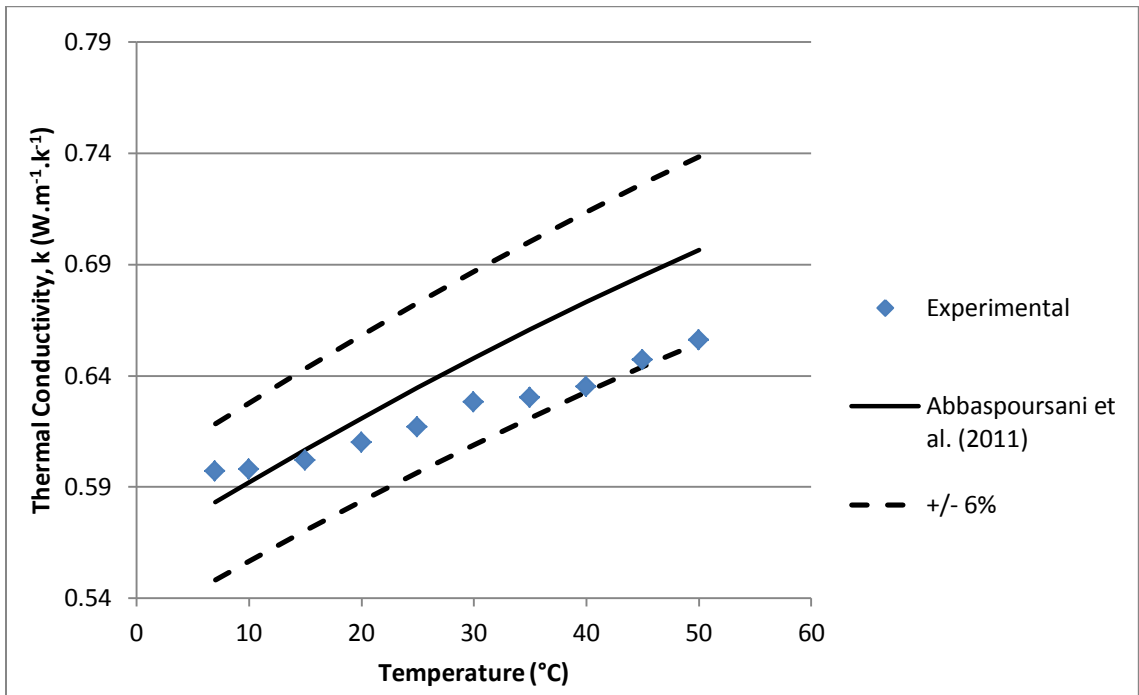
Figure 4.19: Comparison between the thermal conductivity values obtained from current experiment and from Abbaspoursani et al. (2011) correlation

Thermal conductivity model developed by Abbaspoursani et al. (2011) predicts our experimental data with an accuracy of ±6% within the temperature range (Figure 4.19). But the relation of thermal conductivity to temperature for their model is different than that of our present work. As the temperature increases, the deviation between our experimental data and prediction from their model increases. The model developed by

Abbaspoursani et al. (2011) considers the interfacial shell between base fluid and nanoparticle and the shell's thickness. It is possible that these two factors do not play any effective role in our prepared suspension and hence, the difference in experimental result and prediction from the model occurs.

4.3 Rheological Behavior of Silica Nanoparticle Colloidal Suspension

Before running the silica suspension through the test section, its rheological properties are examined. Two different concentrations of the suspension are prepared to study the rheological behavior. One solution contains 4.5% silica particle by volume. The concentration of the other solution is 9.58% silica by volume. At first, experiment is conducted to see if the test fluid behaves as Newtonian or non-Newtonian fluid. Newtonian fluids obey Newton's law of viscosity which is

$$\tau = \mu \frac{du}{dy} \tag{4.3}$$

For Newtonian fluid, the value of viscosity remains constant at a certain temperature irrespective of the shear stress applied on it. If shear stress is plotted against shear rate, then a straight line is found which passes through the origin. The slope of the curve gives the viscosity of the fluid. But for non-Newtonian fluid, the viscosity changes depending on the stress it is subjected to.

The behavior of the silica colloidal suspension with respect to shear stress is observed. The experiment is carried out from 7° to 60°C temperature. At each temperature point, the fluid is sheared at six different RPM and the corresponding shear rate, shear stress and viscosity data are obtained from the viscometer. The highest RPM that can be

achieved by the viscometer is 200. So, test is conducted up to 200 RPM which provides a shear rate of 244.6 s^{-1}.

Shear stress for 9.58% vol. solution is plotted against shear rate and shown in Figure 4.20 and 4.21. From 7°C, the starting temperature point of the experiment, up to 10°C, the plot shows a straight line within the experimental shear rate range (Figure 4.20). But as we reach 15°C, the plot of shear stress against shear rate is no longer a straight line i.e. the fluid starts to show non-Newtonian behavior. This behavior is observed until the end point temperature of the experiment.
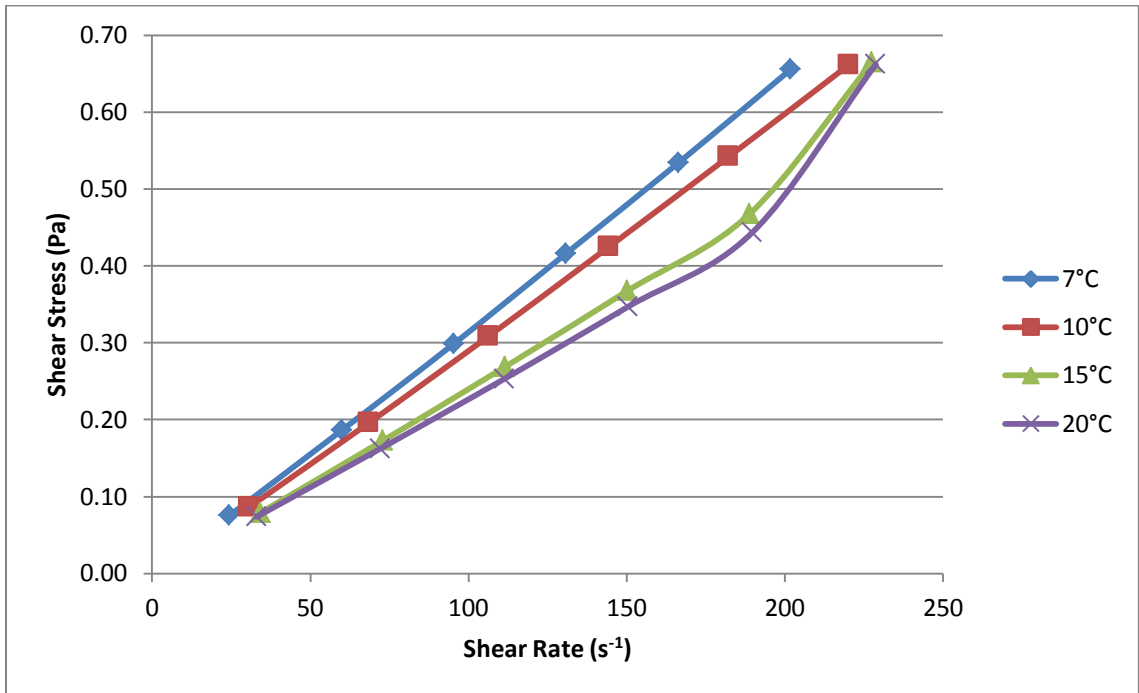
Figure 4.20: Change of shear stress with shear rate at 7°, 10°, 15° and 20°C for silica nanoparticle colloidal suspension (9.58% by volume)

An analysis of the shear stress and shear rate curves after 10°C exhibits that there is a sudden rise in shear stress when a certain point of shear rate is passed. This point shifts down to lower shear rate as the temperature increases (Figure 4.21). So, it is possible that, if higher shear rate could be applied to the fluid, the sudden rise in shear stress could have

76

been observed at lower temperature (less than 15°C) also. Or in other words, the fluid would have behaved as non-Newtonian. The fluid exerts less shear stress at a certain shear rate when the temperature is increased.

There are two theories describing the mechanism behind the sudden rise in the shear stress, Maranzano and Wagner (2002). Experimental evidence can be found in support of both theories. The first theory is known as order-disorder transition (ODT). The argument for order–disorder shear thickening proposes that colloidal particles organize into layers or strings at low shear rates which results in a lower viscosity than would be obtained for a flowing, disordered suspension. But, as the shear rate increases, lubrication forces between adjacent particles in the highly organized, layered flow cause the particles to rotate out of alignment and destabilize the flow. Hence, the viscosity of the suspension increases due to this increase in interparticle interactions in the flowing, disordered state.

The other theory, known as the "hydrocluster" mechanism, states that shear thickening is the result of stress-bearing clusters of particles which are created by self-organization when shear is induced. The dominance of short-range hydrodynamic lubrication forces results in this self-organized microstructure, whereby the flow generates transient packed clusters of particles which are separated from one another only by a thin solvent layer. Percolation of these hydroclusters leads to ''jamming,'' which in turn causes the discontinuous, often irregular increase in shear viscosity at a critical shear stress.
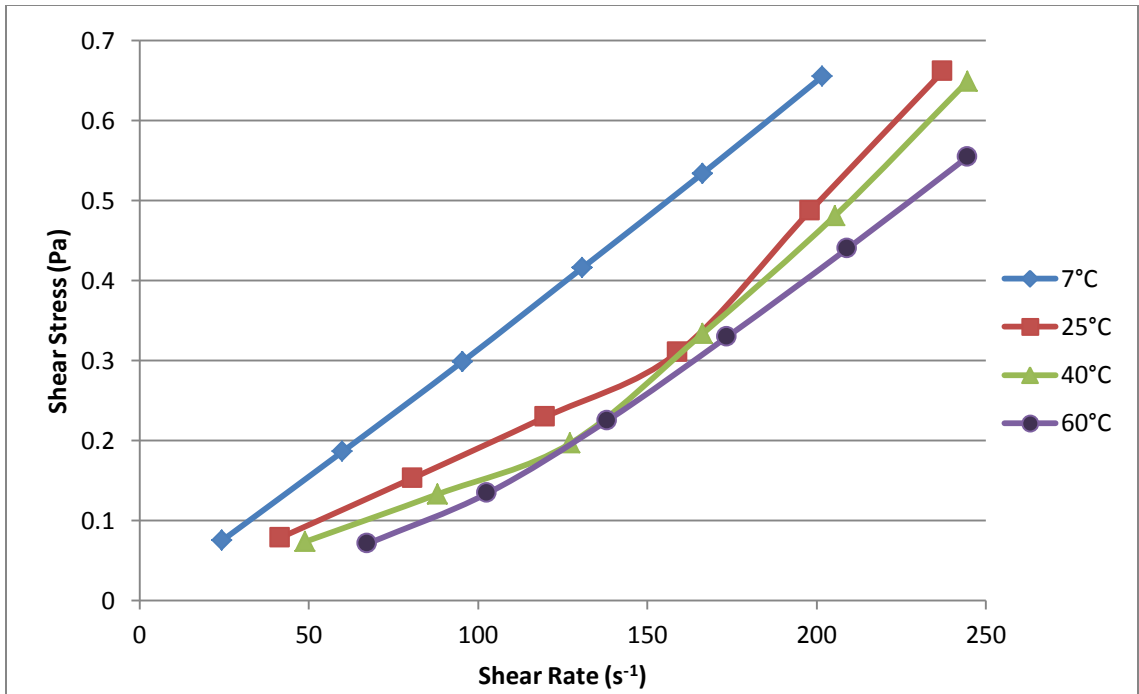
Figure 4.21: Change of shear stress with shear rate at 7°, 25°, 40° and 60°C for silica nanoparticle colloidal suspension (9.58% by volume)

For the fluid suspension of 4.5% by volume, similar characteristics are observed (Figure 4.22). In this case, the fluid exhibits non-Newtonian behavior at all temperatures. The sudden rise in shear stress is also prominent up to 35°C and the point of rise shifts to lower shear rate with increasing temperature. After 35°C, experiment cannot be conducted at shear rate lower than 85.61 s^{-1} as the torque applied by the apparatus falls down below 10% of the full scale torque and hence, readings are not accurate. Otherwise, it might have been possible to observe the sudden rise in shear stress at temperatures higher than 35°C. Shear stress falls down at same shear rate if temperature is increased, which is also the case for 9.58% volume solution.

78

For both suspensions, the shear stress and shear rate curves seem to be originated from the origin of the axis. So, it can be concluded that there is no yield stress associated with the fluids.
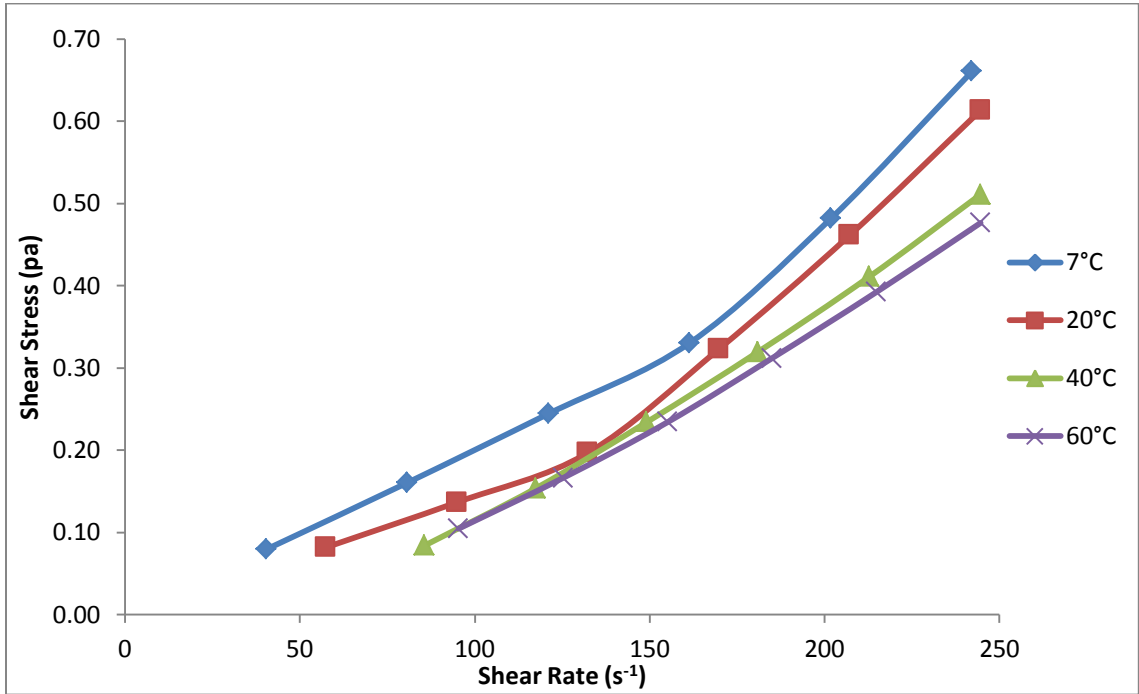
Figure 4.22: Change of shear stress with shear rate at different temperatures for silica nanoparticle colloidal suspension (4.50% by volume)

Change of viscosity with shear rate and temperature is also observed for both concentration of nanoparticle suspension (Figures 4.23 and 4.24). It is apparent that viscosity of the solution increases as the shear rate increases. This implies that the solutions are shear-thickening non-Newtonian fluids. Viscosity increases abruptly after a certain point which is due to the sudden shear stress rise discussed earlier. The percentage of increase in viscosity with shear rate at a certain temperature increases as the temperature goes up. At 7°C, the viscosity increases by 5.88% for 9.58% vol. suspension and by 38.57% for 4.50% vol. suspension within experimental shear rate range. At 60°C,

the increase of the same property for 9.58% and 4.50% vol. suspensions is found to be 107.7% and 77.2% respectively. When the shear rate is fixed and the temperature increases, the viscosity of the fluid decreases which is very common for liquids. At 244.6 s^{-1} shear rate, the viscosity decreases by 39.48% from 10° to 60°C for 4.50% vol. suspension. For the 9.58% vol. suspension, from 35°C to 60°C at same shear rate, the decrease in viscosity is observed to be 21.59%.
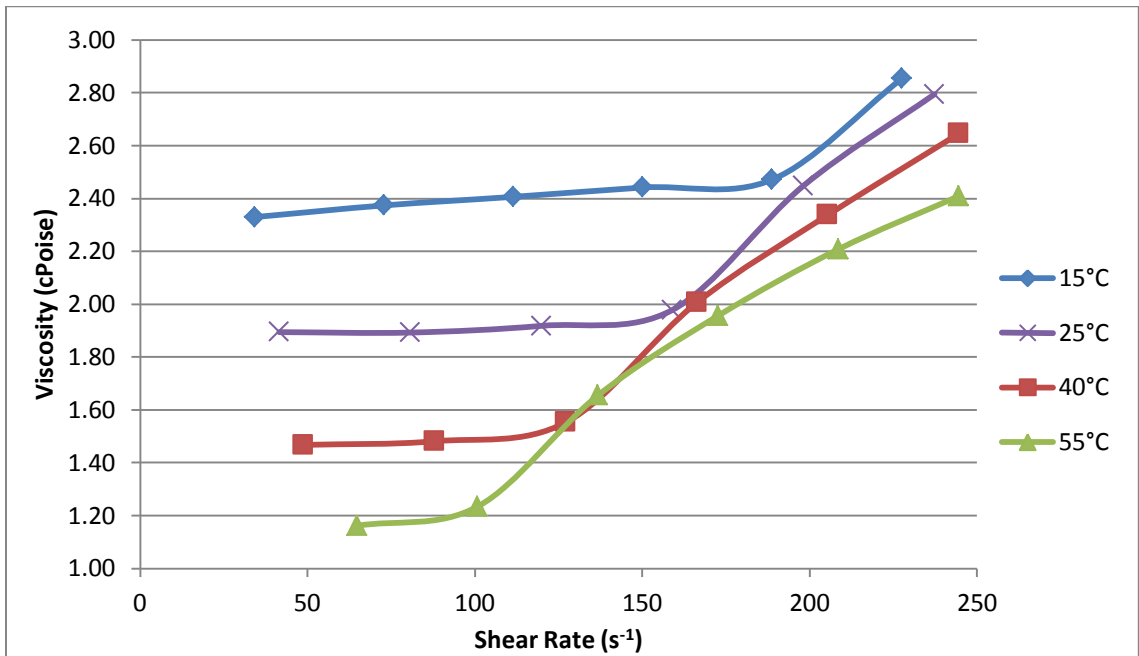
Figure 4.23: Change of viscosity with shear rate at different temperatures for silica nanoparticle colloidal suspension (9.58% by volume)

Figure 4.24: Change of viscosity with shear rate at different temperatures for silica nanoparticle colloidal suspension (4.50% by volume)

When the volume concentration is increased, the viscosity of the solution also increases (Figure 4.25). At lower shear rate, the ratio of viscosity of the higher concentrated solution to the viscosity of the lower concentrate solution is high. But, as the shear rate increases, the ratio decreases. At 35°C and a shear rate of 75 s^{-1}, the viscosity of the 9.58% vol. fluid increased by almost 49% compared to th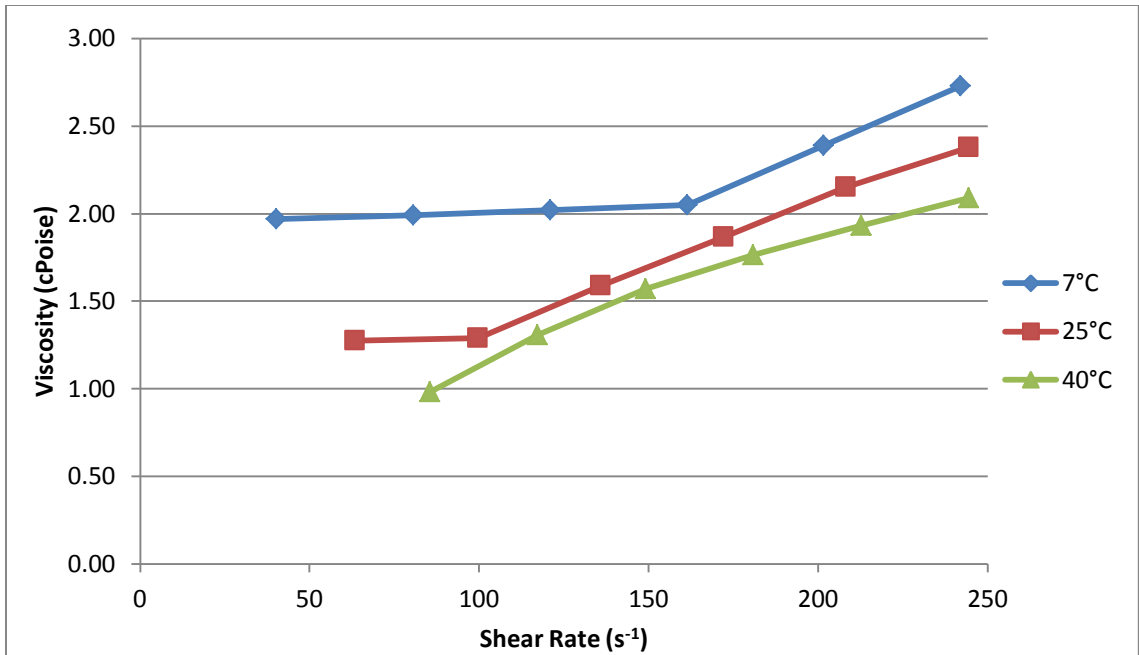e viscosity of the 4.50% vol. fluid. Keeping temperature constant, when shear rate is increased to 244.60 s^{-1}, the increase in the viscosity of 9.58% vol. solution compared to the viscosity of 4.50% vol. solution is 28.4%. For 15°C temperature, the highest and lowest increase in viscosity with volume concentration is found to be 53% and 16.8% respectively, within a shear rate range of 75 to 227 s^{-1}.
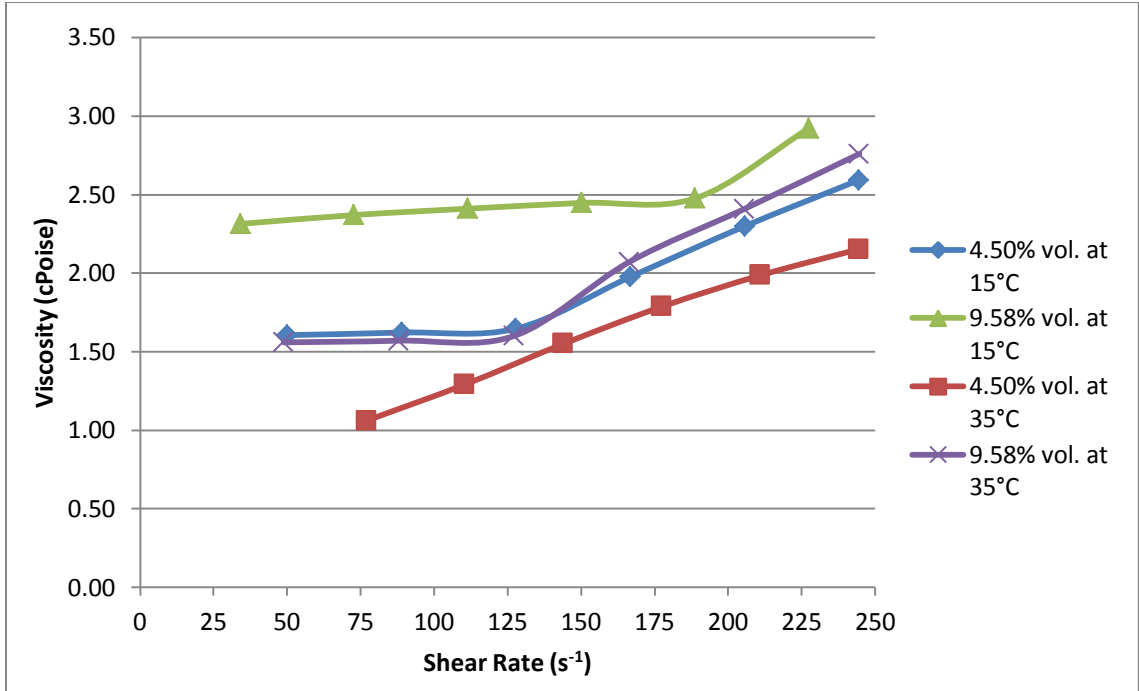
Figure 4.25: Change of viscosity with shear rate at different concentrations for silica nanoparticle colloidal suspension

Researchers developed several models to relate the shear stress and shear rate of non-Newtonian fluids. The most widely used model is the "Power law" model or "Ostwald-deWaele" model. In equation form, the power law can be written as

$$\tau = k\left(\frac{du}{dy}\right)^{n}$$

(4.4)

A logarithmic plot of shear stress vs. shear rate is often found to be linear over a wide range of shear rate. The parameter n is called "flow behavior index" which is the slope of the logarithmic plot. For shear thinning non-Newtonian fluid, the value of n varies between unity and zero. It is greater than unity when the fluid is shear-thickening. The term k is called "consistency index" and is calculated from the intercept on the shear stress axis at unit shear rate.

A term, apparent viscosity can be calculated at a certain shear rate for power law fluid once the flow behavior index and consistency index are known. The following equation can be used to find the apparent viscosity.

$$\mu_a = k\left(\frac{du}{dy}\right)^{n-1} \tag{4.5}$$

For the current experiment, logarithmic plot of shear stress and shear rate is prepared from 7°C to 60°C for both 9.58% vol. and 4.58% vol. solutions to see if they obey the power law. The range of shear rate, within which the experiment is conducted, is from 24.46 s^{-1} to 244.60 s^{-1}. As can be seen from Figures 4.26 and 4.27, the plots are straight lines. Therefore, the silica suspensions are found to be power law fluid within experimental range.
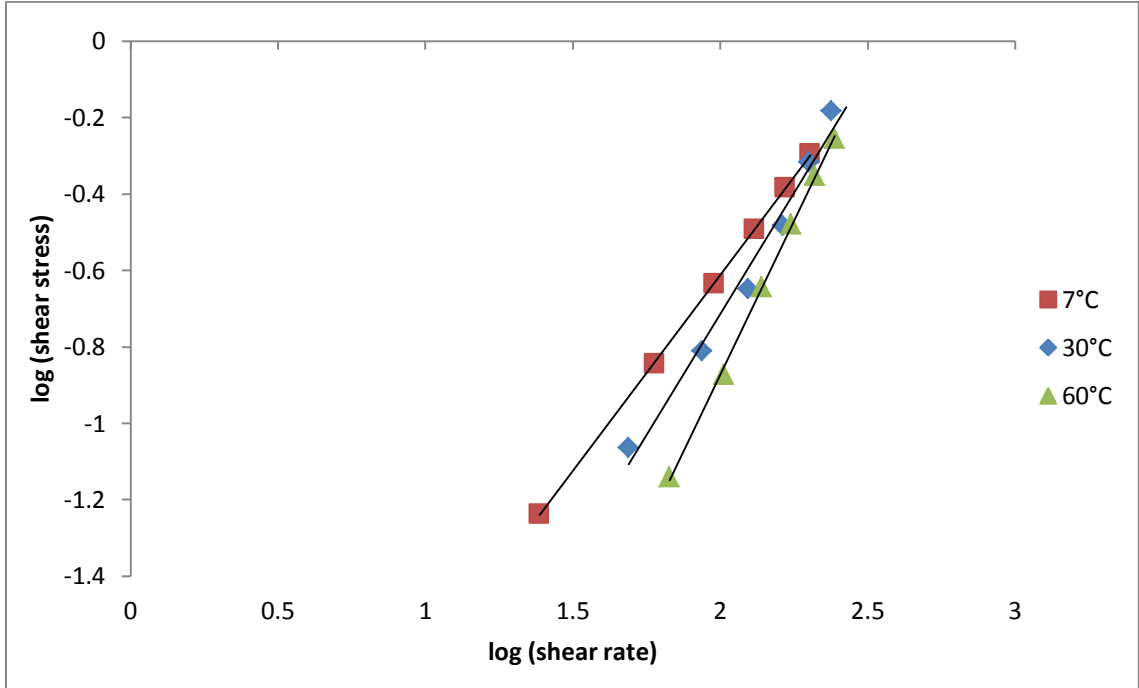
Figure 4.26: logarithmic plot of shear stress vs. shear rate at different temperatures for 9.58% vol. silica colloidal suspension
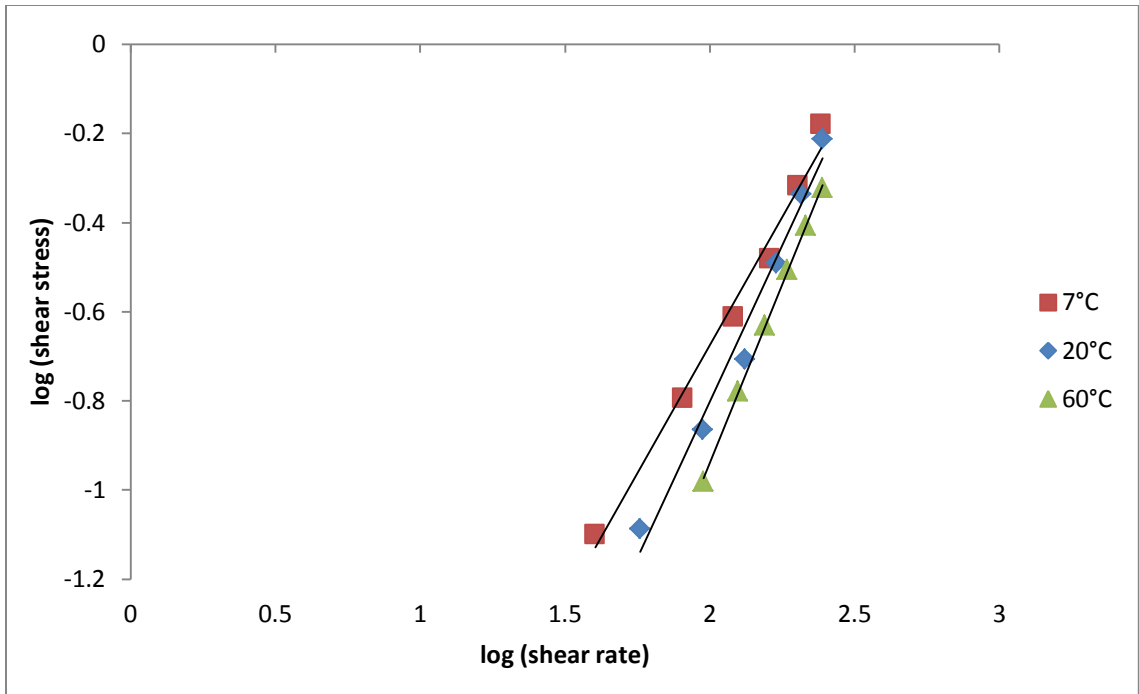
Figure 4.27: logarithmic plot of shear stress vs. shear rate at different temperatures for 4.50% vol. silica colloidal suspension

Flow behavior index, n and consistency index, k are calculated from the logarithmic plot of the shear stress vs. shear rate. The change in flow behavior index for 9.58% vol. and 4.50% vol. solutions with temperature is shown in Figure 4.28. For both solutions, the value of n is always greater than 1, which indicates that the solutions behave as shear-thickening fluid within experimental range. For 9.58% vol. solution, the value of n increases with increasing temperature which indicates that the logarithmic stress-strain curve is getting steeper. That is, the shear-thickening behavior is getting stronger with increase in temperature. The value of n increases by 56.5% from 7°C to 60°C. For the other solution, flow behavior index increases up to 40°C, then its value starts to decrease indicating a decline in shear-thickening behavior. The maximum increase achieved is 48.7% from 7°C to 40°C.
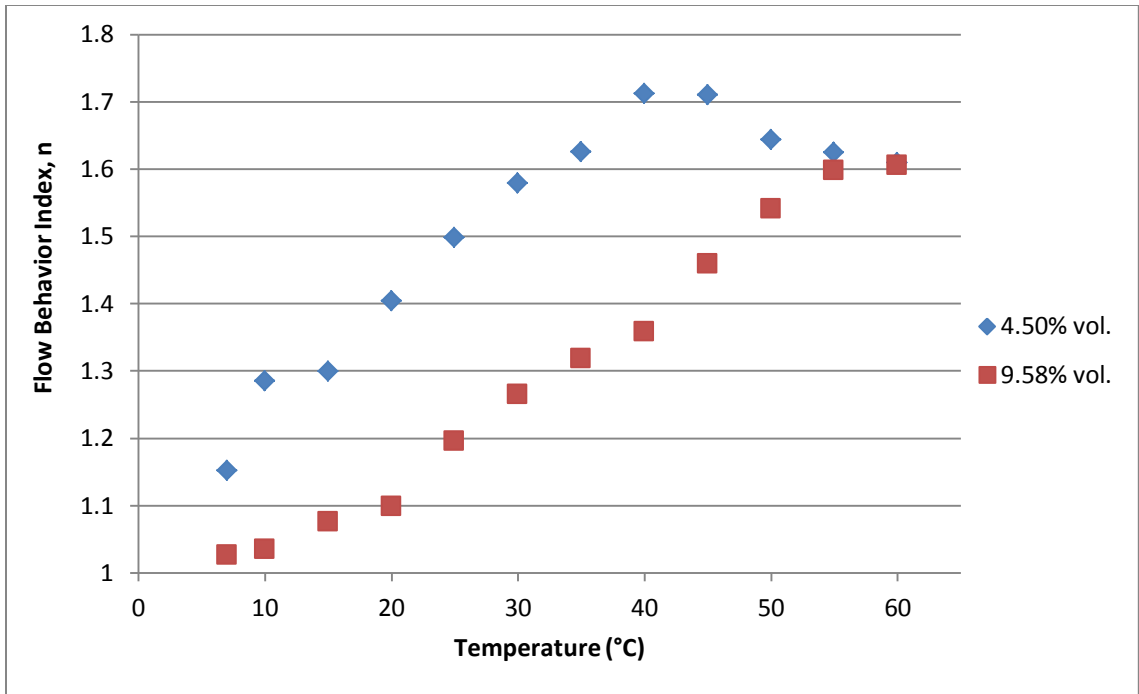
Figure 4.28: Flow behavior index (n) vs. temperature for 9.58% vol. and 4.50% vol. silica colloidal suspension
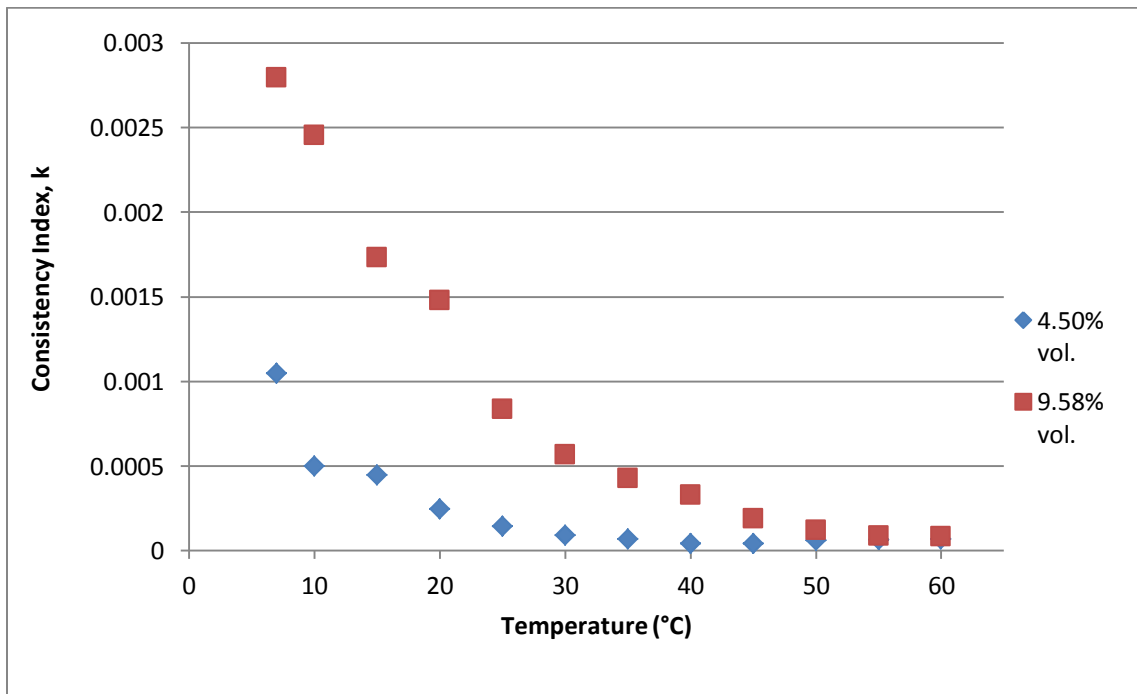
Figure 4.29: Consistency index (k) vs. temperature for 9.58% vol. and 4.50% vol. silica colloidal suspension

Figure 4.29 depicts the relation of consistency index, k and temperature at different

concentrations. The value of k decreases as the temperature increases. The change in k

with temperature is much more sensitive than change in n with temperature. Consistency

index decreases by almost 3400% when temperature of the 9.58% solution rises from 7°C

to 60°C. For the same temperature range, the decrease is 1518% for 4.50% vol. solution.

When temperature is fixed, higher concentrated solution has higher consistency index.

The ratio of the index of higher concentrated solution to that of the lower concentrated

solution increases with temperature from 7°C to 40°C. After 40°C, the ratio starts to

decrease. The highest increase in k with concentration is 771% at 40°C and the lowest

increase with concentration is 19% at 60°C.

Using the values of the flow behavior index and the consistency index at different

temperatures, apparent viscosity at various shear rates is calculated. The calculated shear

rate is then compared with the result obtained from the experiment. Analyzing the

calculated data and the experimental data from Figures 4.30 and 4.31, it can be

established that the power law model can predict the apparent viscosity of both solutions

well within an accuracy range of ±15%.
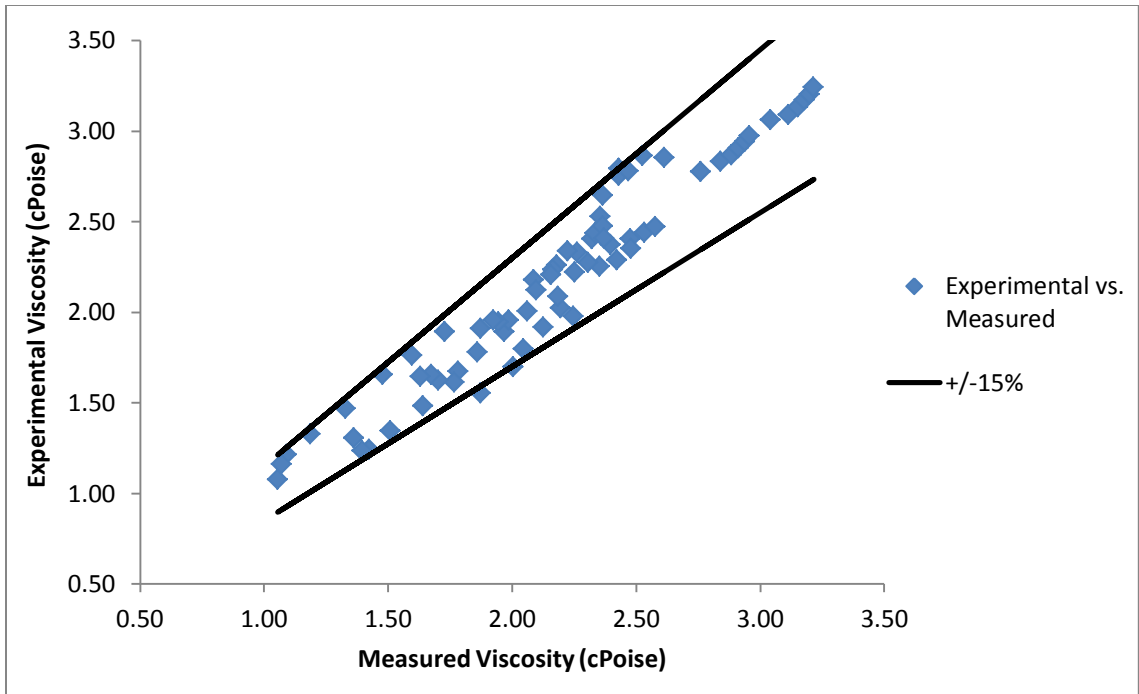
Figure 4.30: Experimental viscosity vs. measured viscosity (using power law equation) of 9.58% vol. silica solution
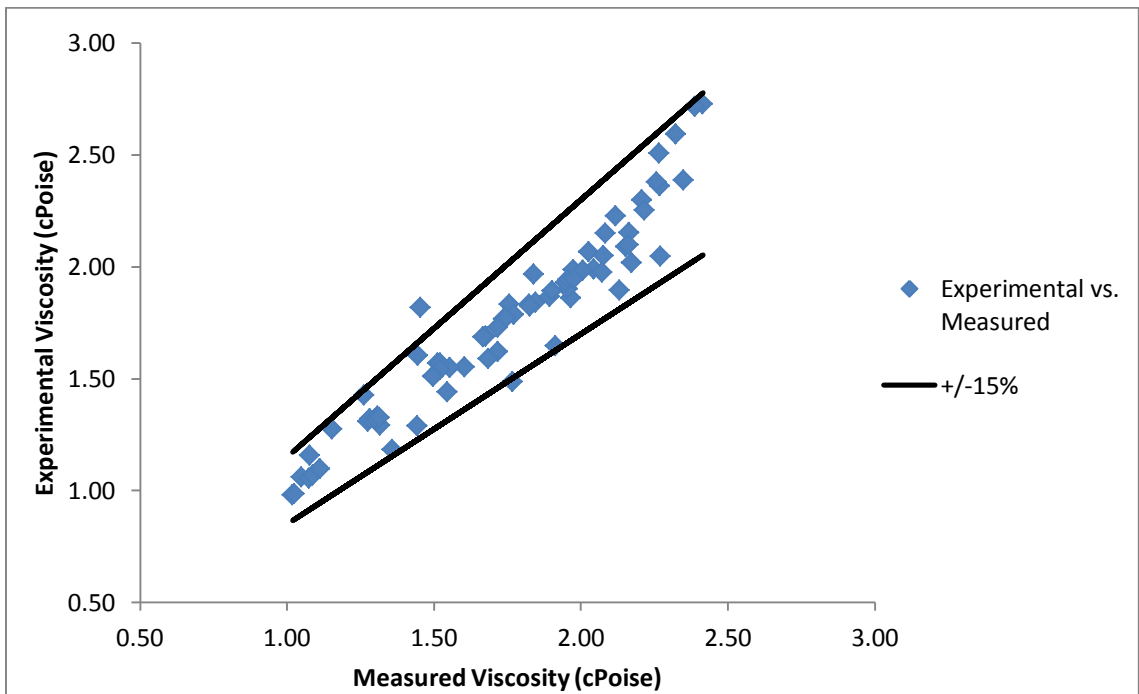
Figure 4.31: Experimental viscosity vs. measured viscosity (using power law equation) of 4.50% vol. silica solution

Non-Newtonian fluids can be grouped into two broad categories depending on their rheological behavior with time. When shear rate at a given point is only dependent on the instantaneous shear stress at that point, the fluid is called time-independent non-Newtonian fluid. In this case, viscosity at a certain temperature remains constant with time if there is no change in shear rate. Time-dependent fluids can be defined as those for which shear rate is a function of both the magnitude and the duration of shear and possibly of the time laps between consecutive applications of shear stress. For this type of fluid, shear stress can either increase or decrease with time at a given shear rate and constant temperature.

The silica colloidal suspension of 9.58% by volume is tested to see if its shear stress is independent of time. This is observed by applying two different methods. First method tests if time laps between consecutive shear rates have any effect on the shear rate. The fluid is subjected to certain shear rate points in increasing order. Then same shear rates are applied, but this time, in decreasing order. The whole process is repeated again. The shear stress of the fluid is then plotted against shear rate and the path of increasing and decreasing shear is examined. Experimental result carried out at 60°C is presented in Figure 4.32. No loop formed by the curves can be observed. Shear stress at a certain shear rate is always located at the same point irrespective of time. The order of RPM change also has no effect on the shear rate.
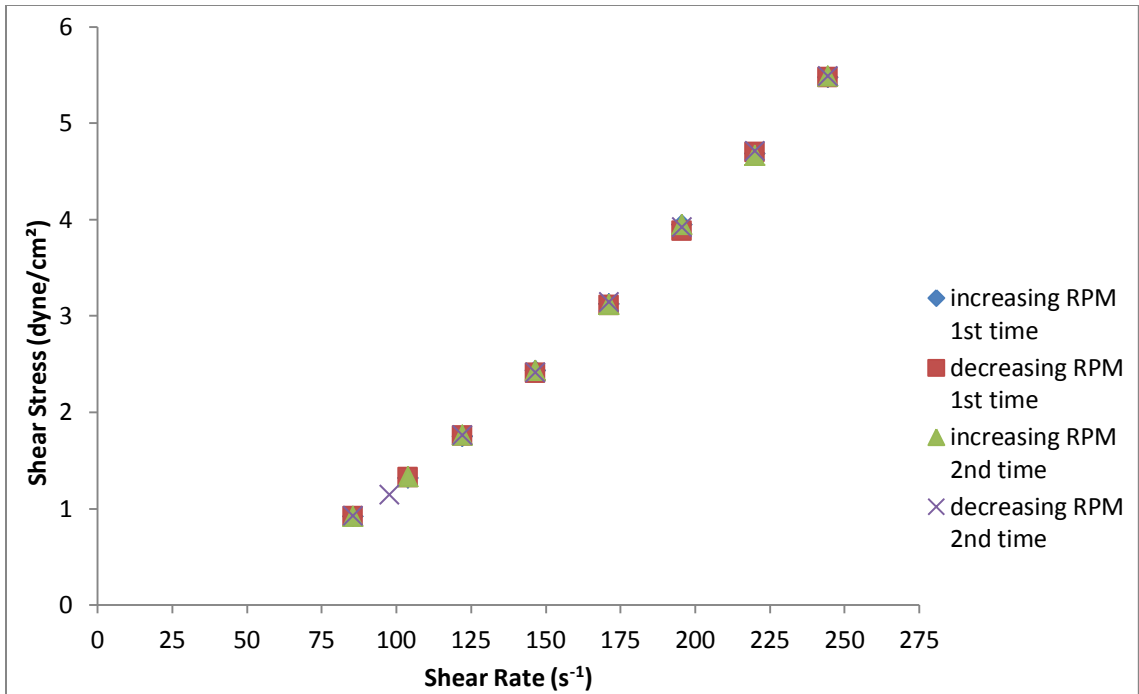
Figure 4.32: Effect of time lapse between consecutive shear rate application on shear stress at 60°C for 9.58% vol. silica suspension

Another method is to apply a certain shear rate on the fluid for a certain amount of time when temperature remains constant and see if the shear stress changes with time. This experiment is carried out at 30°C, 40°C, 50°C and 60°C applying four different shear rates at each temperature. Shear rates are applied for 90 seconds and data point is taken at 1 second interval. From the graph of shear stress against time at 60°C (Figure 4.33), it can be seen that the value of shear stress fluctuates at the beginning of time. After 12-15 seconds, the value of shear stress stabilizes and does not change with time. Dupuis et al. (1994), Hu et al. (1998) and Hess et al. (2006) experimented with shear thickening fluid and reported about time dependency of viscosity for a certain period of time before it reaches steady value. But the reason behind this phenomenon is not explained.

When the current test fluid is run inside tube for measuring heat transfer performance and pressure drop, it is given enough time to reach steady state. So, it can be considered as a time-independent non-Newtonian fluid within the experimental shear rate range. How the fluid will behave beyond this range, is subjected to further testing.
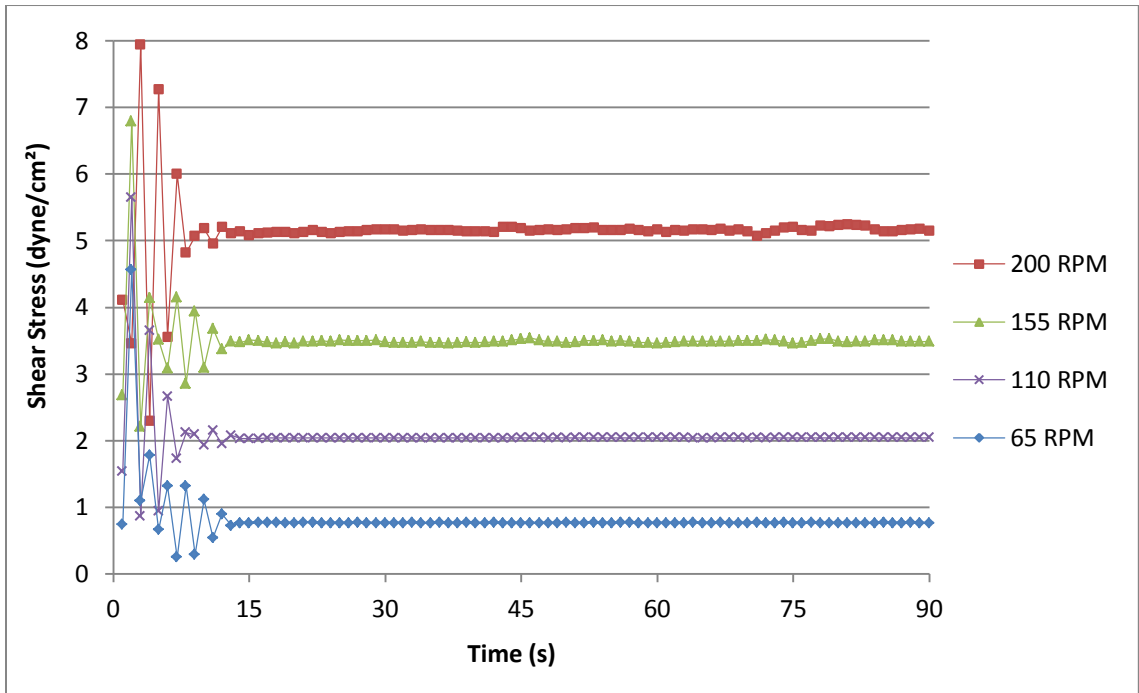
Figure 4.33: Shear stress at different RPMs vs. time conducted at 60°C, data point taken at 1 second interval

To analyze the relation of shear stress and time before the shear stress stabilizes, further experiment is conducted. This time, a certain shear rate is applied and corresponding shear stresses are recorded with a time interval no longer than 0.2 second. The result obtained at 30°C and 60°C are shown in Figures 4.34 and 4.35, respectively. The change of shear stress with time takes an oscillatory shape before getting constant. The amplitude of the oscillation decreases gradually. Also, it is noticeable that shear stress becomes steady a little earlier in time when higher RPM is applied.

90
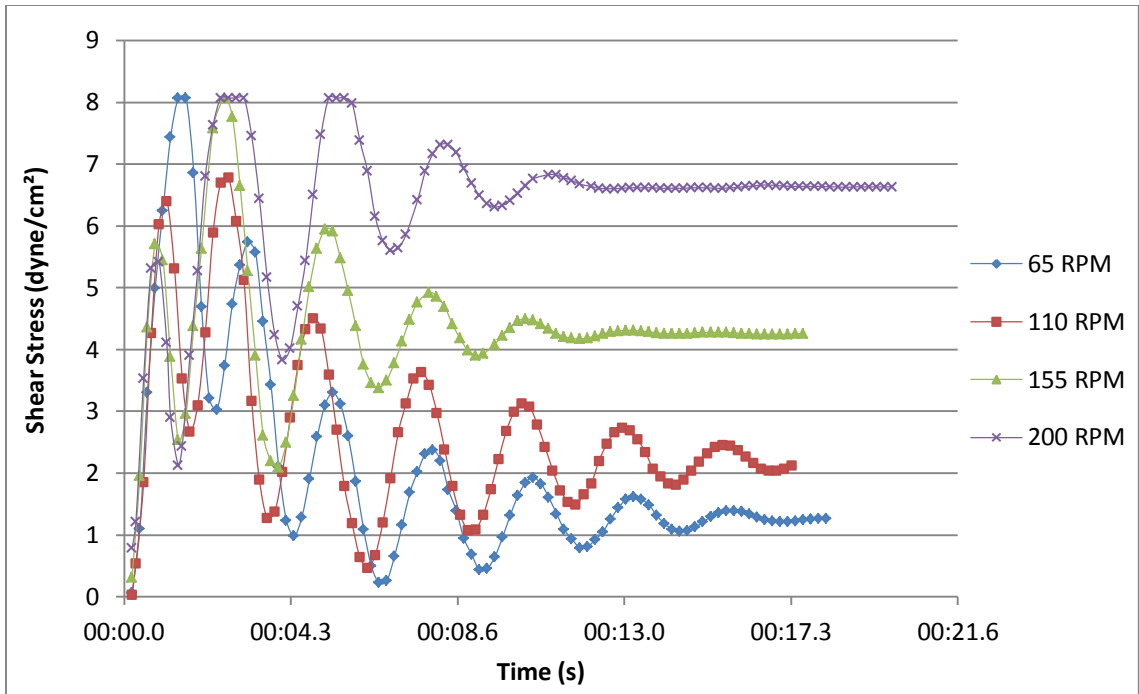
Figure 4.34: Shear stress at different RPMs vs. time conducted at 30°C, data point taken at time interval no longer than 0.2 second
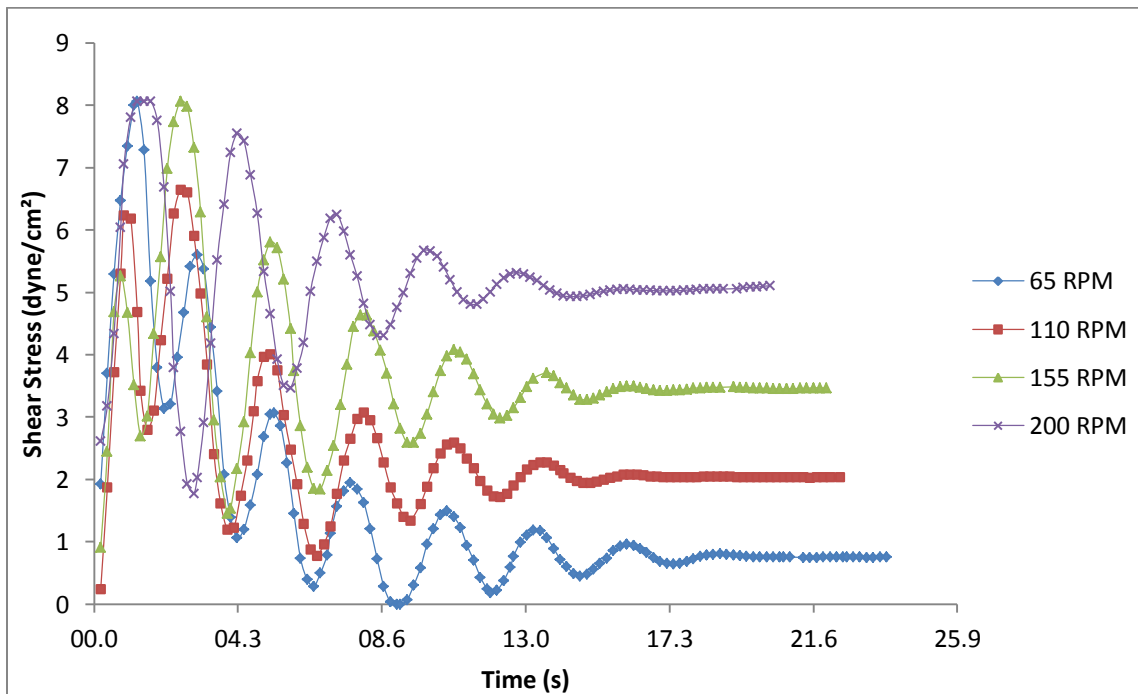
Figure 4.35: Shear stress at different RPMs vs. time conducted at 60°C, data point taken at time interval no longer than 0.2 second

91

Shear stress-time relation when same shear rate is applied at different temperatures is analyzed from the experimental data. Results for 65 RPM and 200 RPM are presented in graphical manner in Figures 4.36 and 4.37 respectively. At a certain RPM, shear stress changes in same way for first few seconds irrespective of temperature. Stress-time curves are found to coincide on each other up to this time period. After that, the oscillation in stress-time curves for different temperature starts to separate. Higher the RPM goes, earlier this separation occurs.

The mechanism of shear thickening non-Newtonian fluid is a complex one. Proper understanding of the rheological behavior of this kind of fluid is yet to be conceived. So, the findings and conclusions about the rheological behavior of 9.58% by volume and 4.50% by volume silica nanoparticle colloidal suspensions are considered to be applicable within current experimental condition and the range of parameters considered.
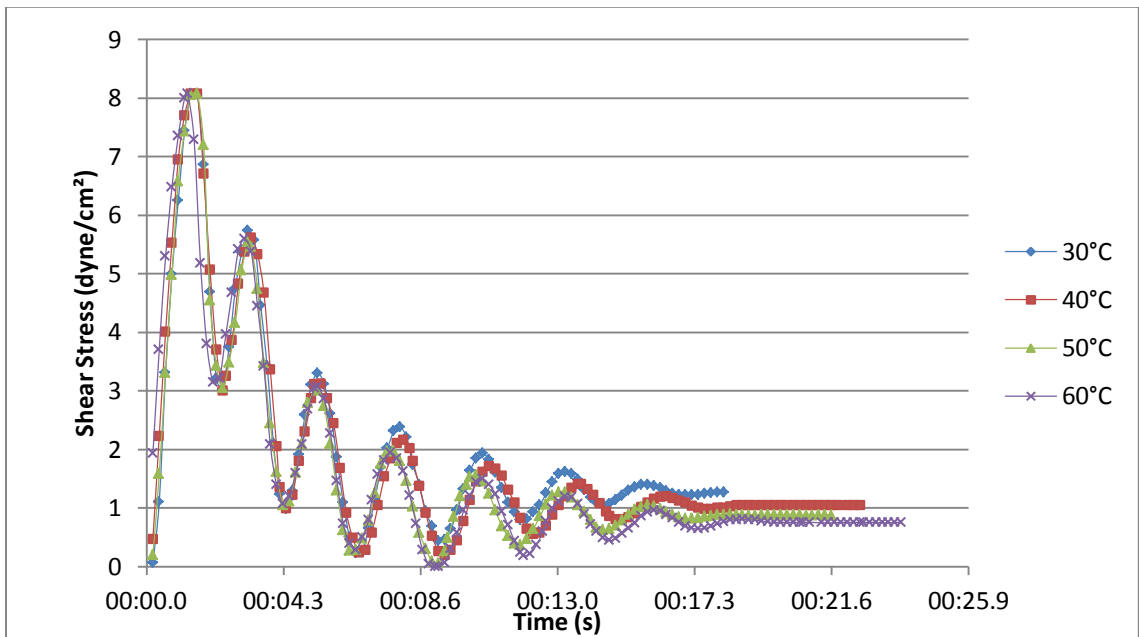
Figure 4.36: Shear stress vs. time at 65 RPM applied on 9.58% by volume silica nanoparticle colloidal suspension at different temperatures
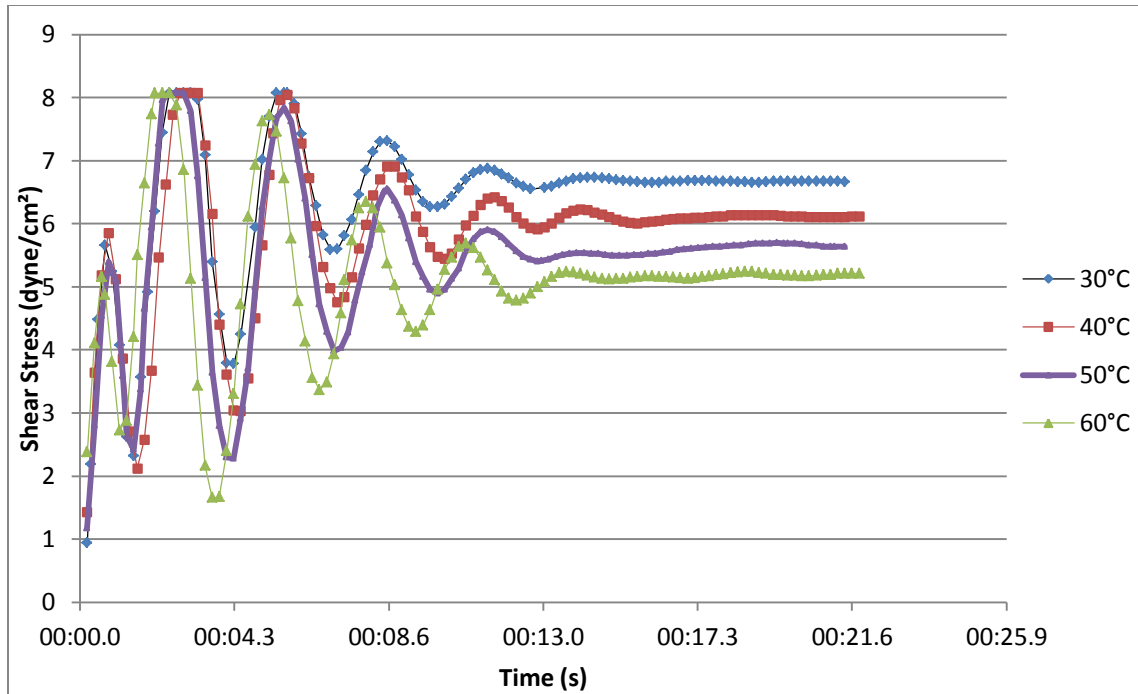
Figure 4.37: Shear stress vs. time at 200 RPM applied on 9.58% by volume silica nanoparticle colloidal suspension at different temperatures

4.4 Pressure Drop of Silica Nanoparticle Colloidal Suspension

Friction factor is measured for the 9.58% vol. silica nanoparticle colloidal suspension flowing through three different test sections. The test sections are 0.125 inch, 0.09375 inch and 0.0625 inch in outer diameter and all of them are 12 inch long. Then the experimental friction factor is compared with that of water. The parameter against which comparison is done is Reynolds number. For non-Newtonian fluid, Reynolds number of pipe flow in the laminar region can be calculated from the following equation Skelland (1967):

$$Re = \frac{D^{n'}V^{2-n'}\rho}{K'8^{n'-1}}$$

(4.6)

The value of K' and n' can be determined from the logarithmic plot of $D\Delta P/4L$ versus $8V/D$. The $D\Delta P/4L$ term represents the wall shear stress. The $8V/D$ term expresses the wall shear rate. Both these terms can be determined from experimental data. The parameter n' is the slope of the curve at any given point, and K' is the intercept of the slope line at a given point on the same plot. It is to be noted that these K' and n' are different from consistency index K and flow behavior index n described in Section 4.3. Both K and n are applicable for shear induced flow, like cylindrical Couette flow. Both K' and n' are used for flow through pipes or pressure driven flow.

To apply Equation 4.6 to determine Reynolds number for silica colloidal suspension, it is necessary to identify the laminar region of the flow for each pipe. For this purpose, friction factor is plotted against wall shear rate. The coordinates are taken in log scale. In laminar region, the curve moves downward. When transition from laminar to turbulent flow starts, the curve moves to an upward direction. When turbulent flow is achieved, the curve again starts to go in downward direction. From Figures 4.38-4.40, it is observed that the laminar flow continues approximately up to a wall shear rate of 6315 s^{-1}, 11540 s^{-1} and 63750 s^{-1} for 0.125 in, 0.09375 in and 0.0625 in OD tube respectively. The corresponding Reynolds number, after which transition to turbulent flow begins, is 1900, 2370 and 2650 for 0.125, 0.09375 and 0.0625 in. OD tube, respectively. These values are close to those Reynolds numbers at which transition for water flow through the same test section begins
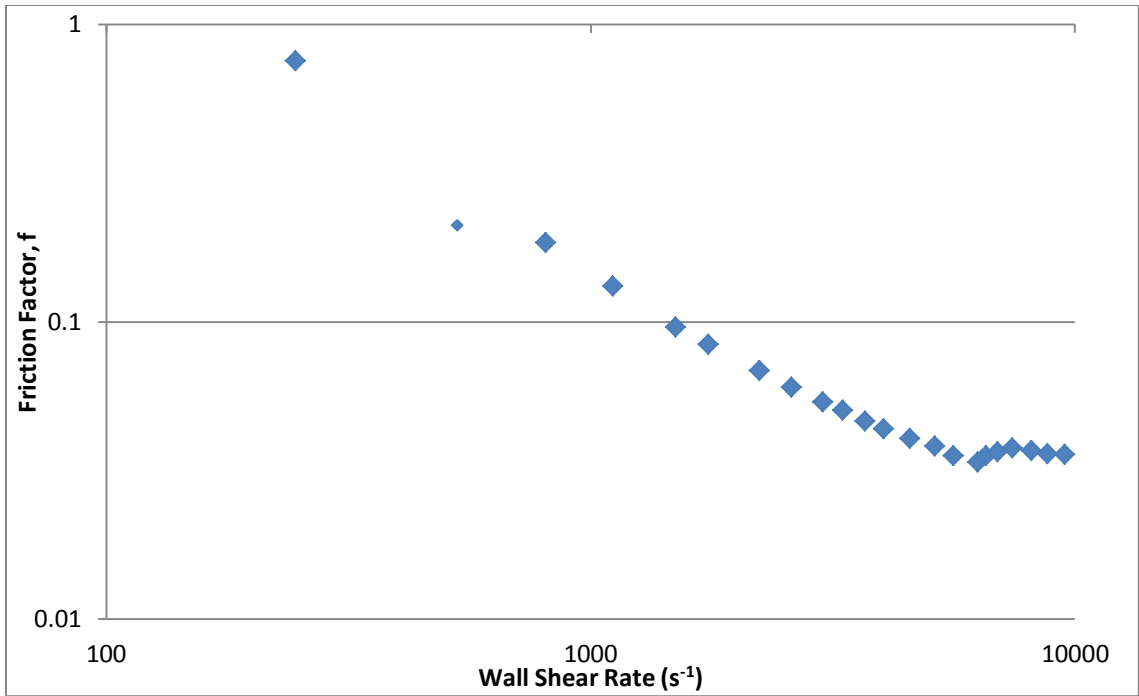
Figure 4.38: Friction factor vs. wall shear rate for 9.58% vol. silica suspension flowing through 0.125 inch OD tube
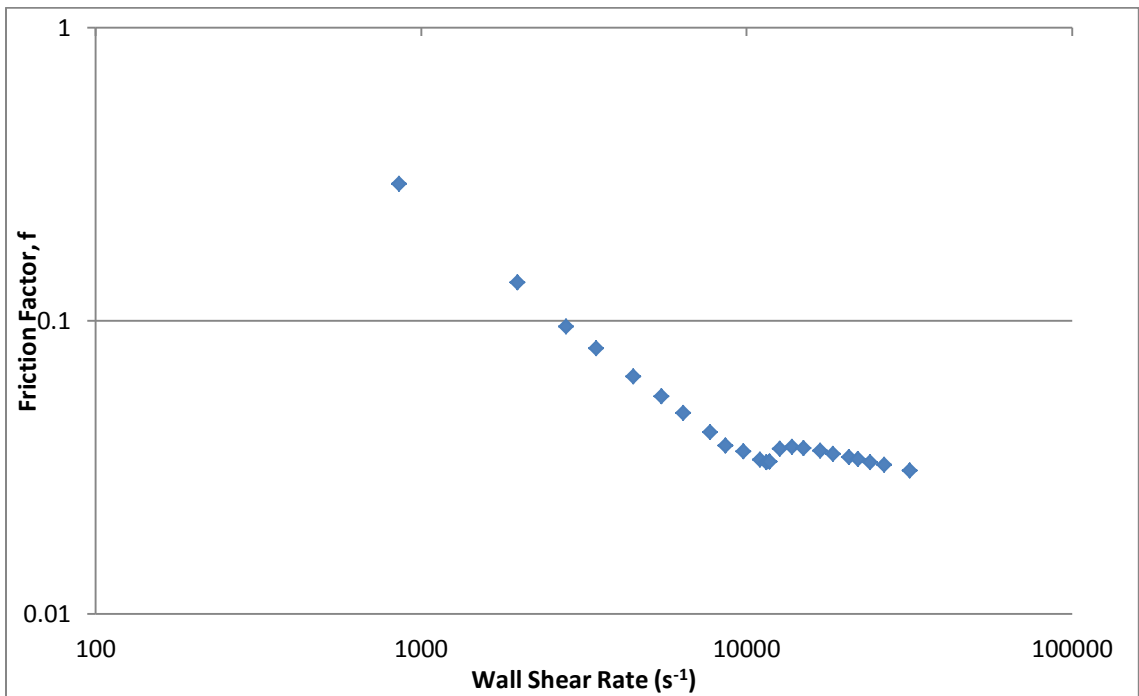
Figure 4.39: Friction factor vs. wall shear rate for 9.58% vol. silica suspension flowing through 0.09375 inch OD tube
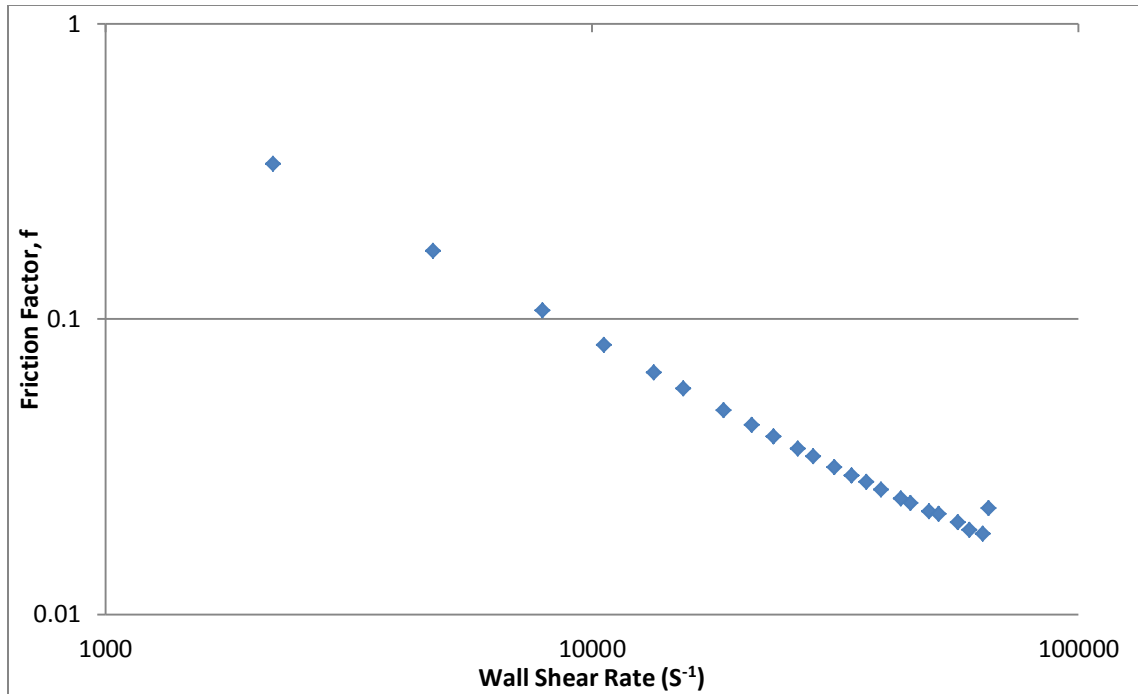
Figure 4.40: Friction factor vs. wall shear rate for 9.58% vol. silica suspension flowing through 0.0625 inch OD tube

Friction Factor for both silica colloidal suspension and water is plotted against Reynolds number. The plots for all test sections, in decreasing order of diameter, are presented in Figures 4.41-4.43. For 0.125 inch OD test section (Figure 4.41), the friction factor of the test fluid remains slightly higher than that of water up to Reynolds number around 950. Then its value starts to decrease for some period compared to water friction factor. At Re 1900, friction factor for both fluids coincide. Friction factor of silica suspension is approximately 4.65% higher at Re 825 and 10% lower at Re 1200.
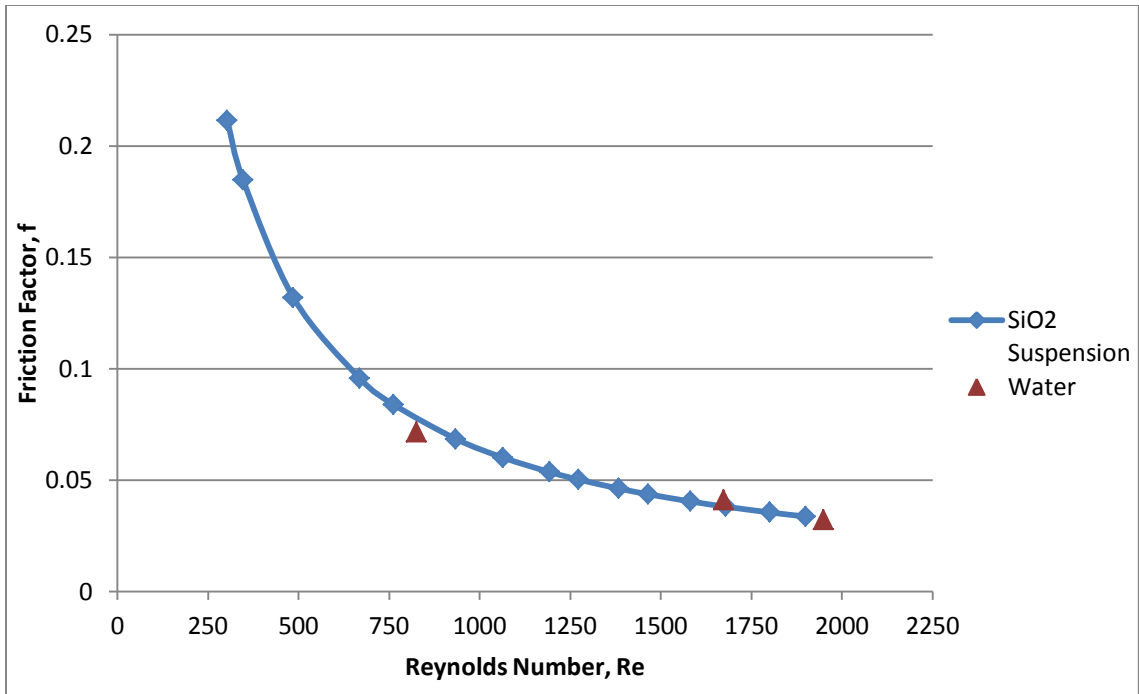
Figure 4.41: Friction factor vs. Reynolds number for 9.58% vol. silica suspension flowing through 0.125 inch OD tube

When the outer diameter of the test section is decreased to 0.09375 inch, we again see that silica suspension's friction factor remains higher than the friction factor of water at the beginning (Figure 4.42). After Reynolds number of 750, friction factor of water and that of test fluid start to get closer. The highest increase and highest decrease in the friction factor of silica suspension compared to the same parameter of water is found to be 31.28% at Re 420 and 16.50% at Re 2340, respectively.
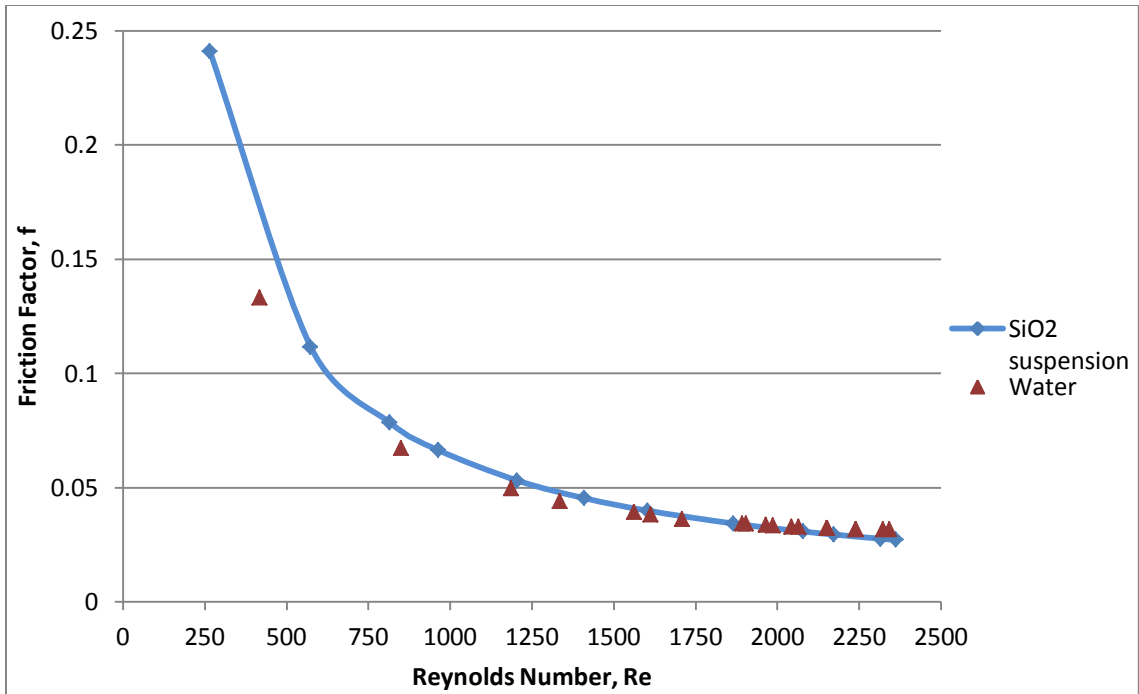
Figure 4.42: Friction factor vs. Reynolds number for 9.58% vol. silica suspension flowing through 0.09375 inch OD tube

For the tube with smallest diameter, the 0.0625 inch OD tube, the friction factor for silica suspension has a higher value at low Reynolds number ($\approx$750) compared to that of water, as can be seen in Figure 4.43. The difference in the friction factor of silica dispersion and water decreases with increasing Reynolds number. At Reynolds number of 600, an approximate increase of 63% is observed for the friction factor of silica nanoparticle dispersion. By the time the Reynolds number reaches around 2630, the increase in friction factor reduces to around 42.28%.

It is observed from the results of all three test sections that, after Reynolds number of 750, silica suspension and water show almost same trend with the friction factor. Transition is getting delayed as the diameter of the test section goes smaller. Also, the

increase in friction factor of silica suspension with respect to the friction factor of water goes higher with decreasing test section diameter.
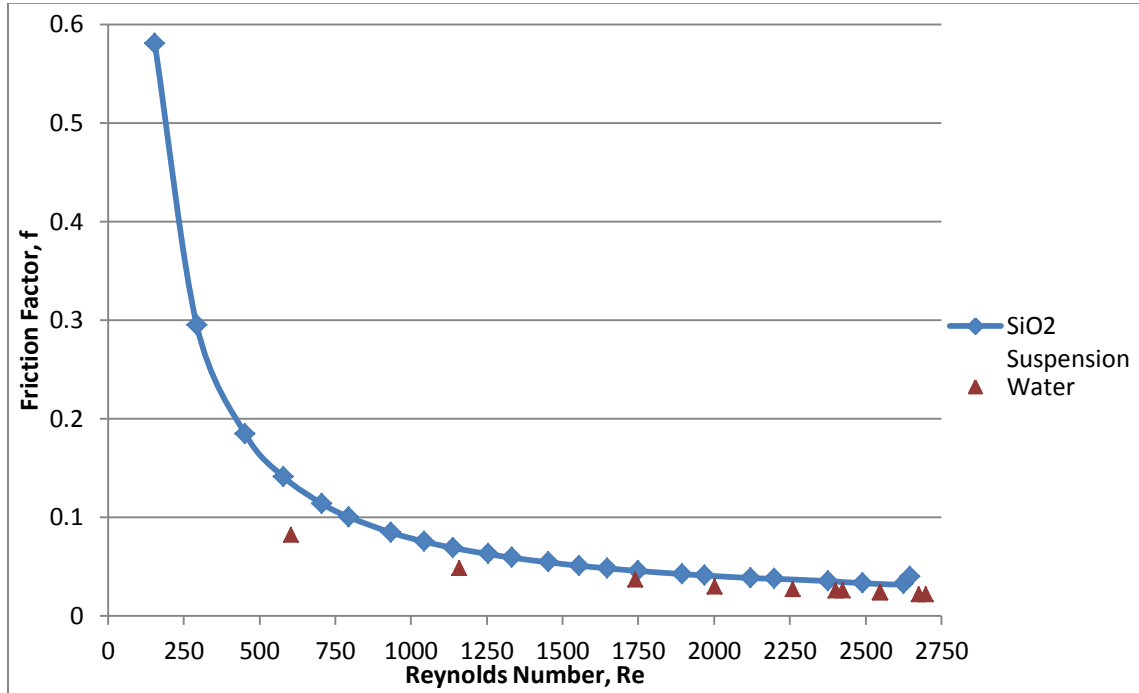
Figure 4.43: Friction factor vs. Reynolds number for 9.58% vol. silica suspension flowing through 0.0625 inch OD tube

4.5 Heat Transfer Performance of Silica Nanoparticle Colloidal Suspension

Nusselt number is calculated for the three test sections. The heat transfer performance of colloidal dispersion and water is compared in terms of Nusselt number against Reynolds number at different axial location of the tubes. Nusselt number of the silica suspension has an increasing trend in the developing region when Reynolds number increases for both fluids.

For 0.125 in OD test section (Figures 4.44 and 4.45), highest Nusselt number achieved for silica suspension and water is 17.54 and 13.42 respectively at 1.5 in from the inlet

when Reynolds number is 2700. Nusselt number of silica suspension from x=1.5 in to 5.5 in is greater than that of water when Re remains constant. From x=6.5 inch to 9.5 inch, Nu of water is almost same or slightly higher than Nu of silica suspension if Re value is close to or less than 1000. At, x=10.5 in, again the silica fluid has higher Nu compared to water Nu at all Reynolds number. Along the axial direction of the test tube, Nu of the colloidal dispersion decreases from inlet to outlet up to x=9.5 in at a certain Re. After that, there is a rise in Nu even when Re is fixed.
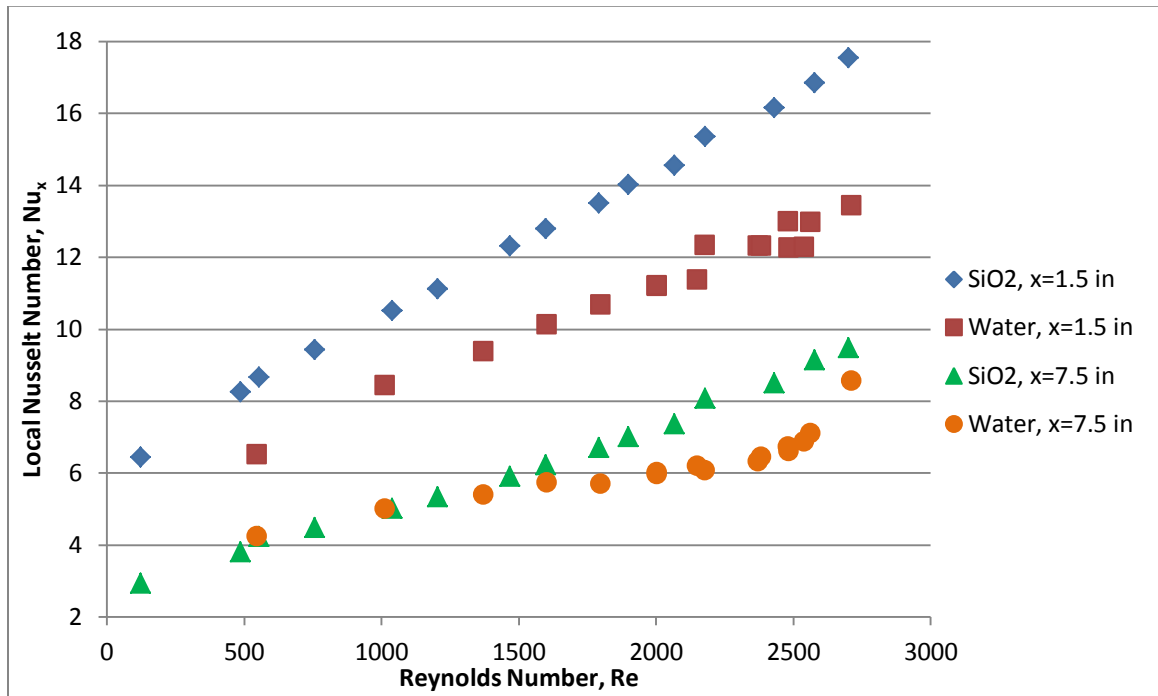
Figure 4.44: Local Nusselt number vs. Reynolds number for 9.58% vol. silica suspension and water flowing through 0.125 in OD tube (x=1.5 and 7.5 in)
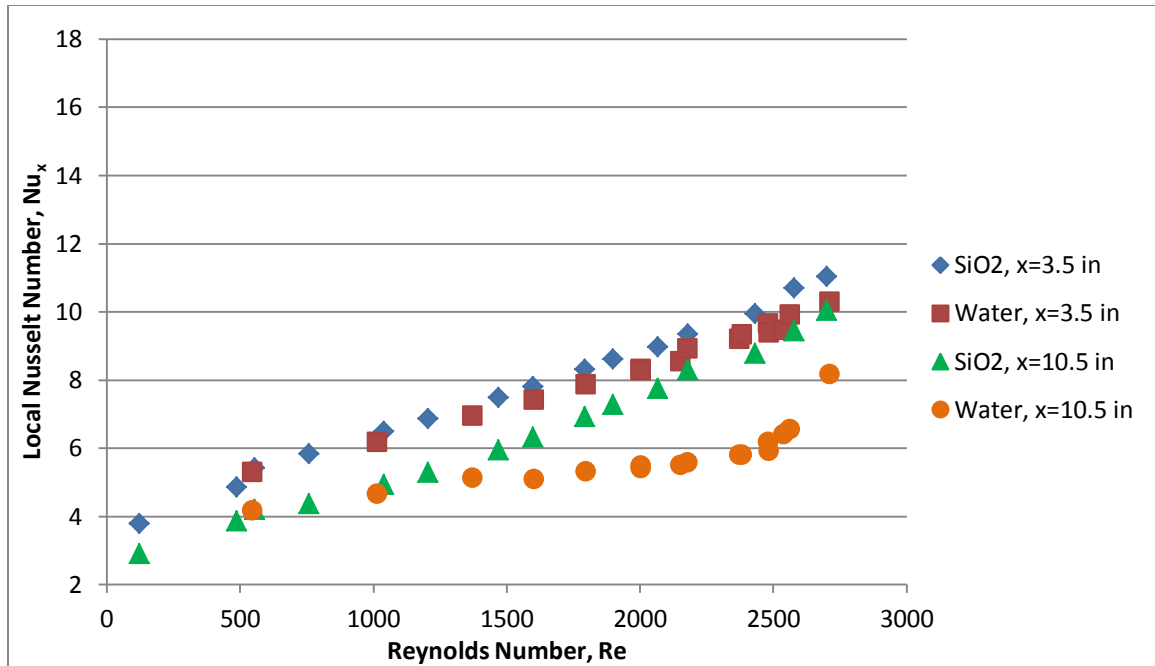
Figure 4.45: Local Nusselt number vs. Reynolds number for 9.58% vol. silica suspension and water flowing through 0.125 in OD tube (x=3.5 and 10.5 in)

The highest value of Nusselt number is 17.50 for silica suspension at Re=2375 and 11.31

for water at Re=2337 when 0.09375 inch OD test section is used for experiment (Figure

4.46). For this test section, Nu of silica suspension is higher than Nu of water when Re

remains constant throughout x=1.5 in to 4.5 in. From next axial point at x=5.5 in, Nu of

water rises slightly higher than Nu of silica suspension until the flow reaches Re≈1200.

This behavior can be observed up to x=9.5 in, after which, the silica fluid again exhibits

higher Nu compared to that of water Nu at same Reynolds number (Figures 4.46 and

4.47). Likewise for the 0.125 in OD test section, Nu of the colloidal dispersion decreases

from inlet to outlet along the axial direction of the test tube until x=9.5 in if Re does not

change. At x=10.5 in, Nu increases compared to the Nu measured at previous axial

location at a certain Re.
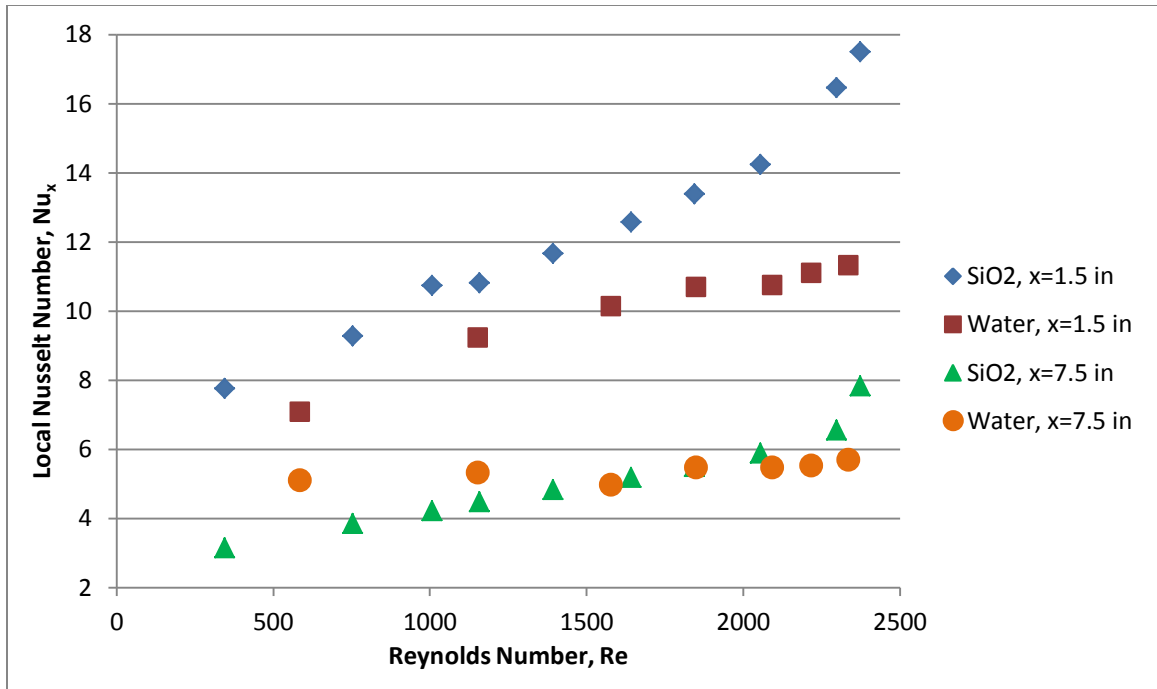
Figure 4.46: Local Nusselt number vs. Reynolds number for 9.58% vol. silica suspension and water flowing through 0.09375 in OD tube (x=1.5 and 7.5 in)
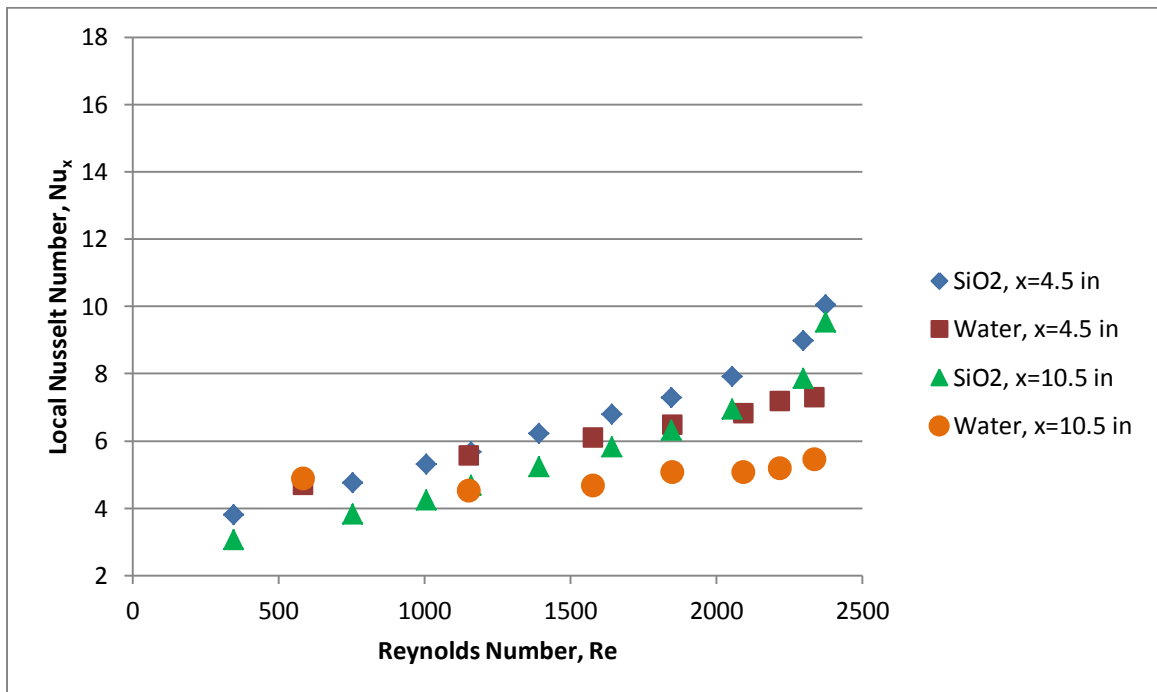
Figure 4.47: Local Nusselt number vs. Reynolds number for 9.58% vol. silica suspension and water flowing through 0.09375 in OD tube (x=4.5 and 10.5 in)

102

Figures 4.48 and 4.49 present the heat transfer result of 0.0625 in OD test section. For this test section, Nu of silica suspension at a certain Re decreases along the axial direction of tube from inlet to outlet. Nu of water surpasses the value of same parameter for silica suspension from x=4.5 in to x=10.5 in, when Re is kept around 1400 or less. In this test section, highest Nu value achieved for silica suspension and water is 16.85 and 10.70 respectively.
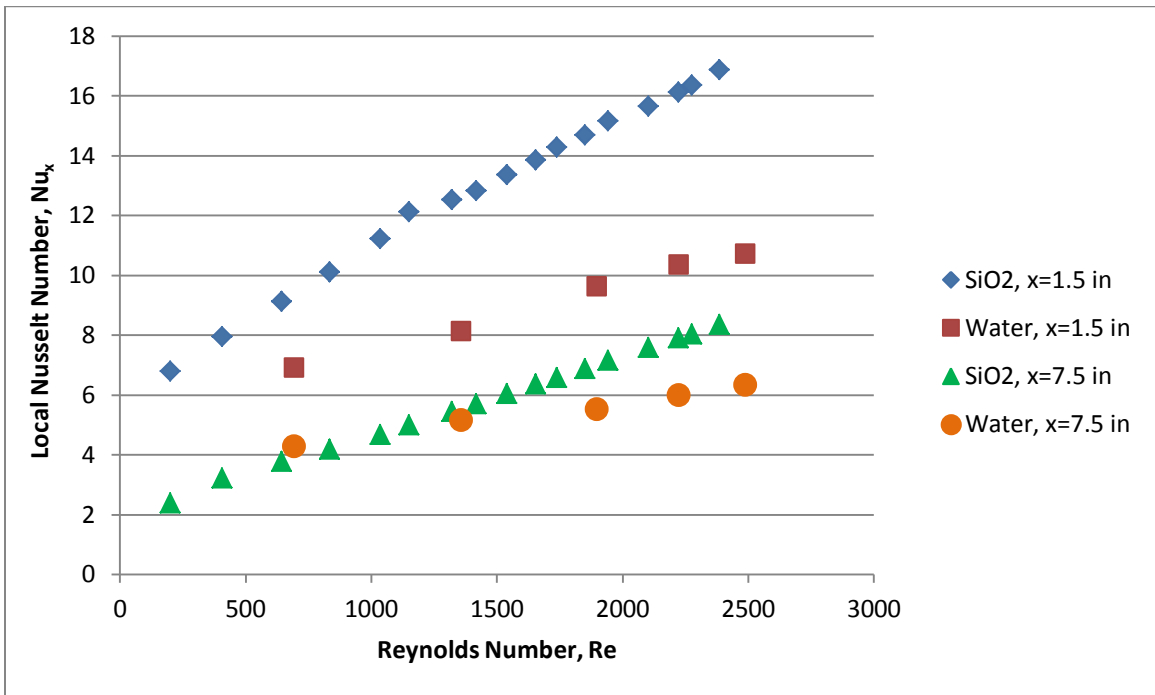
Figure 4.48: Local Nusselt number vs. Reynolds number for 9.58% vol. silica suspension and water flowing through 0.0625 in OD tube (x=1.5 and 7.5 in)
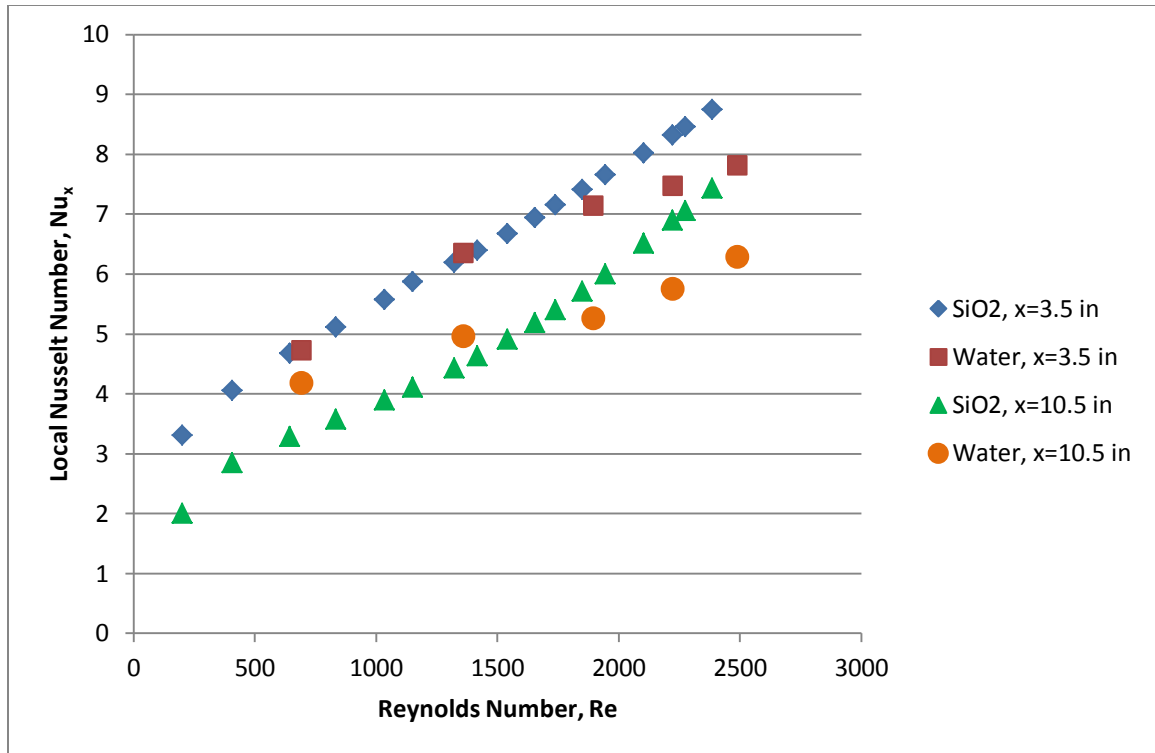
Figure 4.49: Local Nusselt number vs. Reynolds number for 9.58% vol. silica suspension and water flowing through 0.0625 in OD tube (x=3.5 and 10.5 in)

Nusselt number for water and silica suspension are compared against a nondimensional length, x^+ which is given by,

$$x^+ = \frac{2\left(\frac{x}{D}\right)}{Re\ Pr}$$
(4.7)

Experimental results for silica suspension and water flow in all test sections are compared with the Nusselt number obtained from Equation 4.3 and presented in Figure 4.50. It can be deduced from the graph that there is no significant change in the local Nusselt number of silica suspension compared to the local Nusselt number of water. Lienhard and

Lienhard (2012) correlation can be used to predict the local Nusselt number for silica colloidal suspension with an accuracy of ±15%.
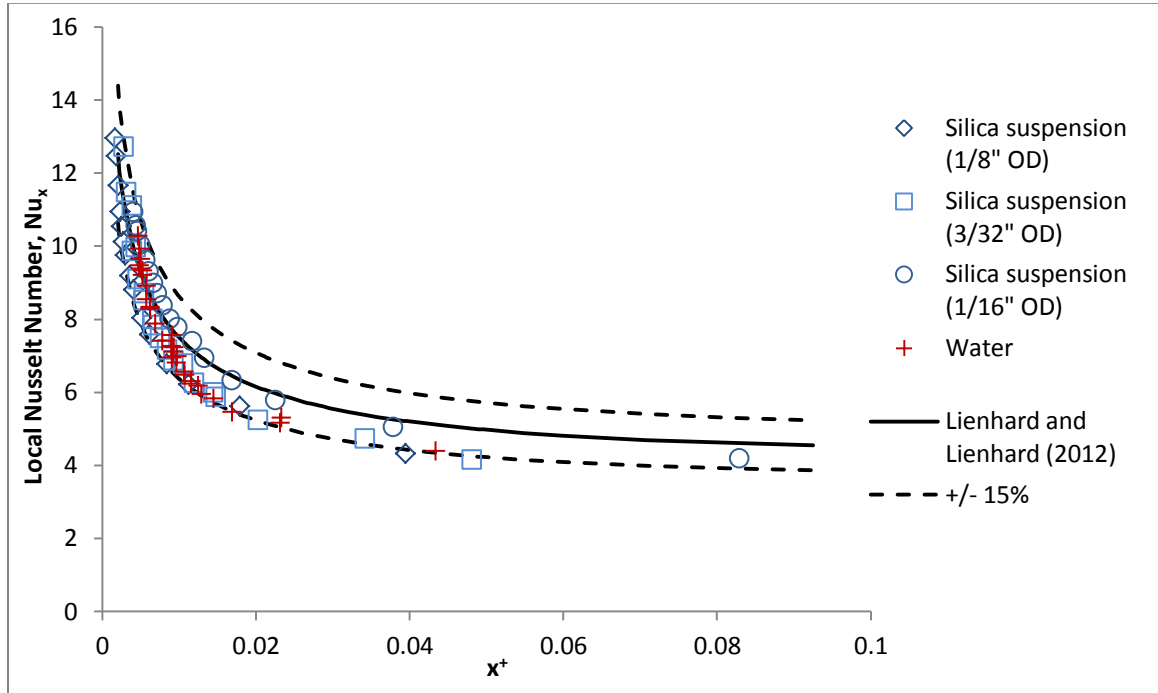
Figure 4.50: Local Nusselt number vs. nondimensional length x$^+$ for the flow of 9.58% vol. silica suspension and water through different test section

In Figures 4.51, 4.52 and 4.53, a comparison of local heat transfer coefficient with mass flow rate is presented. For 0.125 inch OD tube and 0.0625 inch OD tube, heat transfer coefficient of silica suspension is higher than that of water near the entrance at same mass flow rate. As the axial length of the flow increases, heat transfer coefficient of water gets higher than that of colloidal dispersion. For 0.09375 inch OD tube, heat transfer coefficient of water remains higher than the heat transfer coefficient of silica dispersion throughout the entire length of the tube.
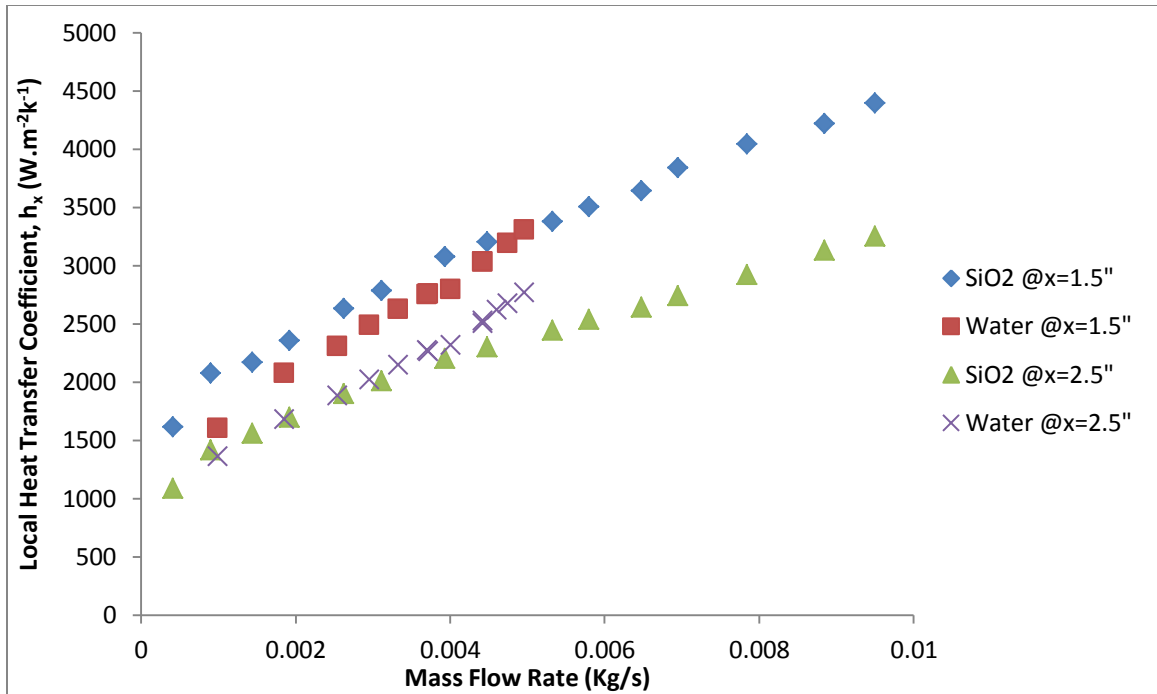
Figure 4.51: Local heat transfer coefficient vs. mass flow rate for 9.58% vol. silica suspension and water flowing through 0.125 in OD tube
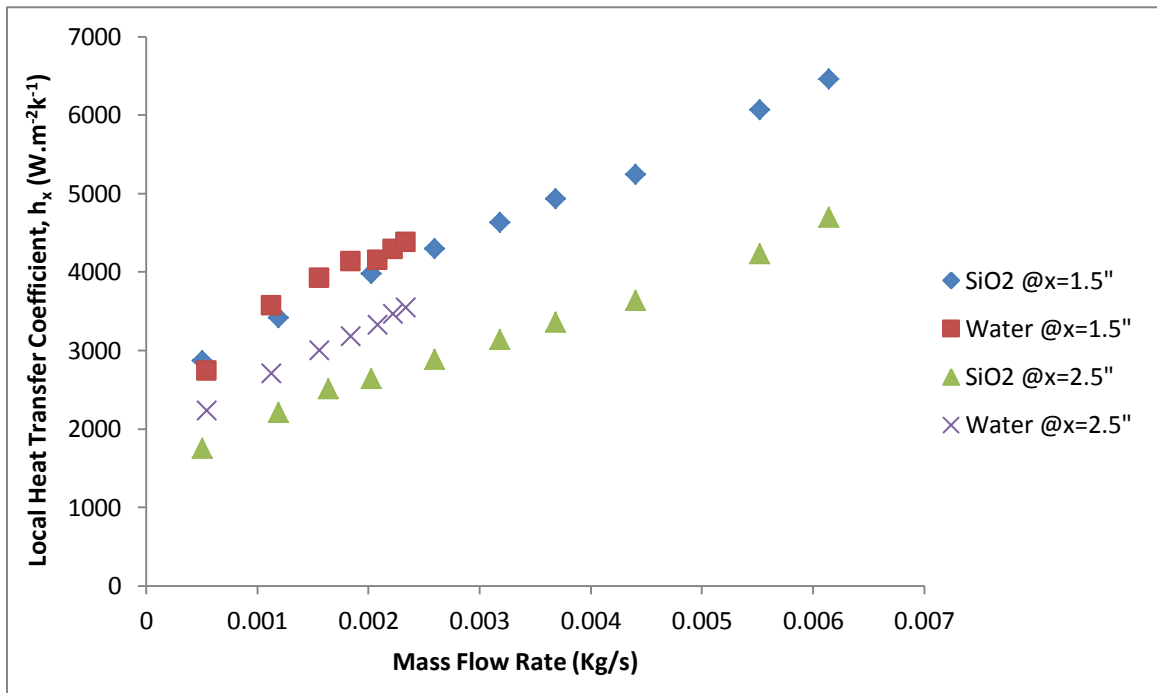
Figure 4.52: Local heat transfer coefficient vs. mass flow rate for 9.58% vol. silica suspension and water flowing through 0.09375 in OD tube
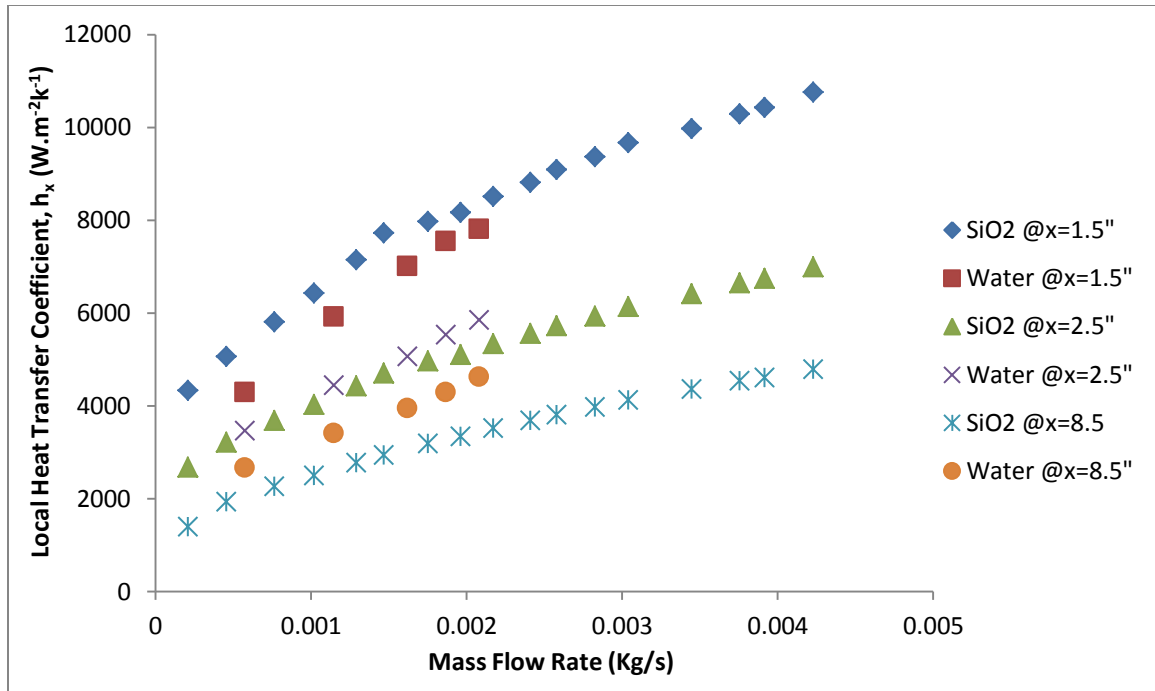
Figure 4.53: Local heat transfer coefficient vs. mass flow rate for 9.58% vol. silica suspension and water flowing through 0.0625 in OD tube

Analyzing the heat transfer data of 9.58% by volume silica nanoparticle colloidal dispersion and water, it can be concluded that the correlation for single phase fluid is also applicable to the colloidal dispersion for predicting its heat transfer performance. When compared at the same nondimensional length, there is no significant difference in the Nusselt number of silica suspension and water. When compared at same Reynolds number, the Nusselt number of the suspension promises better heat transfer performance in laminar convective flow compared to water at shorter tube length (1.5 in to 3.5 in) or at high Reynolds number.

CHAPTER V

CONCLUSION AND FUTURE DEVELOPMENT SCOPE

An experimental study was carried out to analyze the thermophysical properties, rheological behavior, pressure drop and convective heat transfer performance of silica nanoparticle colloidal suspension of 9.58% volume concentration. Obtained results of different properties of the fluid was analyzed and compared with those of water, a conventional heat carrier. The study left scope for future development and improvement of experimental condition.

5.1 Conclusion

Thermal conductivity of silica solution was measured from 7°C to 50°C and found to increase by 9.88%. Also, it has higher thermal conductivity than that of water, 3.6% being the highest increment and 0.99% being the lowest increment. Classical model for thermal conductivity of suspension developed by Maxwell (1954) and recently developed model by Kihm et al. (2011) could predicted our experimental thermal conductivity of silica suspension to within ±1% and ±4% agreement.

While studying the rheological properties of the test fluid within 7°C to 60°C temperature range, it was found to be non-Newtonian shear thickening fluid, which is considered to be a complex fluid type. The fluid was sheared up to a rate of 244.6 s^{-1} and its shear stress

and viscosity were analyzed at different temperatures. Sudden rise in shear stress was observed when applied shear rate passes a certain value at constant temperature. Viscosity of the fluid decreases when temperature goes up, and increases when its volume concentration is enhanced. The silica suspension was found to be obeying power law model which is most widely used model to describe the relation of shear stress and shear rate for non-Newtonian fluid. Viscosity was predicted by the power law with a highest error of 15%. Viscosity changed in oscillatory manner for 12-15 seconds from the time the fluid was exposed to a certain shear rate. After that, viscosity reached a plateau and no further change in its value is observed. No hysteresis was observed in shear stress-strain curve. Hence, the test fluid was considered to be a time-independent shear thickening non-Newtonian fluid.

Water and silica colloidal dispersion were circulated through test sections of 0.125 in OD, 0.09375 in OD and 0.0625 in OD tubes. Each tube was 12 in long. The friction factor of both fluids in laminar region was measured and compared. Before Reynolds number of 750, the silica suspension had higher friction factor than that of water. But as Reynolds number kept increasing, there was no significant difference in the friction factor of both fluids.

Heat transfer performance in the laminar region was assessed using Nusselt number with Reynolds number and a nondimensional length. The performance of silica suspension and water showed little variation at same dimensionless length. Colloidal suspension heat transfer could be predicted with correlation for single phase fluid. The highest value of Nusselt number for silica suspension was 17.54, whereas for water, the highest value of

the same parameter was 13.42. Both of these values were found for the flow through 0.125 in OD tube.

5.2 Scope of Development and Future Work

The thermal properties analyzer used to measure thermal conductivity is very sensible to external disturbances. If a vibration isolation table can be used to place the apparatus, the uncertainty in the measurement will reduce.

The viscometer could not obtain rheological data beyond a shear rate of 244.6 s^{-1} due to its working range limit. But when the colloidal dispersion was circulated through test section, it was subjected to wall shear rate as high as 63750 s^{-1}. So, an instrument with higher capability will help to better understand the rheological behavior of the suspension and come to a more accurate conclusion.

Few data point could be achieved for laminar flow of water with the gear pump used to circulate the fluid. If a sophisticated pump can be used to control the flow rate more precisely, then the pressure drop and heat transfer performance of water can be studied to a greater extent. This, in turn, will enable more accurate quantitative comparison between the performance of silica colloidal dispersion and water.

In future, experiment can be carried out at turbulent regime with necessary experimental setup. Further investigation of the effect of different nanoparticle material, volume concentration and particle size on the properties of colloidal suspension can help understanding the mechanism of the suspension to a greater extent.

Table A1: Energy Balance for water flow inside 0.125 inch OD tube

Flow rate, m (kg/s)	Inlet T (°C)	Outlet T (°C)	Mean T (°C)	Specific Heat, Cp (J/kg/k)	DC Voltage, V (V)	DC Current, I (amp)	Heat supplied, VI (Watt)	Heat absorbed, m*Cp*ΔT (Watt)	Heat Balance % diff.
0.00099	22.96	34.60	28.78	4178.29	0.52	91.73	48.03	48.28	-0.53
0.00186	22.98	33.97	28.47	4178.34	0.70	122.04	85.70	85.22	0.56
0.00254	23.20	32.61	27.91	4178.45	0.76	132.25	100.58	100.00	0.58
0.00296	23.36	32.77	28.07	4178.42	0.82	142.49	116.93	116.39	0.46
0.00333	23.48	32.48	27.98	4178.44	0.85	147.68	125.47	125.10	0.30
0.00371	23.65	32.31	27.98	4178.44	0.88	152.81	134.33	134.12	0.15
0.00371	23.53	32.25	27.89	4178.45	0.88	153.18	134.78	135.48	-0.52
0.00401	23.64	31.69	27.66	4178.50	0.88	153.00	134.11	134.75	-0.48
0.00403	24.05	31.99	28.02	4178.43	0.88	152.59	133.96	133.56	0.30
0.00442	23.74	31.52	27.63	4178.51	0.91	158.12	143.23	143.74	-0.36
0.00442	23.99	31.74	27.87	4178.46	0.91	157.88	143.35	143.18	0.12
0.00460	23.84	31.83	27.83	4178.47	0.94	163.34	152.90	153.65	-0.49
0.00462	23.78	31.63	27.71	4178.49	0.94	163.12	152.56	151.71	0.56
0.00476	23.51	31.24	27.37	4178.57	0.93	163.17	152.38	153.66	-0.84
0.00475	24.01	31.75	27.88	4178.46	0.94	163.19	152.77	153.60	-0.54
0.00496	23.80	33.22	28.51	4178.33	1.06	183.93	194.52	195.30	-0.41

Table A2: Energy Balance for water flow inside 0.09375 inch OD tube

Flow rate, m (kg/s)	Inlet T (°C)	Outlet T (°C)	Mean T (°C)	Specific Heat, Cp (J/kg/k)	DC Voltage, V (V)	DC Current, I (amp)	Heat supplied, VI (Watt)	Heat absorbed, m*Cp*ΔT (Watt)	Heat Balance % diff.
0.00113	23.09	37.92	30.50	4178.05	0.79	91.17	72.40	69.82	3.56
0.00156	23.29	36.59	29.94	4178.12	0.88	101.38	88.71	86.68	2.29
0.00184	23.41	35.84	29.63	4178.16	0.91	106.48	97.42	95.52	1.95
0.00209	23.48	35.55	29.51	4178.17	0.96	111.57	106.97	105.14	1.71
0.00222	23.43	35.19	29.31	4178.20	0.99	114.11	112.60	109.14	3.07
0.00234	23.47	35.25	29.36	4178.20	1.00	116.72	117.15	114.92	1.90

Table A3: Energy Balance for water flow inside 0.0625 inch OD tube

Flow rate, m (kg/s)	Inlet T (°C)	Outlet T (°C)	Mean T (°C)	Specific Heat, Cp (J/kg/k)	DC Voltage, V (V)	DC Current, I (amp)	Heat supplied, VI (Watt)	Heat absorbed, m*Cp*ΔT (Watt)	Heat Balance % diff.
0.00057	24.09	40.24	32.16	4177.94	0.70	55.82	39.21	38.75	1.18
0.00115	23.59	38.77	31.18	4177.99	0.96	76.20	73.34	72.95	0.54
0.00162	23.77	37.53	30.65	4178.04	1.09	86.37	94.39	93.31	1.14
0.00187	23.95	38.99	31.47	4177.97	1.23	96.58	118.62	117.46	0.98
0.00208	24.18	39.21	31.70	4177.96	1.29	101.75	131.74	130.72	0.77

Table A4: Energy Balance for silica suspension flow inside 0.125 inch OD tube

Flow rate, m (kg/s)	Inlet T (°C)	Outlet T (°C)	Mean T (°C)	Specific Heat, Cp (J/kg/k)	DC Voltage, V (V)	DC Current, I (amp)	Heat supplied, VI (Watt)	Heat absorbed, m*Cp*ΔT (Watt)	Heat Balance % diff.
0.00091	24.37	39.91	32.14	3487.49	0.53	91.68	48.59	49.13	-1.12
0.00192	21.45	33.18	27.32	3488.80	0.67	116.91	78.12	78.60	-0.61
0.00262	21.97	33.04	27.51	3488.74	0.76	132.28	100.41	101.33	-0.91
0.00311	22.15	32.24	27.20	3488.84	0.79	137.42	108.36	109.52	-1.07
0.00394	22.27	31.84	27.06	3488.89	0.86	150.16	129.77	131.59	-1.40
0.00448	22.31	30.98	26.65	3489.04	0.88	152.79	134.15	135.61	-1.09
0.00532	22.42	30.24	26.33	3489.16	0.91	157.96	143.25	145.25	-1.40
0.00580	22.71	30.36	26.54	3489.08	0.94	163.13	152.93	154.59	-1.09
0.00648	22.82	30.15	26.49	3489.10	0.97	168.32	162.85	165.65	-1.72
0.00695	22.71	29.88	26.30	3489.17	1.00	173.12	172.79	173.98	-0.69
0.00784	22.99	29.75	26.37	3489.14	1.03	178.44	183.39	184.85	-0.79
0.00884	23.49	29.86	26.68	3489.03	1.06	183.73	194.22	196.60	-1.23
0.00950	23.69	29.77	26.73	3489.01	1.07	185.97	199.23	201.42	-1.10

Table A5: Energy Balance for silica suspension flow inside 0.09375 inch OD tube

Flow rate, m (kg/s)	Inlet T (°C)	Outlet T (°C)	Mean T (°C)	Specific Heat, Cp (J/kg/k)	DC Voltage, V (V)	DC Current, I (amp)	Heat supplied, VI (Watt)	Heat absorbed, m*Cp*ΔT (Watt)	Heat Balance % diff.
0.00051	20.89	43.28	32.08	3487.50	0.55	73.26	40.10	39.53	1.44
0.00119	20.69	36.52	28.60	3488.39	0.70	93.95	66.13	65.84	0.44
0.00164	22.19	35.85	29.02	3488.27	0.77	101.57	77.84	78.09	-0.32
0.00203	21.04	33.19	27.11	3488.87	0.80	106.75	85.37	85.93	-0.66
0.00260	21.26	31.70	26.48	3489.10	0.84	111.88	93.68	94.55	-0.92
0.00319	21.48	31.21	26.35	3489.15	0.90	119.55	107.13	108.12	-0.93
0.00368	21.67	31.22	26.44	3489.11	0.96	127.24	121.60	122.73	-0.93
0.00440	21.86	30.53	26.19	3489.21	0.99	132.39	131.57	133.22	-1.25
0.00552	22.17	29.91	26.04	3489.26	1.05	140.08	147.22	149.13	-1.30
0.00615	22.49	30.24	26.37	3489.14	1.11	147.80	163.65	166.19	-1.55

Table A6: Energy Balance for silica suspension flow inside 0.0625 inch OD tube

Flow rate, m (kg/s)	Inlet T (°C)	Outlet T (°C)	Mean T (°C)	Specific Heat, Cp (J/kg/k)	DC Voltage, V (V)	DC Current, I (amp)	Heat supplied, VI (Watt)	Heat absorbed, m*Cp*ΔT (Watt)	Heat Balance % diff.
0.00076	20.02	37.07	28.55	3488.41	0.76	60.85	46.42	45.49	2.00
0.00102	20.06	36.36	28.21	3488.51	0.86	68.48	58.96	58.00	1.63
0.00129	20.10	36.62	28.36	3488.46	0.98	77.38	75.63	74.45	1.56
0.00147	20.12	36.15	28.14	3488.53	1.03	81.16	83.33	82.18	1.38
0.00175	20.26	35.53	27.90	3488.61	1.09	86.29	94.29	93.44	0.90
0.00196	20.36	34.03	27.19	3488.84	1.09	86.31	94.10	93.57	0.55
0.00217	20.48	34.37	27.42	3488.77	1.16	91.40	105.80	105.21	0.56
0.00241	20.64	33.88	27.26	3488.82	1.19	93.96	111.81	111.33	0.43
0.00258	20.74	33.82	27.28	3488.81	1.22	96.51	118.08	117.73	0.30
0.00283	20.92	33.51	27.22	3488.84	1.26	99.07	124.47	124.14	0.26
0.00304	21.09	33.42	27.25	3488.82	1.29	101.63	131.07	130.84	0.17
0.00345	21.43	32.86	27.15	3488.86	1.32	104.19	137.73	137.52	0.16
0.00376	21.65	32.68	27.16	3488.86	1.36	106.74	144.64	144.52	0.08
0.00392	21.81	32.38	27.09	3488.88	1.35	106.74	144.57	144.44	0.09
0.00423	22.05	32.32	27.18	3488.85	1.39	109.29	151.67	151.59	0.05

REFERENCES

Abbaspoursani, K., Allahyari, M., & Rahmani, M. (2011). An improved model for prediction of the effective thermal conductivity of nanofluids. *Journal of Engineering and Technology, 58*, 234-237.

Aladag, B., Halelfadl, S., Doner, N., Maré, T., Duret, S., & Estellé, P. (2012). Experimental investigations of the viscosity of nanofluids at low temperatures. *Applied Energy, 97*(0), 876-880. doi: http://dx.doi.org/10.1016/j.apenergy.2011.12.101

Baghbanzadeh, M., Rashidi, A., Soleimanisalim, A. H., & Rashtchian, D. (2014). Investigating the rheological properties of nanofluids of water/hybrid nanostructure of spherical silica/MWCNT. *Thermochimica Acta, 578*(0), 53-58. doi: http://dx.doi.org/10.1016/j.tca.2014.01.004

Beck, M., Yuan, Y., Warrier, P., & Teja, A. (2009). The effect of particle size on the thermal conductivity of alumina nanofluids. *Journal of Nanoparticle Research, 11*(5), 1129-1136. doi: 10.1007/s11051-008-9500-2

Chan Hee, C., Kihm, K. D., Shin Pyo, L., & Choi, S. U. S. (2005). Empirical correlation finding the role of temperature and particle size for nanofluid (Al_2O_3) thermal conductivity enhancement. *Applied Physics Letters, 87*(15), 153107. doi: 10.1063/1.2093936

Darzi, A. A. R., Farhadi, M., Sedighi, K., Shafaghat, R., & Zabihi, K. (2012). Experimental investigation of turbulent heat transfer and flow characteristics of SiO_2/water nanofluid within helically corrugated tubes. *International Communications in Heat and Mass Transfer, 39*(9), 1425-1434. doi: http://dx.doi.org/10.1016/j.icheatmasstransfer.2012.07.027

Duan, F., Wong, T., & Crivoi, A. (2012). Dynamic viscosity measurement in non-Newtonian graphite nanofluids. *Nanoscale Research Letters, 7*(1), 360.

Duangthongsuk, W., & Wongwises, S. (2010). An experimental study on the heat transfer performance and pressure drop of TiO_2-water nanofluids flowing under a turbulent flow regime. *International Journal of Heat and Mass Transfer, 53*(1–3), 334-344. doi: http://dx.doi.org/10.1016/j.ijheatmasstransfer.2009.09.024

Dupuis, D., Lewandowski, F. Y., Steiert, P., & Wolff, C. (1994). Shear thickening and time-dependent phenomena: the case of polyacrylamide solutions. *Journal of Non-Newtonian Fluid Mechanics, 54*(0), 11-32. doi: http://dx.doi.org/10.1016/0377-0257(94)80013-8

Fotukian, S. M., & Nasr Esfahany, M. (2010). Experimental study of turbulent convective heat transfer and pressure drop of dilute CuO/water nanofluid inside a circular tube. *International Communications in Heat and Mass Transfer, 37*(2), 214-219. doi: http://dx.doi.org/10.1016/j.icheatmasstransfer.2009.10.00

Hamilton, R. L., & Crosser, O. K. (1962). Thermal Conductivity of Heterogeneous Two-Component Systems. *Industrial & Engineering Chemistry Fundamentals, 1*(3), 187-191. doi: citeulike-article-id:1033567

Hashemi, S. M., & Akhavan-Behabadi, M. A. (2012). An empirical study on heat transfer and pressure drop characteristics of CuO–base oil nanofluid flow in a horizontal helically coiled tube under constant heat flux. *International Communications in Heat and Mass Transfer, 39*(1), 144-151. doi: http://dx.doi.org/10.1016/j.icheatmasstransfer.2011.09.002

Hess, O., Goddard, C., & Hess, S. (2006). From shear-thickening and periodic flow behavior to rheo-chaos in nonlinear Maxwell-model fluids. *Physica A: Statistical Mechanics and its Applications, 366*(0), 31-54. doi: http://dx.doi.org/10.1016/j.physa.2005.10.007

Heyhat, M. M., Kowsary, F., Rashidi, A. M., Momenpour, M. H., & Amrollahi, A. (2013). Experimental investigation of laminar convective heat transfer and pressure drop of water-based Al_2O_3 nanofluids in fully developed flow regime. *Experimental Thermal and Fluid Science, 44*(0), 483-489. doi: http://dx.doi.org/10.1016/j.expthermflusci.2012.08.009

Hojjat, M., Etemad, S. G., Bagheri, R., & Thibault, J. (2011a). Convective heat transfer of non-Newtonian nanofluids through a uniformly heated circular tube. *International Journal of Thermal Sciences, 50*(4), 525-531. doi: http://dx.doi.org/10.1016/j.ijthermalsci.2010.11.006

Hojjat, M., Etemad, S. G., Bagheri, R., & Thibault, J. (2011b). Rheological characteristics of non-Newtonian nanofluids: Experimental investigation. *International Communications in Heat and Mass Transfer, 38*(2), 144-148. doi: http://dx.doi.org/10.1016/j.icheatmasstransfer.2010.11.019

Hong, J., & Kim, D. (2012). Effects of aggregation on the thermal conductivity of alumina/water nanofluids. *Thermochimica Acta, 542*(0), 28-32. doi: http://dx.doi.org/10.1016/j.tca.2011.12.019

Hu, Y., Boltenhagen, P., Matthys, E., & Pine, D. (1998). Shear thickening in low-concentration solutions of wormlike micelles. II. Slip, fracture, and stability of the shear-induced phase. *Journal of Rheology (1978-present), 42*(5), 1209-1226.

Huifei, J., Andritsch, T., Tsekmes, I. A., Kochetov, R., Morshuis, P. H. F., & Smit, J. J. (2014). Properties of Mineral Oil based Silica Nanofluids. *Dielectrics and Electrical Insulation, IEEE Transactions on, 21*(3), 1100-1108. doi: 10.1109/TDEI.2014.6832254

Hwang, Y. J., Ahn, Y. C., Shin, H. S., Lee, C. G., Kim, G. T., Park, H. S., & Lee, J. K. (2006). Investigation on characteristics of thermal conductivity enhancement of nanofluids. *Current Applied Physics, 6*(6), 1068-1071. doi: http://dx.doi.org/10.1016/j.cap.2005.07.021

Jo, B., & Banerjee, D. (2014). Viscosity measurements of multi-walled carbon nanotubes-based high temperature nanofluids. *Materials Letters, 122*(0), 212-215. doi: http://dx.doi.org/10.1016/j.matlet.2014.02.032

Kannadasan, N., Ramanathan, K., & Suresh, S. (2012). Comparison of heat transfer and pressure drop in horizontal and vertical helically coiled heat exchanger with CuO/water based nano fluids. *Experimental Thermal and Fluid Science, 42*(0), 64-70. doi: http://dx.doi.org/10.1016/j.expthermflusci.2012.03.031

Kayhani, M., Soltanzadeh, H., Heyhat, M., Nazari, M., & Kowsary, F. (2012). Experimental study of convective heat transfer and pressure drop of TiO_2/water nanofluid. *International Communications in Heat and Mass Transfer, 39*(3), 456-462.

Kays, W. M., Crawford, M. E., & Weigand, B. (2004). *Convective Heat and Mass Transfer* (4th ed.): McGraw-Hill.

Kihm, K., Chon, C., Lee, J., & Choi, S. (2011). A new heat propagation velocity prevails over Brownian particle velocities in determining the thermal conductivities of nanofluids. *Nanoscale Research Letters, 6*(1), 361.

Kole, M., & Dey, T. (2010). Thermal conductivity and viscosity of Al_2O_3 nanofluid based on car engine coolant. *Journal of Physics D: Applied Physics, 43*(31), 315501.

Lienhard, J. H., & Lienhard, J. H. (2012). *A Heat Transfer Textbook* (4 ed.): Phlogiston Press.

Maranzano, B. J., & Wagner, N. J. (2002). Flow-small angle neutron scattering measurements of colloidal dispersion microstructure evolution through the shear thickening transition. *The Journal of chemical physics, 117*(22), 10291-10302.

Mariano, A., Pastoriza-Gallego, M. J., Lugo, L., Camacho, A., Canzonieri, S., & Piñeiro, M. M. (2013). Thermal conductivity, rheological behaviour and density of non-Newtonian ethylene glycol-based SnO_2 nanofluids. *Fluid Phase Equilibria, 337*(0), 119-124. doi: http://dx.doi.org/10.1016/j.fluid.2012.09.029

Masoumi, N., Sohrabi, N., & Behzadmehr, A. (2009). A new model for calculating the effective viscosity of nanofluids. *Journal of Physics D: Applied Physics, 42*(5), 055501.

Maxwell, J. C. (1954). *A Treatise on Electricity and Magnetism* (3 ed. Vol. 1): New York Dover Publications.

Namburu, P. K., Kulkarni, D. P., Dandekar, A., & Das, D. K. (2007). Experimental investigation of viscosity and specific heat of silicon dioxide nanofluids. *Micro & Nano Letters, IET, 2*(3), 67-71. doi: 10.1049/mnl:20070037

Namburu, P. K., Kulkarni, D. P., Misra, D., & Das, D. K. (2007). Viscosity of copper oxide nanoparticles dispersed in ethylene glycol and water mixture. *Experimental Thermal and Fluid Science, 32*(2), 397-402.

Pastoriza-Gallego, M., Lugo, L., Legido, J., & Pineiro, M. (2011). Rheological non-Newtonian behaviour of ethylene glycol-based Fe_2O_3 nanofluids. *Nanoscale Research Letters, 6*(1), 560.

Philip, J., & Shima, P. D. (2012). Thermal properties of nanofluids. *Advances in Colloid and Interface Science, 183–184*(0), 30-45. doi: http://dx.doi.org/10.1016/j.cis.2012.08.001

Prasher, R., Song, D., Wang, J., & Phelan, P. (2006). Measurements of nanofluid viscosity and its implications for thermal applications. *Applied Physics Letters, 89*(13), -. doi: doi:http://dx.doi.org/10.1063/1.2356113

Sahoo, B. C., Das, D. K., Vajjha, R. S., & Satti, J. R. (2013). Measurement of the Thermal Conductivity of Silicon Dioxide Nanofluid and Development of Correlations. *Journal of Nanotechnology in Engineering and Medicine, 3*(4), 041006-041006. doi: 10.1115/1.4024003

Sajadi, A. R., & Kazemi, M. H. (2011). Investigation of turbulent convective heat transfer and pressure drop of TiO_2/water nanofluid in circular tube. *International Communications in Heat and Mass Transfer, 38*(10), 1474-1478. doi: http://dx.doi.org/10.1016/j.icheatmasstransfer.2011.07.007

Skelland, A. H. P. (1967). *Non-Newtonian Flow and Heat Transfer*: John Wiley & Sons, Inc.

Sun, C., Bai, B., Lu, W.-Q., & Liu, J. (2013). Shear-rate dependent effective thermal conductivity of H_2O+SiO_2 nanofluids. *Physics of Fluids, 25*(5), 052002. doi: 10.1063/1.4802049

Tiwari, S. (2012). *Evaluation of Thermophysical Properties, Friction Factor and Heat Transfer of Alumina Nanofluid Flow in Tubes.* (MS), University of North Dakota.

Wang, H., Zhao, H., & Liu, S. (2011). Preparation and Thermal Conductivity of Nanofluids Consisting of SiO_2-Organic Composite Nanorods. *Journal of Inorganic and Organometallic Polymers and Materials, 21*(4), 946-949. doi: 10.1007/s10904-011-9545-z

Wang, J., Zhu, J., Zhang, X., & Chen, Y. (2013). Heat transfer and pressure drop of nanofluids containing carbon nanotubes in laminar flows. *Experimental Thermal and Fluid Science, 44*(0), 716-721. doi: http://dx.doi.org/10.1016/j.expthermflusci.2012.09.013

Wu, X., Wu, H., & Cheng, P. (2009). Pressure drop and heat transfer of Al_2O_3-H_2O nanofluids through silicon microchannels. *Journal of Micromechanics and Microengineering, 19*(10), 105020.

Yang, J.-C., Li, F.-C., Zhou, W.-W., He, Y.-R., & Jiang, B.-C. (2012). Experimental investigation on the thermal conductivity and shear viscosity of viscoelastic-fluid-based nanofluids. *International Journal of Heat and Mass Transfer, 55*(11–12), 3160-3166. doi: http://dx.doi.org/10.1016/j.ijheatmasstransfer.2012.02.052

Zhou, S.-Q., Ni, R., & Funfschilling, D. (2010). Effects of shear rate and temperature on viscosity of alumina polyalphaolefins nanofluids. *Journal of Applied Physics, 107*(5), 054317-054322. doi: 10.1063/1.3309478